MICROGRAVITY FLOW PATTERN IDENTIFICATION USING VOID FRACTION SIGNALS

A Thesis

by

LUCA VALOTA

Submitted to the Office of Graduate Studies of
Texas A&M University
in partial fulfillment of the requirements for the degree of

MASTER OF SCIENCE

May 2004

Major Subject: Nuclear Engineering

MICROGRAVITY FLOW PATTERN IDENTIFICATION USING VOID FRACTION SIGNALS

A Thesis

by

LUCA VALOTA

Submitted to the Office of Graduate Studies of
Texas A&M University
in partial fulfillment of the requirements for the degree of

MASTER OF SCIENCE

Approved as to style and content by:

Frederick R. Best (Chair of Committee)	Yassin A. Hassan (Member)
Marvin L. Adams (Member)	Ali Beskok (Member)
William E. Burchill (Head of Department)	

May 2004

Major Subject: Nuclear Engineering

ABSTRACT

Microgravity Flow Pattern Identification Using Void Fraction Signals. (May 2004)

Luca Valota, B.S., Politecnico di Milano

Chair of Advisory Committee: Dr. Frederick R. Best

Knowledge of the two-phase flow state is fundamental for two-phase flow system design and operation. In traditional two-phase flow studies, the flow regime refers to the physical location of the gas and liquid in a conduit. Flow configuration is important for engineering correlations of heat and mass transfer, pressure drop, and wall shear. However, it is somewhat subjective since it is mostly defined by experimental observation, resulting in an approximate and equivocal definition. Thus, there is need for a better, objective flow regime identification. The void fraction is a key parameter in monitoring the operating state of a two-phase system and several tools have been developed in order to measure it. The purpose of this study is to use the void fraction and other parameters of the system to achieve a model for flow pattern identification.

Recently, an experimental program using the Foster-Miller two-phase flow test bed and Creare Inc. capacitance void fraction sensors was conducted in the microgravity environment of the NASA KC-135 aircraft. Several data types were taken for each phase, such as flow rate, superficial velocity, density and transient void fraction at 100Hz. Several analytical approaches were pursued, including a statistical approach of the fluctuation of the void fraction, Martinelli analysis, and

Drift Flux analysis, in order to reach a model for flow pattern identification in microgravity conditions.

Several parameters were found to be good flow pattern identifiers such as the statistical moments variance and skewness, Signal -to- noise ratio (SNR), Half Height Value (HHV) and Linear Area Difference (LAD). Moreover, relevant conclusions were achieved using the Martinelli parameter and the Drift Flux model in microgravity conditions. These results were compared with the basic literature.

ACKNOWLEDGEMENTS

I would like to express my gratitude to a number of individuals and organizations who have contributed to this thesis and to my research.

First of all, I would like to thank Dr. Frederick Best, my thesis advisor, for his willingness to share his insights in two-phase flow in microgravity. I am very grateful for his passion and for the patient guidance throughout this work, and in particular thankful for his proof that, like Alexis Carrel once said, “a few observations and much reasoning lead to error, many observations and a little reasoning lead to truth“.

I would also like to acknowledge all the assistance from Cable Kurwitz and the members of the ITP group at Texas A&M University for the laboratory work done together. In particular Mike Ellis for the computational consulting, Charlie Neill for the lab organization, Filip Finodeyev for the proof that even with few concepts anyone can come out with something interesting and last but not least Jonathan Braisted because of your scacciafiga, my future wife will thank you.

Sincere thanks go to NASA Johnson Space Center, NASA Glenn Space Center, CREARE Inc. in the person of Chris Crowley and the Texas A&M Center for Space Power (CSP) for all the technical support.

In a less technical level, I would like to thank all the friends that have gone with me in this adventure, in particular Vittorio (Tolo) and all the “ragazzi del Poli”, the scec, Mike Eppler and the CL guys, because I felt at home. Thank you also to

all the friends from the Nuclear Engineering department that introduced me in this strange world called Texas A&M. A special thank to Atalanta, because you never give up and at the end we are still here singing.

Finally I would like to thank my parents, Giacomo Valota and Adelisa Manfredi, and my brother and sister Matteo (Teo) and Valentina for their loving and endless support throughout my life.

TABLE OF CONTENTS

Chapter Page

LIST OF TABLES

LIST OF FIGURES

Page

Page

Page

NOMENCLATURE

Symbol	Description
α	Void Fraction (dimensionless)
$\langle \alpha \rangle$	Average Void Fraction (dimensionless)
α_c	Centerline Void Fraction (dimensionless)
α_w	Wall Void Fraction (dimensionless)
A	Test Section Cross Sectional Area (m^2)
C_0	Distribution Parameter (dimensionless)
d_h	Hydraulic Diameter (m^2)
g	Gravitational Acceleration (one-g = 9.81 m/s^2)
g_x	x-Axis Acceleration (g's or m/s^2)
g_y	y-Axis Acceleration (g's or m/s^2)
g_z	z-Axis Acceleration (g's or m/s^2)
j	Total Volumetric Flux (m/s)
j_g	Gas Volumetric Flux (m/s)
j_l	Liquid Volumetric Flux (m/s)
$\langle j \rangle$	Total Average Volumetric Flux or Total Superficial Velocity (m/s)
$\langle j_g \rangle$	Average Gas Volumetric Flux or Gas Superficial Velocity (m/s)
$\langle j_l \rangle$	Average Liquid Volumetric Flux or Gas Superficial Velocity (m/s)

σ	Surface Tension (N/m)
ρ_g	Gas Density (kg/m^3)
ρ_l	Liquid Density (kg/m^3)
$\bar{\rho}$	Two-Phase Mixture Density (kg/m^3)
Q_g	Volumetric Gas Flow Rate (m^3/s)
Q_l	Volumetric Liquid Flow Rate (m^3/s)
v_g	Gas Velocity (m/s)
v_l	Liquid Velocity (m/s)
v_r	Relative Velocity (m/s)
v_{gj}	Drift-Flux or Drift-Velocity (m/s)
V_{gj}	Void-Fraction Weighted Mean Drift Velocity (m/s)
W_g	Gas Mass Flow Rate (kg/s)
W_l	Liquid Mass Flow Rate (kg/s)
X	Martinelli Parameter
f	Probability density function
F	Cumulative probability function
p	Pressure (psi)
Φ_{fo}	Two phase flow multiplier
μ_f	Viscosity fluid (Pa-s)
μ_g	Viscosity gas (Pa-s)
x	Volumetric quality

CHAPTER I

INTRODUCTION AND LITERATURE REVIEW

1.1 INTRODUCTION

The application of fluids is widely used in current space programs. This includes bioreactors and life-support systems, storage and transport of cryogenics, tank filling and fluid management and design of many cold plate assemblies where heating (or cooling) takes place at the instrument/utility interface. In particular, fluids are widely used as coolant in high power thermal management energy-transport systems. The importance of this study is further enhanced due to the fact that power requirements for future spacecraft and satellites are expected to increase due to incremented technology and capabilities.

At this time single-phase liquids or gasses are used as the principal coolant fluid in transport of heat in space systems. These systems require a thorough understanding of the mechanism of single-phase flow under microgravity conditions; understanding that was achieved with years of experiments and

---

The thesis follows the style of Fusion Engineering and Design.

theoretical investigation. But considering the restrictions in volume and mass imposed by space applications, achieving a high level of power, future space mission should take advantage of two-phase flow technology. In fact, in comparison with single-phase flow, two-phase flow (gas-liquid) has several advantages:

- Carry more energy per fluid unit mass
- Work at almost constant temperature
- Require less pumping power per unit mass thermal energy carried
- Better heat transfer characteristics

These features allow us to reduce the volume, the mass and the cost and to increase the performance of the system in comparison with single-phase equivalent systems.

Reliable design of such systems requires a thorough understanding of the two-phase phenomena under microgravity conditions. At this time a complete theoretical scheme for the behavior of two-phase flow is not yet developed. Consequently we use approximate theory or correlations applicable under particular conditions. Moreover most of experiments are KC-135 reduced gravity of very short duration limiting the experimental data and reducing the range of empirical models.

For the purpose of understanding two-phase flow, several quantities must be considered, such as pressure drop, void fraction and heat transfer coefficient.

The pressure drop is the difference in pressure in a conduit. The void fraction indicates how much of a mixture is liquid or vapor. The heat transfer coefficient regulates the heat exchange capability of the two-phase mixture. All analyses and correlations will be functions of the two phase flow phenomenon and of the properties of the fluids (density, viscosity, temperature, etc…). Fundamental information is the flow pattern, or flow regime.

In traditional two-phase flow studies, the flow regime refers to the physical location of the gas and liquid in a conduit. It is essential information since the basic empirical equations that describe the behavior of the fluid are strongly dependent on it. In particular the flow configuration is important for engineering design such as heat and mass transfer and wall shear. However, its identification is somewhat subjective since it is mostly defined by the experimenter's eye, which results in an approximate definition. Hence, most investigations performed on this subject have tried to determine, through experimental and empirical means when each flow regime configuration is likely to occur given the system parameters.

Usually all the parameters (phase velocities, densities, temperatures, viscosities, flow rates) of the system are necessary to make a prediction of which flow pattern will occur. However in the present work a possible way to identify the flow pattern using only the void fraction fluctuation measurement is analyzed. In order to do this the probability density function (PDF) of the

measurement of the void fraction and several other statistical parameters were developed.

In the literature several methods have been developed to measure void fraction in a system including quick-closing valves, neutron scattering, optical probes, gamma-ray and x-ray absorption, hot-film anemometry, and impedance methods using conductance probes, or capacitance probes. In the present work a CREARE Inc. Capacitance Void Fraction probe is used.

1.2 FLOW PATTERN CLASSIFICATION

As just said, the analysis of the flow pattern and its identification is based on visual recognition, and so it's a subjective and not clearly determined categorization. Under microgravity conditions, the general classification that is accepted is three flow patterns: bubbly flow, annular flow and slug flow (also called intermittent flow). Bubbly flow is a Capillary dominated regime with dispersed bubbles in liquid. Annular flow is an inertial dominated regime characterized by a symmetric liquid film surrounding a vapor core. Waves may or may not be present. The annular core may be centered or not depending on residual acceleration. Finally slug flow is a capillary dominated regime characterized by the presence of large Taylor bubbles separated by liquid slugs. Taylor bubbles are produced by the packing and subsequent coalescence of smaller bubbles.

An example and a description of the visual characteristics of these different flows is provided by Fabre [1]. Figure 1.1 shows the general visual identification for different flow patterns.

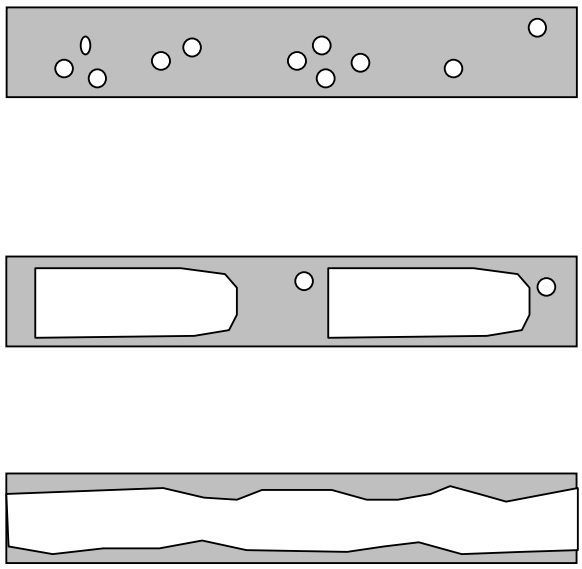

Fig. 1.1. Flow patterns

Because of the complexity of two-phase flow modeling, the flow patterns shown in figure 1.1 could be not well defined and so flow patterns intermediate between the basic three flows patterns are recognized too. In particular lately the flow pattern “transition”, also called “churn flow”, will be analyzed and it consists in an intermediate condition between annular and slug flow.

1.3 LITERATURE REVIEW

The behavior and nature of two-phase flow technology under earth-gravity conditions are widely developed due to the extensive use of this technology in many different applications. This provides us with a large literature base.

This literature review is concerned with three different aspects of the previous studies: analysis of all void fraction measurement probes, analysis of the statistical approaches to the void fraction data, and, finally, analysis of the general theoretical scheme where all these results are applied. While the technology of the probes and the statistical approaches are similar for earth-gravity and micro-gravity conditions, the theoretical fluid basis is different.

Several methods have been developed to measure void fraction in a system including quick-closing valves, optical probes, gamma-ray and x-ray absorption, hot-film anemometry, neutron scattering, electrical resistance tomography and capacitance probes.

In 1962 Govier and Omer [2] used a horizontal pipeline flow of an air-water mixture and quick-closing valves in order to quantify the amount of air and water in a cylinder and to collect the volumetric void fraction in the pipe. This approach is mechanical and the measurement (the amount of water in a column of mixture) doesn't imply any special electronic or digital conversion. Weak points of this method are the imprecision of the measurement and that the measurement can't be continuous.

In 1969 Miller and Mitchie [3] developed a universal probe for measurement of local void in liquid/gas two phase flow systems using optical technology. Advantages of this method are the fast response and the real-time monitoring of the void fraction fluctuations, but the disadvantage is the calibration difficulty due to lost signals.

Gamma-ray and x-ray absorption were considered by Schrock [4] and recently by others [5] as a good technology for the investigation of void fraction. It consists in the analysis of the absorption of x-rays or gamma-rays by the mixture. This approach can give us data in real time and with good precision, but the large and sometimes dangerous instrumentation (radioactive sources or generators) become restrictive.

Delhaye [6] developed in 1969 a technology for the measurement of void fraction using hot film anemometry. The disadvantage of this probe was the interpretation of the output signal.

Electrical Resistance Tomography (ERT) [7-11] consists of reconstructing an image of a body interior from the electrical characteristic measurements made on its surface. In other words, it is measurement of the resistance R (correlated with the electrical conductivity σ and with the form) of an unknown body, in order to ascertain properties of the body, and in particular the shape.

The use of the conductivity of a two-phase mixture to indicate the void fraction averaged over a cross section of the channel has been demonstrated by Petrick and Lee (1965). It consists of a series of electrodes placed all around

(but in contact) with the operating fluid. Measurements of the potential between the electrodes are collected. Knowing the current and the voltage we can calculate the value of the resistance and some physical properties of the fluid like the void fraction.

Several others studies have been focused on the performance of the conductance probe. A basic description of it could be found in Geraets and Borst [12]. Difficulties associated with this technology are the correlation between the conductance and the void fraction and the reconstruction of the input signal.

Jones and Zuber [13] were the first to apply the statistical examination of fluctuations of the void fraction for flow pattern recognition. They used a fast response X-ray void fraction measurement system of air-water in a rectangular channel. They concluded that fundamental information regarding the structure of two-phase flow may be obtained from the analysis of the Probability Density Function of the void fraction. In that study other quantities were analyzed, like the film thickness, the slug residence time fractions and the bubble length.

In 1981 Vince and Lahey [14] used a similar X-ray system to make chordal-average void fraction measurements. Using the Probability Density Function (PDF) and the Power Spectra Density (PSD) they tried to develop an objective flow regime indicator. The first four statistical moments associated with these distributions were studied. They concluded that the moments of the PDF indicated various flow regime transitions. The moments also show some flow regime transition information, but were sensitive to liquid phase velocity.

Annunziato and Girardi [15] presented an experimental work concerning the use of statistical methods to identify upward air-water two-phase flow regimes by pressure drop and local void fraction fluctuation. Tests were made in a vertical Perspex tube 92 mm I.D. for a wide range of gas and liquid flow rates by using optical probes, a pressure transducer and gamma-ray apparatus. In order to quantify the differences of signal fluctuations depending on the flow regime, statistical functions and parameters were identified as having different physical meanings. A complete set of flow pattern identification parameters were chosen in characteristic ranges. Annunziato and Girardi supported their experiment with a detailed mathematical description of the binomial shape of the PDF.

Song et al. [16] in 1994 studied the propagation properties of void fraction waves in vertical upward, air-water flow. Their experiment used a conductance probe. Several statistical parameters were evaluated from the void fraction signal to objectively characterize the developing flow structure and to investigate the wave propagation properties. The statistical signal processing system investigated the PDF, the Signal Noise Ratio (SNR), the power-spectral density function and the autocorrelation function.

Lowe and Rezkallah [17] used a capacitance sensor to measure the two-phase flow void fraction for the purpose of objectively identifying flow regimes. The sensor has been used in conjunction with a two-phase flow loop aboard the NASA Lewis DC-9 microgravity aircraft. They discovered that the examination of

the PDF is a useful way to identify the flow pattern, but they didn't provide any quantifiable statistical parameter to describe it.

A helical wound capacitance sensor was used to obtain void fraction measurement in adiabatic two-phase flow in a small diameter tube by Elbow and Rezkallah [18]. Statistical analysis using the PDF was applied to the temporal void fraction signals. It was found that there was a wider fluctuation in void fraction values for the bubble and slug flow regime. They didn't provide any quantifiable value for the description of the PDF but they provided a large collection of pictures for a visual classification.

The Probe used for the experiment described in the present study is a CREARE Inc. Capacitance, Void Fraction Probe and it's described in Chapter II.

1.4 THESIS GENERAL ORGANIZATION

In the second chapter the experiment and the procedure are described. A general overview of the package and detailed information on the CREARE Capacitance Void Fraction Sensors are presented.

In the third chapter the relevant theory concerning this study is analyzed. Its application to a statistical drift flux and Martinelli analysis is presented.

The results of the experiment are listed in Chapter IV.

In chapter V statistical, drift flux and Martinelli analysis of the experimental data are given. Also differences and analogies with other studies are proposed, including their explanation.

The last chapter proposes conclusions to the entire thesis proposing a unique flow pattern identifier.

CHAPTER II

EXPERIMETAL DESCRIPTION AND PROCEDURE

2.1 INTRODUCTION

A general overview of the experiment is presented in this chapter. The chapter is divided in to three sections. In the first section the experimental package flown aboard the NASA KC-135, the Forster Miller test bed and the Interphase Transport Phenomena (ITP) KC-135 flight equipment are described. The second section describes the general performance of the CREARE Inc. Void Fraction Sensor. The third section describes the flight procedures aboard the NASA KC-135 that were applied during this experiment.

2.2 EXPERIMENTAL PACKAGE

A schematic of the Foster Miller/Texas A&M University ITP Lab two-phase flow test package used in the current thesis is shown in Figure 2.1. Figure 2.2 shows the legend, Figure 2.3 is a void fraction sensor schematic and Table 2.1 is a list of the instruments present in the test bed. Figures 2.4 and 2.5 show pictures of the Forster Miller package.

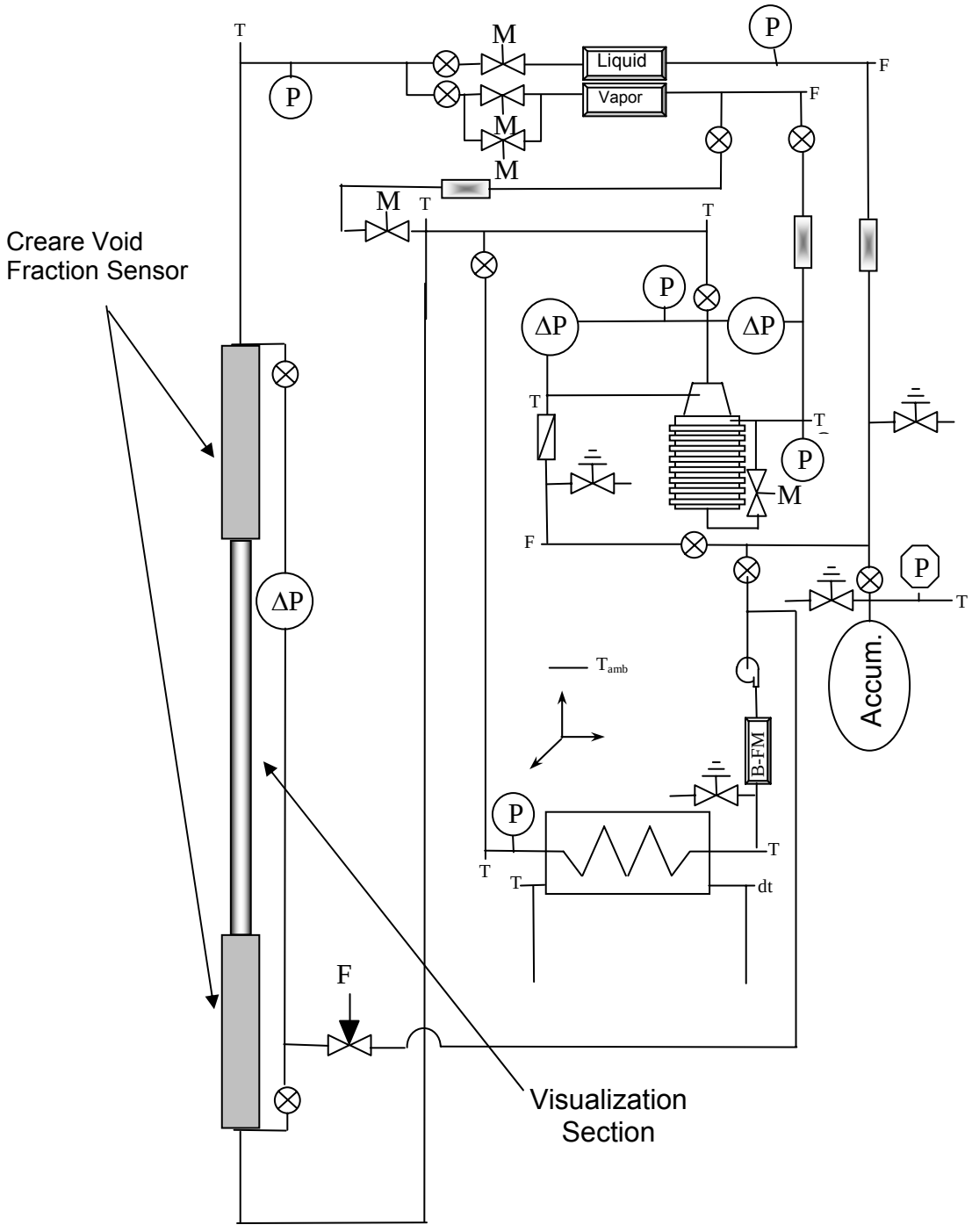

Fig. 2.1. Experiment schematic

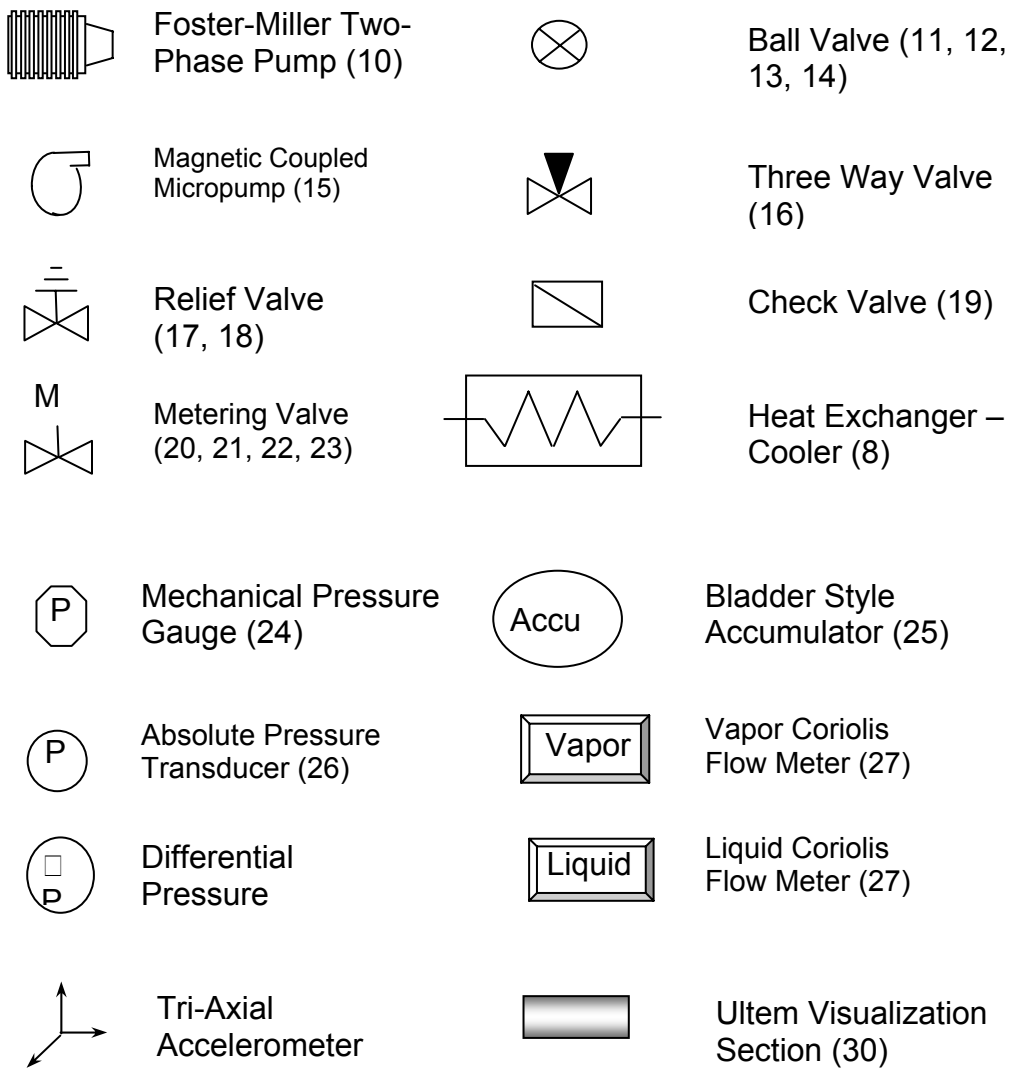

Fig. 2.2. Legend for figure 2.1

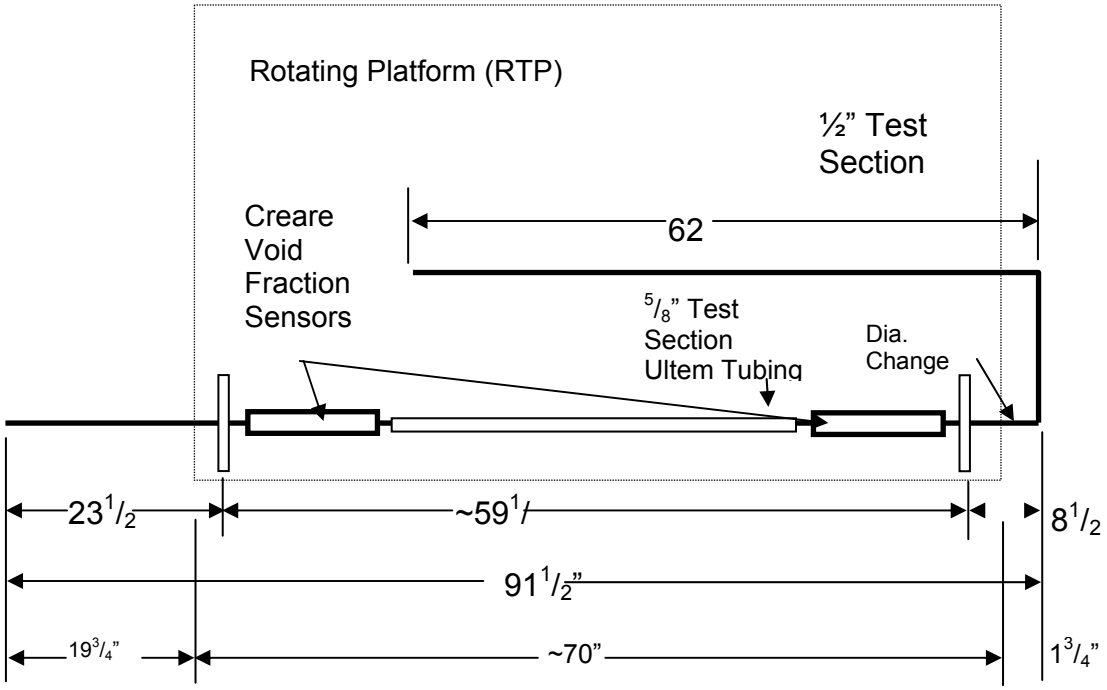

Fig. 2.3. Test section schematic

Table 2.1. Sensor list for the test bed

Sensor #	Sensor Code	Sensor Name	Sensor #	Sensor Code	Sensor Name	Sensor #	Sensor Code	Sensor Name
0	AP1	Pump Vapr Outlet Absolute Pressure	14	TE2	Heat Exchanger R-12 Outlet Temperature	28	GY	Transverse Acceleration
1	AP2	Pump Inlet Absolute Pressure	15	TW1	Heat Exchanger H2O Differential Temperature	29	GZ	Vertical Acceleration
2	AP3	Pump Liquid Outlet Absolute Pressure	16	TWD	Heat Exchanger H2O Differential Temperature	30	VF1-1	Void Fraction Sensor 1 3mm
3	AP4	Heat Exchanger Outlet Absolute Pressure	17	TL1	Pump Liquid Outlet Temperature	31	VF1-2	Void Fraction Sensor 1 6mm
4	AP5	Section 1 Inlet Absolute Pressure	18	TL2	Accumulator Outlet Temperature	32	LD	Micromotion Liquid Density
5	DP1	Pump Vapor Differential Pressure	19	TL3	Micromotion Vapor Temperature	33	VD	Micromotion Vapor Density
6	DP2	Pump Liquid Differential Pressure	20	TV1	Pump Vapor Outlet Temperature	34	VF1-3	Void Fraction Sensor 1 135mm
7	DP3	Section 1 Differential Pressure	21	TV2	Micromotion Vapor Temperature	35	VF2-1	Void Fraction Sensor 2 3mm
8	AP6	Heat Exchanger Inlet Absolute Pressure	22	TA	Ambient Temperature	36	VF2-2	Void Fraction Sensor 2 6mm
9	T1	Section 1 Inlet Temperature	23	ME	Hrat Exchanger R-12 Flowwrate	37	VF2-3	Void Fraction Sensor 2 135mm
10	T2	Section 2 Inlet Temperature	24	MF	Heat Exchanger H2O Flowrate	38	Shear Top	
11	T3	Section 2 Outlet Temperature	25	ML	Micromotion Liquid Mass Flowrate	39	Shear Bottom	
12	T4	Pump Inlet Temperature	26	MV	Micromotion Vapor Mass Flowrate			
13	TE1	Heat Exchanger R-12 Inlet Temperature	27	GX	Axial Acceleration			

Fig. 2.4. Foster Miller package, front view

Fig. 2.5. Foster Miller package, back view

All testing was performed using R-12 dichlorodifluoromethane as the working fluid. It was chosen for its low toxicity, low heat of vaporization, and material compatibility properties and in particular for high vapor density at low pressure. The facility operates at a temperature of about 295 K. The corresponding saturation pressure is about 600 kPa. Table 2.2 summarizes the fluid properties.

Table 2.2. Properties for the working fluid R-12

Property	*Value for R-12*	*Value for Air/Water*	*Ratio*
Liquid density (Kg/m3)	1320	1000	1.3:1
Vapor density (kg/m3)	34	1	34:1
Liquid viscosity (Pa-s)	2.3X10-4	1X10-5	1:4
Vapor viscosity (Pa-s)	1.2X10-5	1.2X10-5	1:1
Surface tension (N/m)	0.01	0.07	1:7

A brief description of the components of the flow loop is now provided.

A Foster-Miller Inc. Two-Phase pump is present. This component works as both a pump and phase separator and the two phases are pumped separately. Sight glasses in the lines were used to visually verify the purity of the phases. Figure 2.6 show the Foster Miller Two Phase Pump.

Fig. 2.6. Foster-Miller two phase pump

Hurlbert [19] and Benner et al. [20] precisely discusses the thermodynamic aspects of the system.

Micro-motion mass flow rate sensors were used to accurately measure the mass flow rate of the liquid and vapor phases. Figure 2.7 show the Coriolis flow meter for gas.

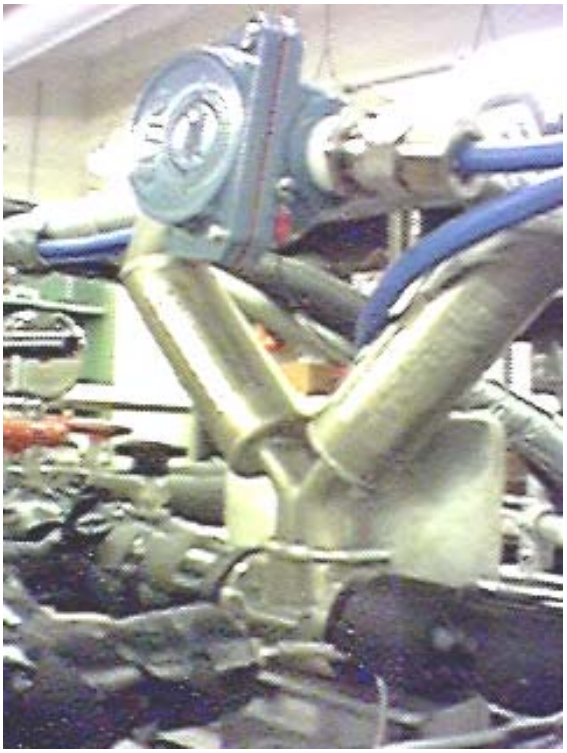

Fig. 2.7. Coriolis flow meter

Pressure drop measurements across the adiabatic test section were taken with a Foxboro Electronic d/p Cell Transmitter and with a Validyne P305D instrument. A description of these devices can be found in Wheeler [21].

For the visual flow regime data, a Kodak Ektapro 1000 Motion Analyzer was used. Data were recorded at a frequency of 500 or 1000 frames per second. The images were used for the visual classification of the flow pattern.

The Data Acquisition System (DAQS) was designed and provided by the Texas A&M ITP Laboratory.

Acceleration measurements were made throughout the flight tests for three directions relative to the test section.

2.3 CAPACITANCE VOID FRACTION SENSORS

The Creare Inc. capacitance void fraction instrumentation described by Crowley et al. [22] is a simple, non-intrusive device to measure void fraction in a pipe. Chang has already described the probe associated with this experiment [23].The instrument uses the electrical capacitance method to measure the void fraction. It consists of three major components, a sensor spool, a printed circuit board, and a remote electronics box. Figure 2.8 is a picture of the capacitance void fraction sensor and the remote electronics box.

The sensor spool includes the end connections and housing compartment for the printed circuit board. The inner diameter is constructed to match the diameter of the system piping. Therefore, the sensor does not interfere with the flow in the system. An array of sensors is placed inside the sensing spool. A Teflon lining is placed over the electrodes to protect the electrodes from the flowing fluids. The housing around the electrodes is constructed to prevent stray capacitance effects. The printed circuit board contains the multiplexer and the housing compartment.

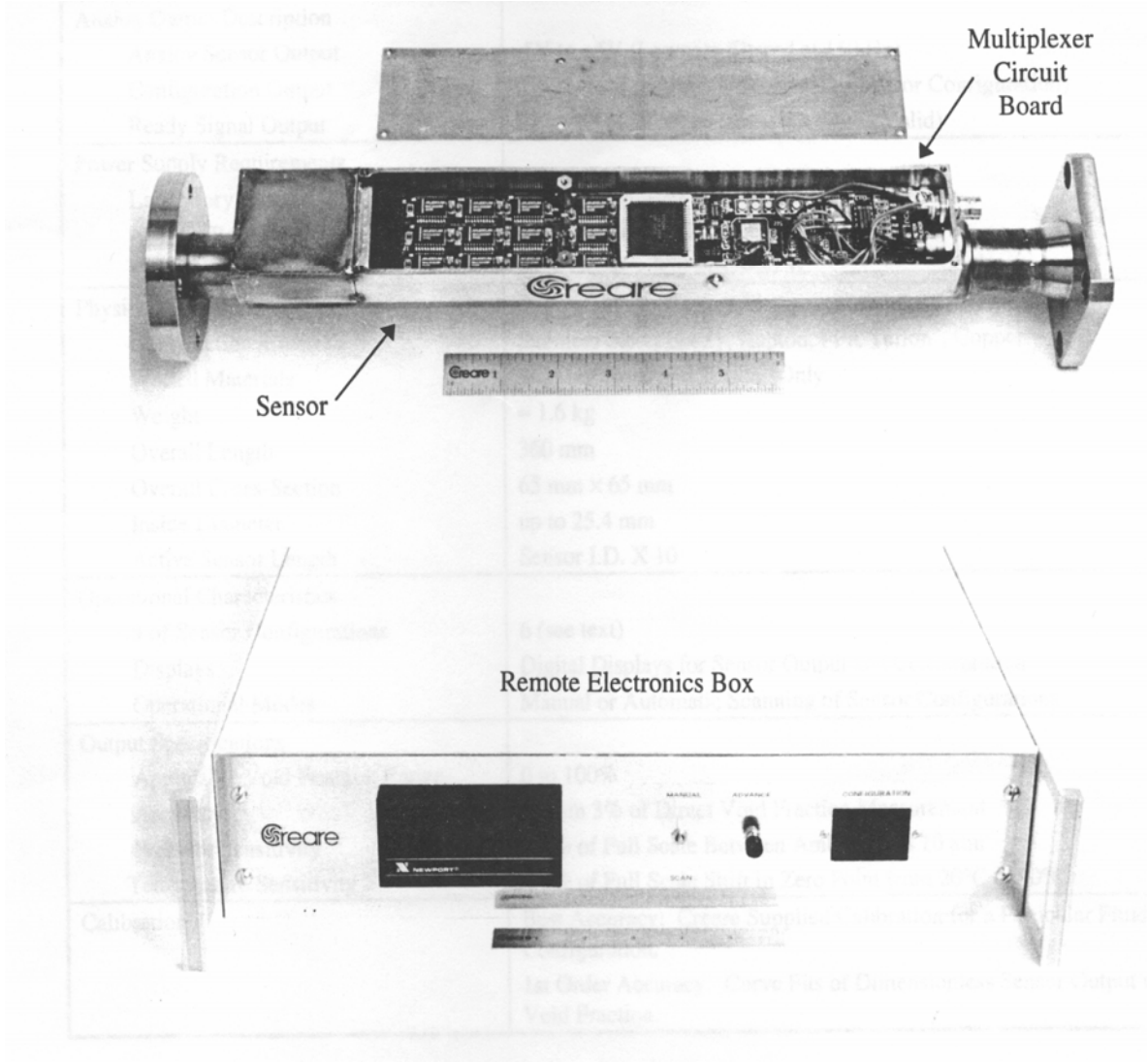

Fig. 2.8. Capacitance void fraction sensor and remote electronic box.

There are two measurement standard arrangements. The electrical configuration of the sensor can be changed by the multiplexer to measure average void fraction in the sensor or measure liquid film thickness at the circumference of the sensor. Figure 2.9 is the electrical configuration of the capacitance sensor used to measure the full volume. Figure 2.10 is the electrical configuration for the thin film measurements. Signal conditioning electronics of the printed circuit board further minimizes the effects of stray capacitance on the output signal.

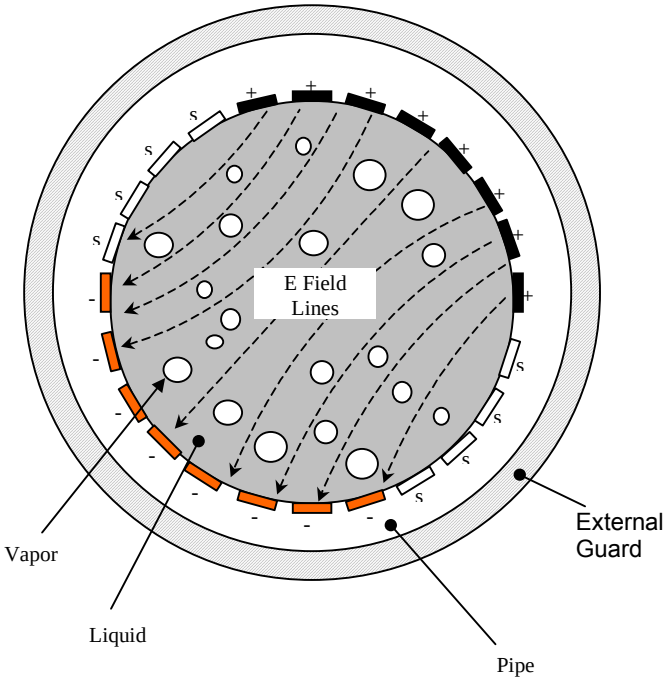

Fig. 2.9. Full volume sensor configuration.

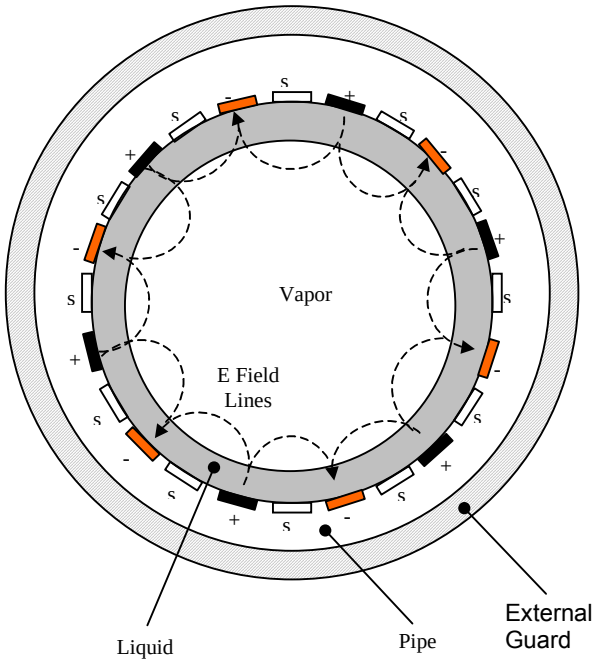

Fig. 2.10. Thin film sensor configuration

Static and dynamic calibration tests performed by Crowley et al. [22] produced equations to determine void fractions. The equation for the void fraction in the full volume configuration is,

$$\alpha = \left[\frac{1 - C^*}{1 + 0.5C^*} \right]^{0.8439} \qquad \text{(Eq. 2.1)}$$

The void fraction in the thin film thickness configuration is,

$$\alpha = 1 + 0.222\ln(1 - 0.9892C^*). \qquad \text{(Eq. 2.2)}$$

Normalized capacitance C* is,

$$C^* = \left[\frac{C_\alpha - C_{\alpha=1}}{C_{\alpha=0} - C_{\alpha=1}} \right], \qquad \text{(Eq. 2.3)}$$

where

C_α = measured capacitance

$C_{\alpha=1}$ = calibrated capacitance for channel filled with vapor

$C_{\alpha=0}$ = calibrated capacitance for channel filled with liquid

Figure 2.11 shows the Void Instrument internals. In each sensor there are three void fraction measurement points: a 3mm ring, a 6.5mm ring and a 135mm volume-average sensor. The behavior of the probes and their performance are analyzed by Crowley and Chen [24]. They concluded that the 9mm and 135mm sensors provide good measurements, while the 19.5mm sensors show some problems of stability and so it can't be used.

For this study only the 3mm sensor was considered because the current analysis is trying to analyze the instantaneous fluctuation of the void fraction, and so a volume-average probe is useful for this purpose.

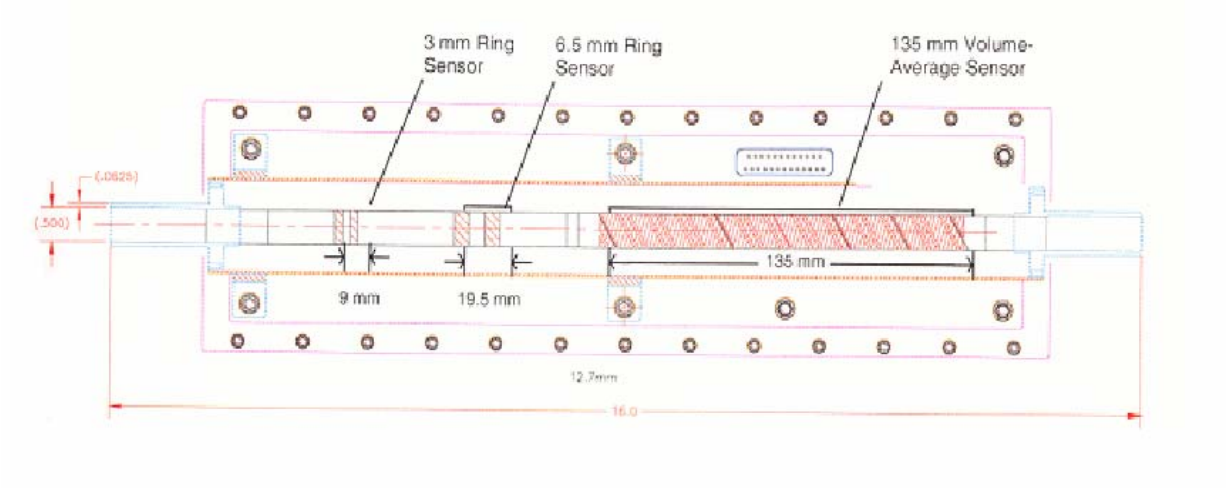

Fig. 2.11. Void fraction sensors in the instruments

The capacitance sensor has an inner diameter of 11.1 mm (0.437 inches). The active sensor length is 111 mm (4.37 inches). The output signal from the remote electronics box is –5V to +5V at 150 Hz. However, the limit on the ITP data acquisition system is about 100 Hz. Therefore, the void fraction sensor output signals were collected at 100 Hz. The power supply to the capacitance sensor is 110 VAC @ 500 mA and 60 Hz.

2.4 FLIGHT PROCEDURE

The experiment was flown aboard the NASA-Johnson Space Center (JSC) KC-135 aircraft stationed at Ellington Field in Houston, Texas. The KC-135 airplane, a modified Boeing 707 also called Weightless Wonder, flies alternating periods of high gravity (~1.8g) and reduced gravity by flying a parabolic path. The aircraft is capable of providing microgravity (~0g), or, a partial gravity environment including Lunar (0.16g) and Martian (0.38g) levels. In the flight sections of this experiment the KC-135 flew only in microgravity mode. A typical mission is 2 to 3 hours long and consists of 30 to 40 parabolas. These parabolas can be flown in succession or with short breaks between maneuvers to reconfigure test equipment. Figure 2.12 is a diagram of the KC-135 flight parabolas.

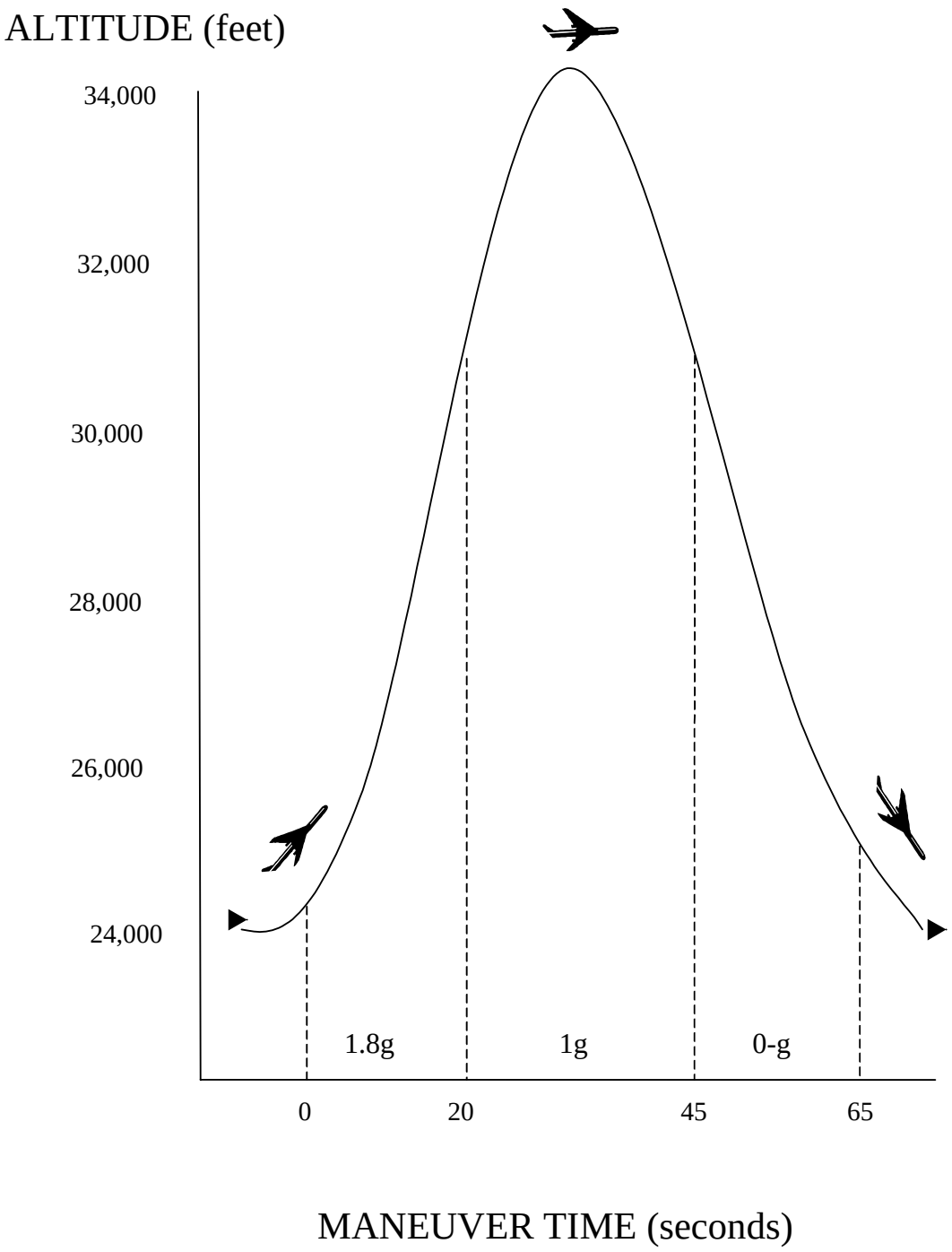

Fig. 2.12. KC-135 Flight parabola trajectory

Marsden and Best [25] analyzed a large number of zero-gravity conditions aboard the airplane and they found a typical duration of 18.6±1.9 seconds followed by a period of 43±6 seconds of high g (~1.8g). The flight schedule consists of about 40 total parabolas per day for four days.

The test environment on the KC-135 is very different than a ground based laboratory and the experiment is taking place in a challenging environment. For example the aircraft acceleration varies in time and direction, the cabin pressure varies through each parabola and cabin temperature varies throughout the flight. For these reasons, it is important to understand instrument responses to the environmental conditions in the KC-135. Therefore, initialization parabolas, where special experimental conditions are set, e.g., no liquid mass flow rate or power to the evaporator, are flown to quantify instrument responses in the aircraft. Two initialization parabola sets were flown during two flights. A particular report of a typical flight procedure in described in Chang's thesis [23].

The operating conditions for the system were set prior to entering the microgravity period. These conditions included the liquid and vapor R-12 mass flow rates, and coolant flow rate. The test system was at steady state. Sensors and data collection system were initiated prior to entering the first microgravity period.

2.5 CHAPTER SUMMARY

In this chapter a general overview of the experiment package was presented. In particular the performance of the CREARE Inc. Void Fraction Sensor and the correlation expression given. Moreover the NASA KC-135 Flight Procedures were given.

CHAPTER III

THEORY

3.1 INTRODUCTION

This chapter describes the statistical analysis developed for the investigation of the void fraction data. The chapter is divided into four sections. In the first section, statistical properties of a measurement are described. In particular the Probability Density Function (*f*) and the Cumulative Probability Function (F) with some of their properties are considered. In the second section a simulation of the statistical approach is provided in order to validate the theoretical approach. The third section describes the basic equation of the Drift Flux Two Phase Flow Theory and its properties. Finally in the fourth section an introduction to the Martinelli Parameter approach to the two-phase flow is given.

3.2 STATISTICAL ANALYSIS

Jones and Zuber [13] and later Annunziato and Girardi [15] and Song et al. [16] provided a theory for the statistical treatment of the measurement of void fraction and for its properties.

The void fraction is considered as a random variable with a range from 0 to 1. If the probability that the void fraction α is less than some specific value is given by P(α), then

$$\frac{dP(\alpha)}{d\alpha} = p(\alpha) \qquad \text{(Eq. 3.1)}$$

Where P(α) is the probability function and p(α) is the probability density function.

Equation 3.1 represents the probability per unit void fraction that the void fraction is between α and α+dα.

Consider now a void-time trace record where the void scale is broken into equal increments of $\Delta\alpha_i$ and the time scale divided into equal increments Δt_j. If during the interval time T the void fraction is seen to be in $\Delta\alpha_i$ a total of n_i times then

$$\frac{n_i/N}{\Delta\alpha_i} = \frac{1}{\Delta\alpha_i}\sum_{j=1}^{n_j}\frac{\Delta t_j}{T} \qquad \text{(Eq. 3.2)}$$

Where N is the total number of void fraction samples.

Since the ratio $\sum \Delta t_i/T$ is the probability that the void fraction is in $\Delta\alpha_i$, then

$$\lim_{\Delta\alpha_i \to 0} \frac{1}{T\Delta\alpha_i} \sum_{j=1}^{n_i} \Delta t_j = f(\alpha) \qquad \text{(Eq. 3.3)}$$

Where f(α) represents the probability density function (PDF) of the void fraction.

Different statistical moments of the distribution [26] [27] have been developed to describe the shape of the PDF. The four moments are the mean or the first moment about the origin, the variance or the second moment about the mean, the skewness or third moment about the mean, and the kurtosis or the fourth moment about the mean. The mean is the average of the distribution. When the distribution is arranged from the lowest to highest, the middle value is defined as the median. Variance is the measure of the distribution about the mean. Skewness is a measure of the asymmetry of a distribution. If the median of the distribution is left of the mean, the skewness is considered to be positive. A positive skewed distribution will have a tail to the left side of the distribution. If the distribution has a negative skewness and a tail on the right side of the distribution, the median of the distribution is right of the mean. For a normal distribution the skewness is zero and the mean and median will be the same. Figure 3.1 provides a visual explanation of the skewness where $\bar{\alpha}$ is the mean of the distribution.

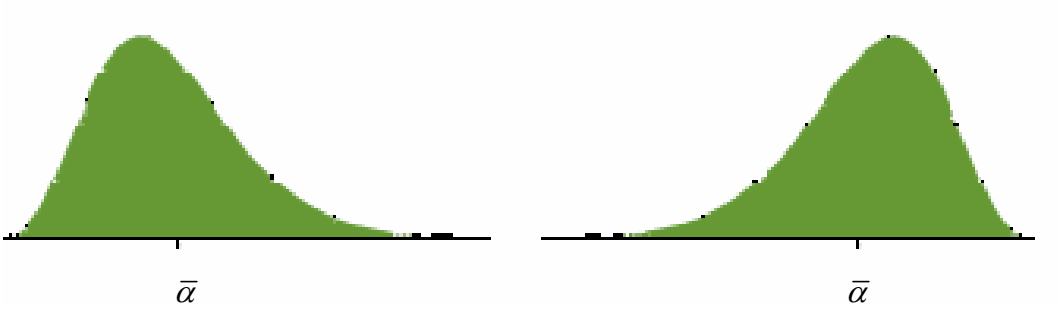

Fig. 3.1. Example of distribution with positive (left) and negative (right) skewness coefficients

Kurtosis measures the peakedness of a distribution. Kurtosis is often compared with the peakedness of a normal distribution, mesokurtic, which has a coefficient of kurtosis of zero. If the distribution is flatter than a normal distribution (platykurtic), then the coefficient of kurtosis is negative. Distributions with more peakedness than normal distributions have positive coefficients of kurtosis and are called leptokurtic, as shown in figure 3.2.

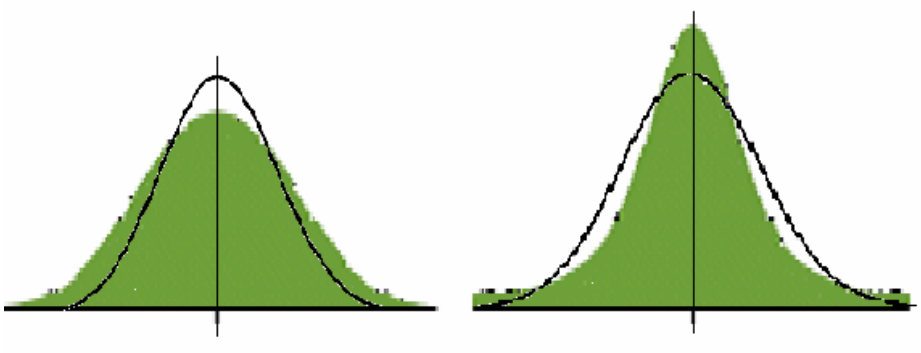

Fig. 3.2. Example of distribution with low (left) and high (right) kurtosis coefficient. The black line is the Gaussian distribution

The formulae for the four discrete moments are listed below [27].

The mean or the sample average is,

$$\bar{X} = \sum_{i=1}^{N} \frac{X_i}{N}. \qquad \text{(Eq. 3.4)}$$

The variance S^2 of the distribution is,

$$S^2 = \sum_{i=1}^{N} \frac{\left(X_i - \bar{X}\right)^2}{N-1}. \qquad \text{(Eq. 3.5)}$$

The coefficient of skewness is defined as,

$$\hat{\gamma}_s = \frac{N\sum_{i=1}^{N} \frac{\left(X_i - \bar{X}\right)^3}{(N-1)(N-2)}}{S^3}. \qquad \text{(Eq. 3.6)}$$

The coefficient of kurtosis is,

$$\hat{\gamma}_k = \frac{\dfrac{\sum_{i=1}^{N}\left(X_i - \bar{X}\right)^4 \left(N^2 - 2N + 3\right)}{(N-1)(N-2)(N-3)} - \dfrac{3\left(S^2\right)^2 (N-1)(2N-3)}{N(N-2)(N-3)}}{S^4} - 3. \qquad \text{(Eq. 3.7)}$$

An additional parameter useful for this investigation is the Signal to Noise Ratio (SNR) defined as

$$SNR = \frac{\sigma^2}{\bar{X}} \qquad \text{(Eq. 3.8)}$$

Where σ is the variance and $\bar{X}$ is the signal mean.

Another useful function is the normalized discrete cumulative density function F(α) defined as

$$F(\alpha) = \frac{\sum_{i=0}^{\alpha} f(\alpha)}{N} \qquad \text{(Eq. 3.9)}$$

The analysis of the shape of the probability density function P(α), consists of the investigation of two parameters: the Half High Value (HHV) and the Linear Area Difference (LAD). The HHV is defined as the value of α when $F(\alpha) = 0.5$:

$$F(HHV) = 0.5 \qquad \text{(Eq. 3.10)}$$

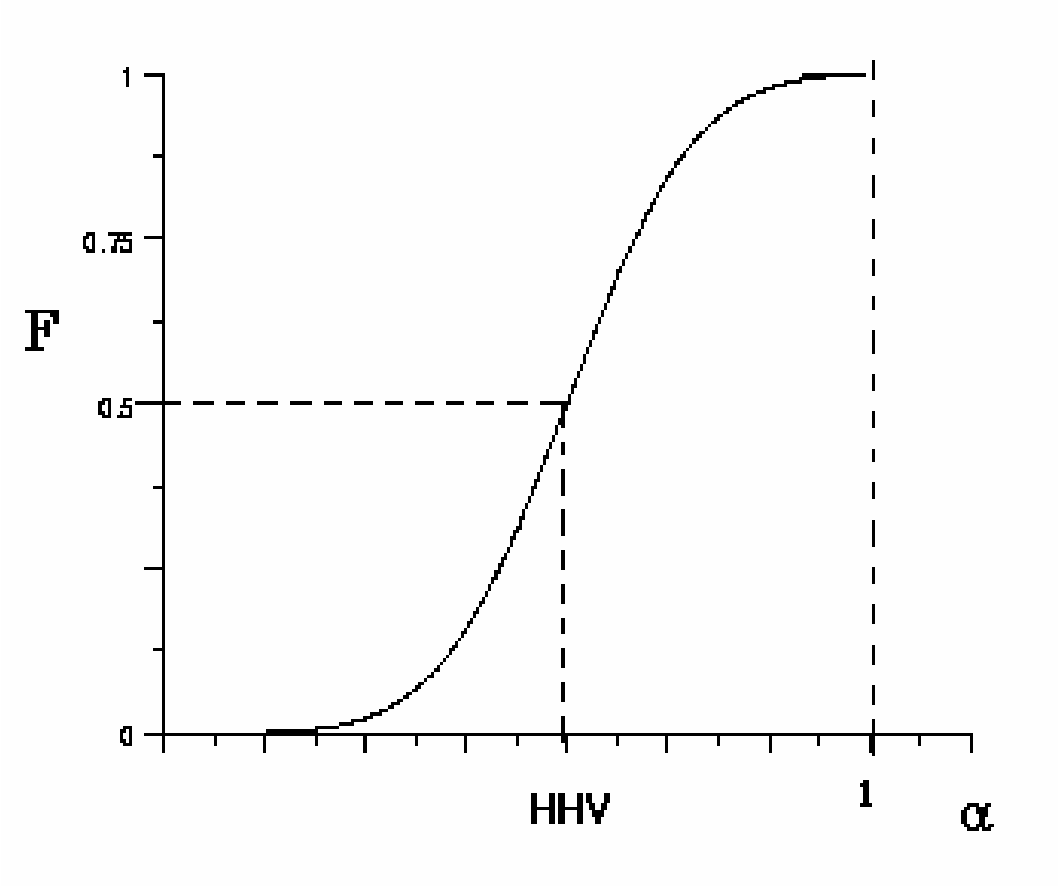

Fig. 3.3. Half high coefficient for a simulated F(x)

Figure 3.3 represents the HHV for a typical Cumulative Function distribution.

The Linear Area Difference (LAD) is the area between the line $F(\alpha)=\alpha$ and $F(\alpha)$. Mathematically the two quantities are both not-dimensional. In formula

$$LAD = \sum_{i=1}^{N} \left(F(\alpha) - \alpha \right) \qquad \text{(Eq. 3.11)}$$

Where $F(x_i)$ is the Cumulative Function at the void fraction alpha. The mathematical meaning is shown in picture 3.4.

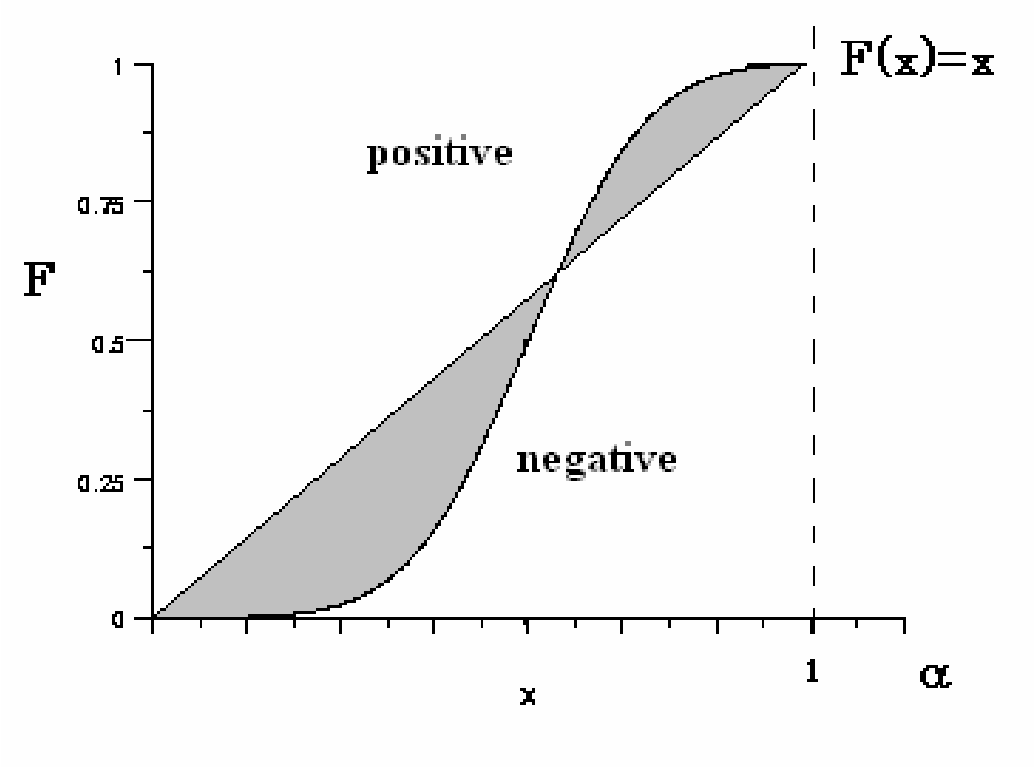

Fig. 3.4. Linear area difference for a simulated F(x)

Both the HHV and LAD are descriptors of the distribution of the void fraction and provide a good measure of two-peakness. Physical meaning and expected results for different flow pattern are presented in the next section.

A brief description of how the parameters should behave for the different flow patterns and why this study considers them useful is presented below.

The variance is reasonably expected to be the same for bubbly and annular flow, while it should assume large values for slug flow because of the intermittent presence of the Taylor bubbles and full fluid regions.

The SNR, because it's defined from the variance, is expected to have the same trend as the variance.

The coefficient of skewness should be positive (right tailed) for bubbly flow and negative (left tailed) for annular flow. In slug flow the PDF has bipolarity and so this coefficient hasn't a useful meaning because it works just for a single-peak function. In fact the values reached in this case could be also similar to the one peak distribution but without any statistical reason and they shouldn't be considered.

The coefficient of kurtosis should be similar for annular and bubbly flow because the peakedness distribution is the same but with a different mean. Again there is no statistical meaning in the case of slug flow because it's a measure of the peakedness of a two peaks distribution and so no useful data are expected.

HHV and LAD are correlated with the double peak of the PDF. HHV should increase from bubbly to annular flow while LAD should decrease. This happens because the slope of the Cumulative density function is greater for high values of void fraction for annular flow and it's small for low void fractions for slug flow.

So for annular flow the intercept for the Cumulative function equals to 0.5 is high (HHV high value) and the area below the straight line y=x is big in absolute value (LAD large in absolute value). While for slug flow the intercept for the Cumulative function equals to 0.5 is smaller (HHV lower value) than annular and the area below the straight line y=x is small (LAD small).

3.3 COMPUTATIONAL SIMULATION

In this section a computer code simulating the capacitance void fraction effects of microgravity two-phase flow is described. It consists of a computational simulation of the flow pattern and of the parameters just described in order to show the capability to identify the flow pattern.

The code generates as output the void fraction from the sensors at 100Hz. As explained in Chapter II, the Data Acquisition System and the CREARE Inc. sensors have the same frequency.

The code was run for three different cases: annular flow, slug flow and bubbly flow. In each case the reconstructions of the signal are based on random processes with particular characteristics for each flow regime. The transient signal and the Probability Density Function are plotted for each case. The statistical moments, HHV and LAD are computed.

3.3.1 Bubbly Flow

The input for bubbly flow was obtained from the output processed signal that Jones and Zuber [13] found. The code emulates their signal and process all the parameters and graphs.

The bubbly flow void fraction trace over time is shown in figure 3.5, the Probability Density Function in figure 3.6 and the Cumulative Probability Function in figure 3.7.

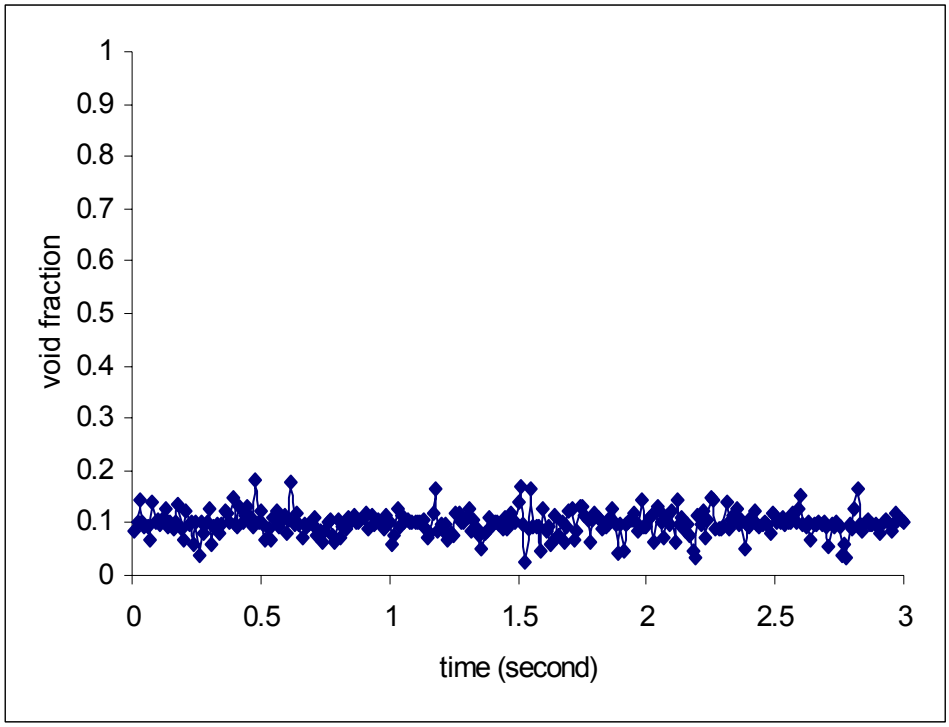

Fig. 3.5. Simulated bubbly flow void fraction trace

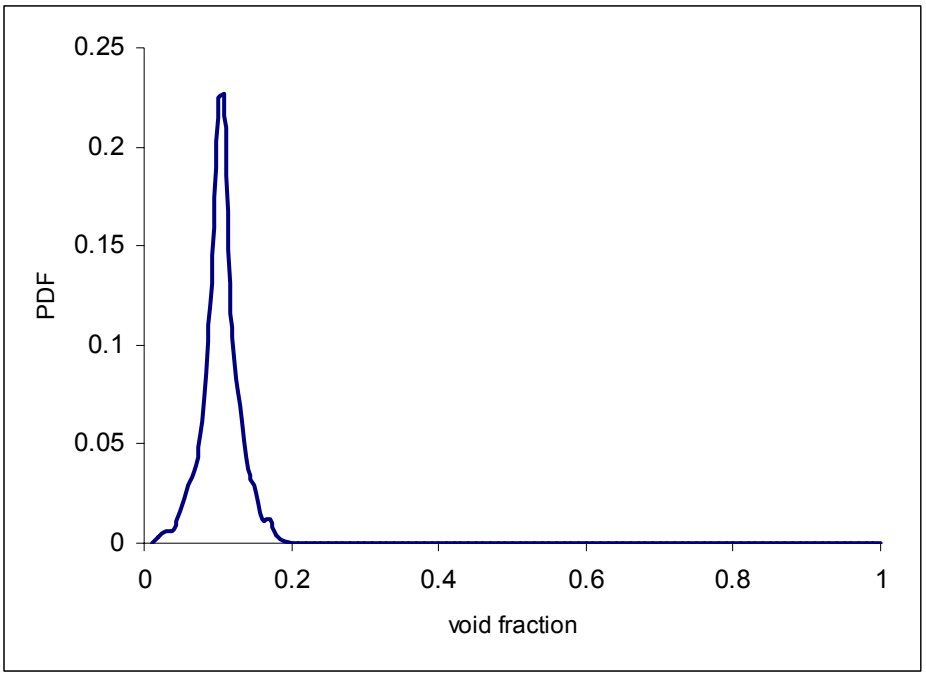

Fig. 3.6. Simulated bubbly flow normalized PDF

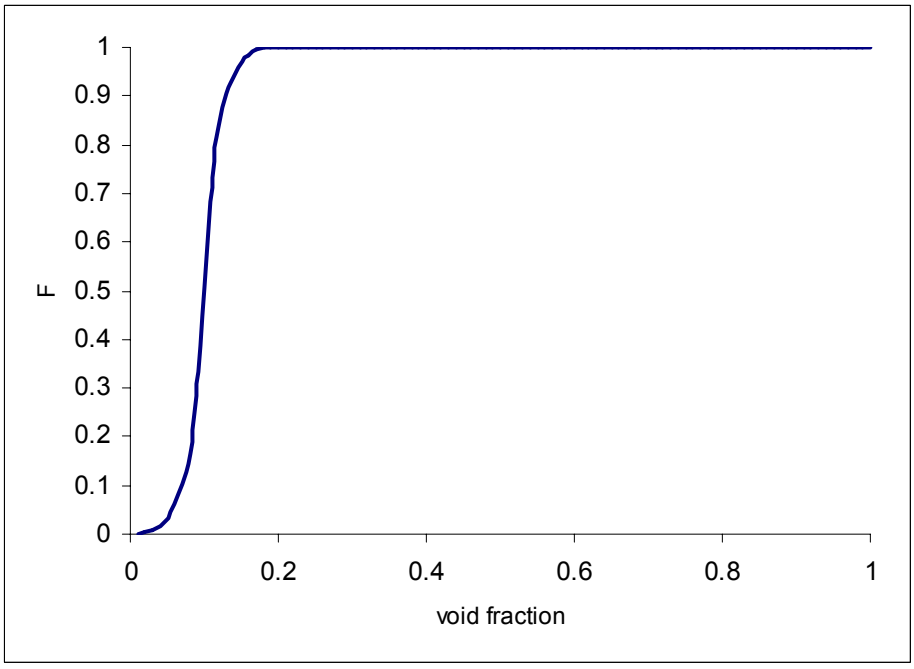

Fig. 3.7. Cumulative probability function for simulated bubbly flow

As expected for bubbly flow the PDF has a peak at low value of the void fraction. The statistical moments and other parameters are listed in Table 3.1.

Table 3.1. Parameters for simulated bubbly flow

Mean	0.0997
Variance	0.0005
Skewness	-0.0161
Kurtosis	1.3549
HHV	0.1260
LAD	40.0346

The mean void fraction (0.0997) of the distribution is slightly less than the median; therefore as definition the coefficient of skewness is negative. As expected the variance (0.0005) is very small since there is very little fluctuation. Vince and Lahey [14] found a smaller variance. The reason why could be that their calculations are experiment-based and not from a simulated code. The HHV and LAD have meaning in comparison with others from the other flow patterns For now one can notice a low value of HHV and a positive value of LAD, as expected.

3.3.2 Annular Flow

The input for annular flow was obtained from the output signal that Jones and Zuber [13] found. The code emulates their signal and process all the parameters and graphs.

The annular flow void fraction trace over time, the Probability Density Function, and the Cumulative Probability Function are shown in Fig.3.8-3.9-3.10.

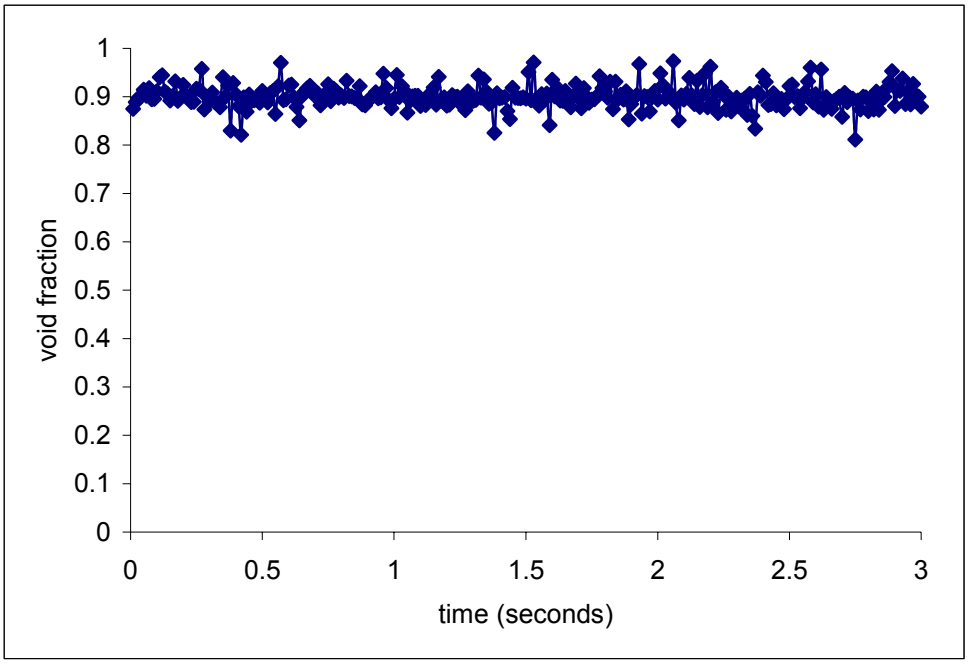

Fig. 3.8. Simulated annular flow void fraction trace

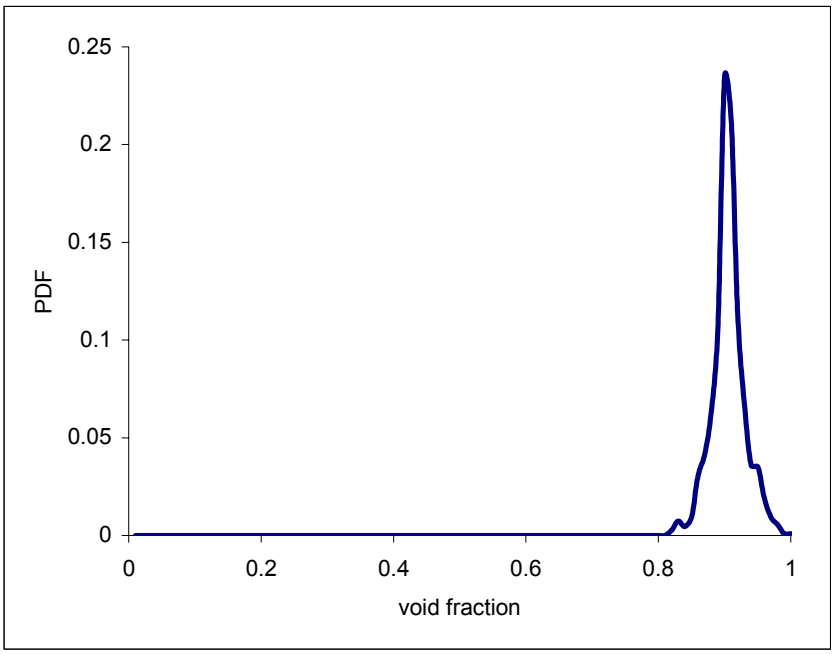

Fig. 3.9. Simulated annular flow normalized PDF

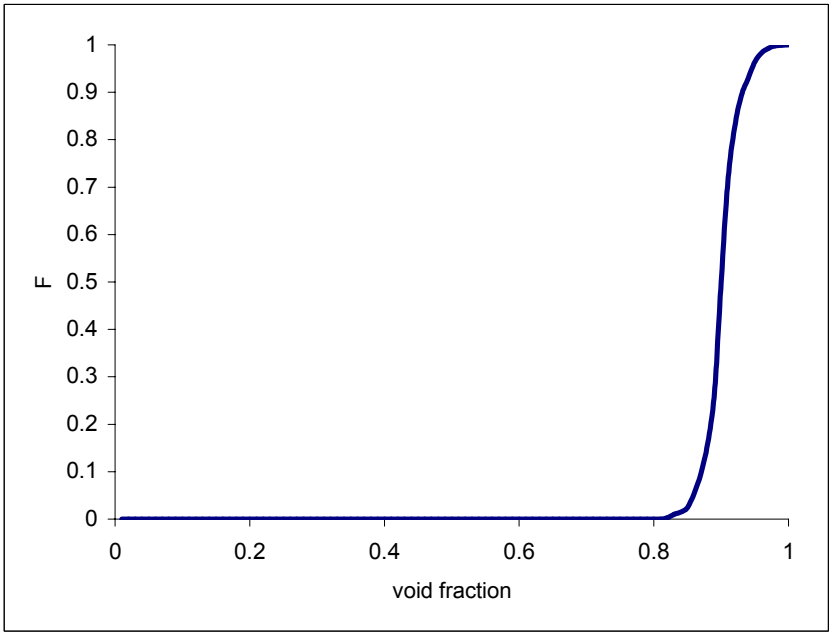

Fig. 3.10. Cumulative probability function for simulated annular flow

With only the difference of the mean, these plots have similar shapes to the bubbly ones. In fact the distribution of the PDF is similar.

The statistical moments and other parameters are listed in Table 3.2.

Table 3.2. Parameters for simulated annular flow

Mean	0.9005
Variance	0.0005
Skewness	0.2120
Kurtosis	1.5469
HHV	0.9000
LAD	-40.0772

The mean (0.9005) is high and the value of the variance is reasonably close to the variance in the bubbly flow pattern. The HHV is high and the LAD strongly negative as expected.

3.3.3 Slug Flow

The input for slug flow was obtained from the combination output signal that Jones and Zuber [13] produced for bubbly and annular flow. As shown in Chapter IV slug flow physically is not a combination of annular and bubbly flow,

but for the purpose of this chapter (observe the behavior of all the parameters) we can assume that to be the case and have input file combinations of bubbly and annular shows.

The slug flow void fraction trace over time is shown in figure 3.11, the Probability Density Function in figure 3.12 and the Cumulative Probability Function in figure 3.13.

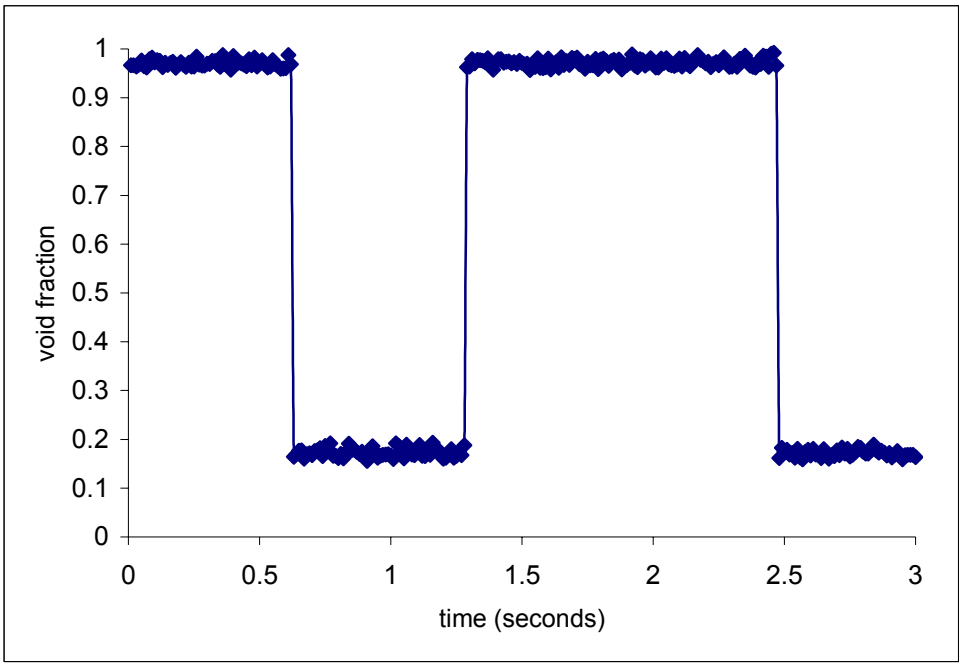

Fig. 3.11. Simulated slug flow void fraction trace

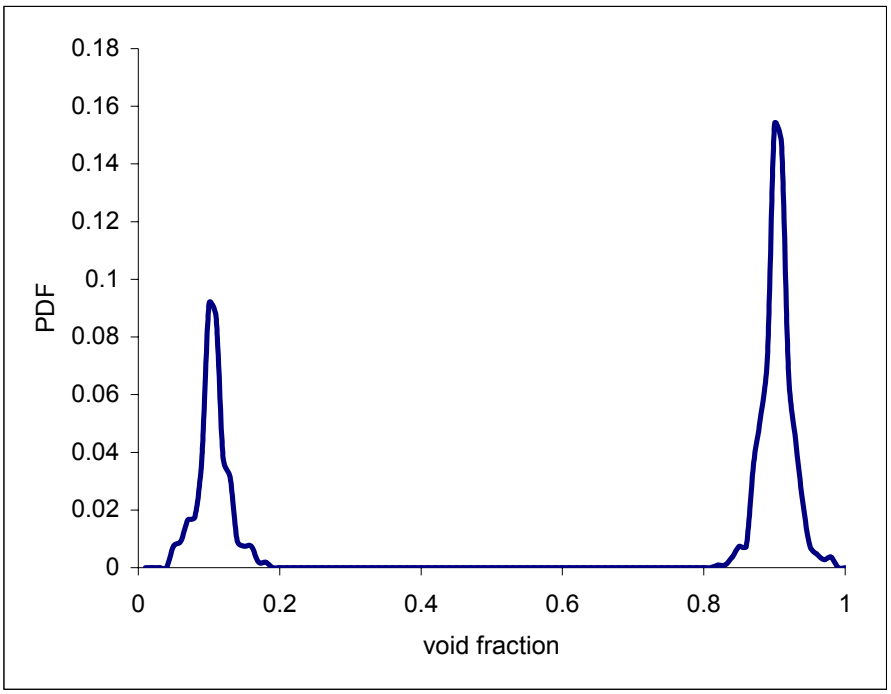

Fig. 3.12. Simulated slug flow normalized PDF

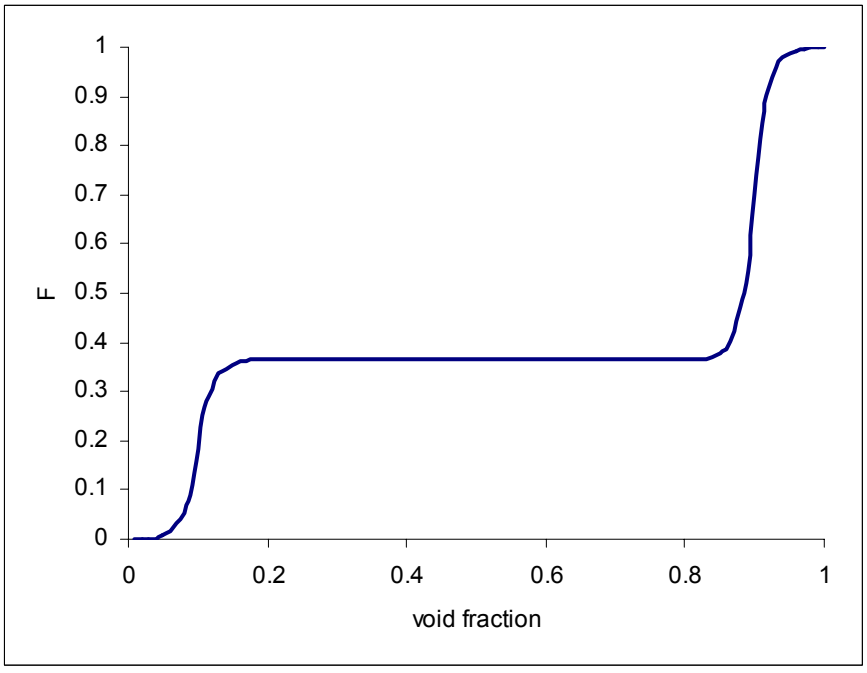

Fig. 3.13. Cumulative probability function for simulated slug flow

As expected the simulated slug flow normalized PDF has a bimodal distribution.

The statistical moments and other parameters are listed in Table 3.3.

Table 3.3. Parameters for simulated slug flow

Mean	0.6076
Variance	0.1495
Skewness	-0.5566
Kurtosis	-1.6791
HHV	0.8500
LAD	-10.7099

The mean of the void fraction is higher than bubbly flow. As expected the variance is the highest due to the largest variation of the void fraction. The kurtosis coefficient is negative due to the low peakness of the distribution.

Due to the bimodal distribution of the PDF the moments don't provide a good identification parameter of the kind of distribution of the PDF. Further descriptors are needed, as Annunziato and Girardi [15] observed. That's why the HHV and LAD are developed in this study.

Table 3.4 summarizes all the parameters from the analysis of the simulated flow regimes.

Table 3.4. Review of parameters from the simulated flows

	BUBBLY	SLUG	ANNULAR
Mean	0.0998	0.6076	0.9005
Variance	0.0006	0.1496	0.0005
Skewness	-0.0161	-0.5566	0.2120
Kurtosis	1.3549	-1.6792	1.5469
HHV	0.1000	0.8500	0.9000
LAD	40.0347	-10.7100	-40.0772

HHV and LAD have a strong dependence on the flow pattern. HHV increases from bubbly to annular flow. LAD decreases strongly. So, theoretically, we can consider these two parameters as good flow pattern identifiers.

3.4 DRIFT FLUX ANALYSIS

The drift flux model is essentially a separated-flow model in which attention is focused on the relative motion rather than on the motion of the individual phases. The approach is general and could be applied to all regimes in all the gravity conditions, even if at the time no attempts have been made to approach

the zero gravity fluid flow. This model is general and has been developed principally by Zuber and Findley [28] and Wallis [29] together with their co-workers.

The basic equations are presented here.

The local vapor velocity u_v can be expressed as

$$u_v = j + u_{vj} \qquad \text{(Eq. 3.12)}$$

Where u_{vj} is the local drift velocity of the vapor and j is the two-phase local volumetric velocity defined by equation 3.13:

$$j = \frac{\dot{Q}_{total}}{A_{total}} \qquad \text{(Eq.3.13)}$$

Where Q is the volumetric flow rate and A is the area of the duct.

Using the definition of the vapor superficial velocity we reach equation 3.13:

$$j_v = \alpha j + \alpha(u_v - j) \qquad \text{(Eq. 3.13)}$$

Rearranging and integrating all over the flow area:

$$< j_v >=< \alpha j > + < \alpha(u_v - j) > \qquad \text{(Eq. 3.14)}$$

Where clearly the second term on the right hand is the rate at which vapor passes through a unit area that's already traveling with the flow at velocity j.

Now, defining the distribution parameter C_0 as

$$C_0 = \frac{<\alpha j>}{<\alpha><j>} \qquad \text{(Eq. 3.15)}$$

and the drift velocity V_{vj} as

$$V_{vj} = \frac{<\alpha(u_v - j)>}{<\alpha>}. \qquad \text{(Eq. 3.16)}$$

These two parameter have been chosen in order to simplify eq. 3.14 in eq. 3.17.

$$<j_v> = C_0 <\alpha><j> + <\alpha> V_{vj} \qquad \text{(Eq 3.17)}$$

A good visualization of equation 3.17 is the plot j_v/α vs. j. In this graph the data should form a straight line with slope C_0 and intercept V_{vj}. Figure 3.14 is the actual plot-space that Zuber and Findlay [28] proposed in their study.

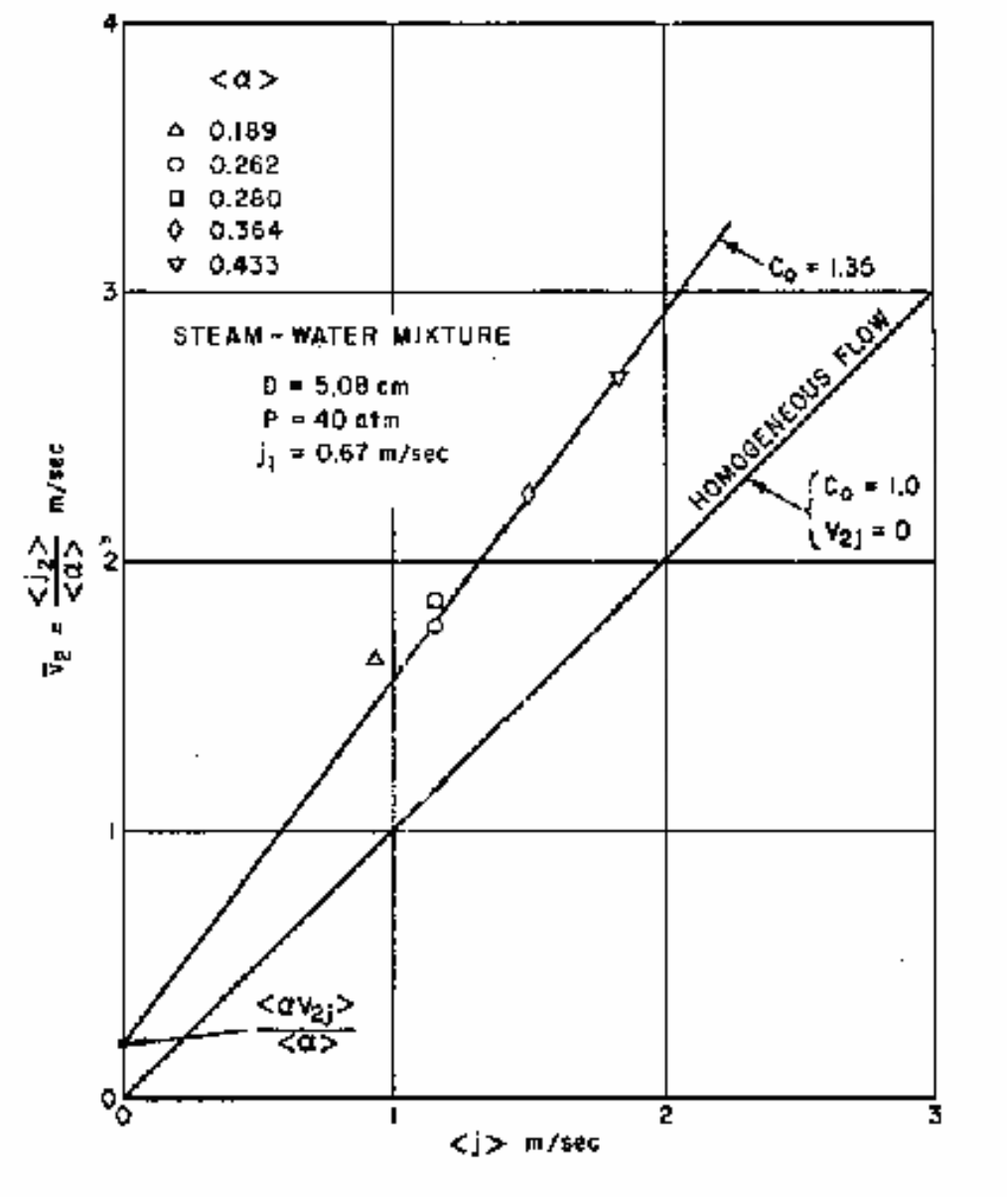

Fig. 3.14. Findlay and Zuber space

Eq 3.17 is the basic equation of the Drift Flux model.

Equation 3.18 defines the volumetric quality β as the ratio between the gas volumetric flow rate Q_g and the total volumetric flow rate Q_f+Q_g.

$$\beta = \frac{Q_g}{Q_g + Q_f} \qquad \text{(Eq.3.18)}$$

So using equation 3.18 and equation 3.17 Equation 3.19 is another expression as function of the volumetric quality β.

$$\frac{<\alpha>}{<\beta>} = \frac{1}{C_0 + \frac{V_{vj}}{<j>}} \qquad \text{(Eq.3.19)}$$

It's now important to go through the specific physical meaning of these quantities.

The drift flux, V_{vj}, physically represents the volumetric rate at which vapour is passing forwards through unit area of a plane normal to the channel axis already traveling with the flow at a velocity j.

The distribution parameter, C_0, physically is the term of the global effect due to radial non-uniform void and velocity profiles. In other words C_0 represents an empirical factor correcting the one-dimension homogeneous theory to account for the fact that the concentration and velocity profiles across the channel can vary independently of one another.

These parameters are very important for the flow pattern description and so a deeper analysis is required

Zuber and Findlay [28] investigated the effect of radially non-uniform flow and concentration distribution on the value of the coefficient C_0. For simplicity they assumed that the flow and the concentration distributions were given by

$$\frac{j}{j_c} = 1 - \left(\frac{r}{R}\right)^m \qquad \text{(Eq. 3.20)}$$

and by

$$\frac{\alpha - \alpha_w}{\alpha_c - \alpha_w} = 1 - \left(\frac{r}{R}\right)^n \qquad \text{(Eq. 3.21)}$$

where the subscript *c* and *w* are for the values evaluated at the center line and at the wall of the circular duct. m and n are two value to be determined experimentally.

Inserting equations 3.20 and 3.21 in equation 3.17 two different expression of C_0 can be obtained: one as function of α_w and the other as function of α_c:

$$C_0 = 1 + \frac{2}{m+n+2}\left[1 - \frac{\alpha_w}{<\alpha>}\right] \qquad \text{(Eq. 3.22)}$$

$$C_0 = \frac{m+2}{m+n+2}\left[1+\frac{\alpha_c}{<\alpha>}\frac{n}{m+2}\right] \qquad \text{(Eq. 3.23)}$$

First, we can note that, if the concentration is uniform across the duct,

$$\alpha_w = \alpha_c = <\alpha> \qquad \text{(Eq. 3.24)}$$

then it follows from equations 3.22 and 3.23 that C_0=1 (homogeneous conditions).

If the concentration at the center line is larger than at the wall (annular conditions), i.e., if

$$\alpha_c > \alpha_w \qquad \text{(Eq. 3.25)}$$

then it follows that C_0>1,

Finally if the concentration at the centerline is smaller than that at the wall, i.e., if

$$\alpha_c < \alpha_w \qquad \text{(Eq. 3.26)}$$

then Co<1.

The values for the distribution parameter C_0 as function of the exponents of the flow and concentration profile curves for axisymmetric vertical up flow through circular ducts proposed by Zuber and Findlay [28] are shown in figure 3.15.

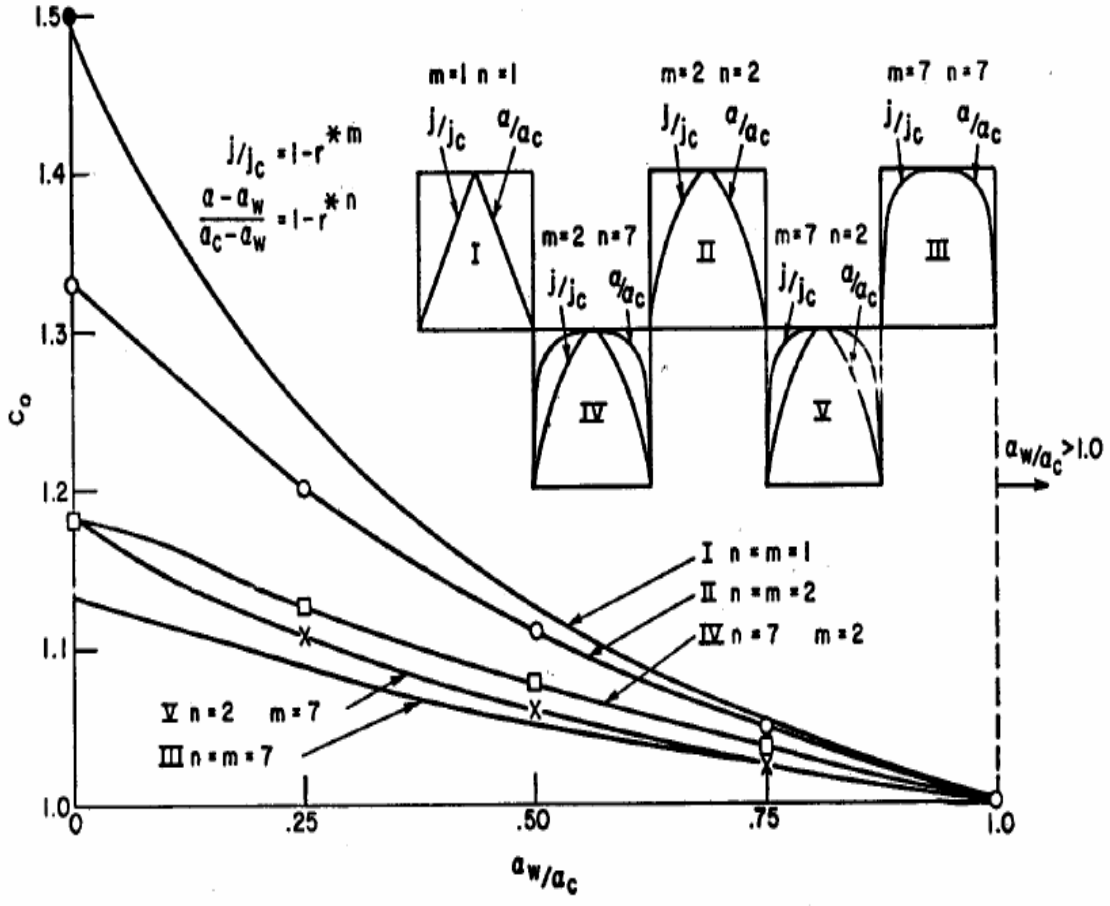

Fig. 3.15. Values for the distribution parameter

Figure 3.15 shows the values of C_0 as a function of the ratio of the void fraction at the wall and at the centerline. The lines represent the theoretical

value of C_0 following the five different void distributions in the duct (Eq. 3.22, 3.23).

From figure 3.15 it can be seen that, with $\alpha_c >> \alpha_w$ then C_0 attains a constant value which depends only on the type of the flow and of the concentration profiles. For pronounced parabolic profiles (curve I in figure 3.15), the distribution parameter attains a value of C_0=1.5, whereas for flat profiles, it tends to reach a value of unity.

These considerations lead to four conclusions:

1- The value of the distribution parameter C_0 depends on the velocity and concentration profiles.

2- For fully established profiles, in axisymmetric two-phase flow, this value may range from about C_0=1.5 to C_0=1.0 when $\alpha_c > \alpha_w$

3- For fully established profiles when $\alpha_c < \alpha_w$, the distribution parameter has a value smaller than unity, i.e., C_0<1.

4- For fully established and uniform concentration, C_0=0.

Consequently Zuber suggested that C_0 and V_{vj} are functions of the flow regime; C_0=1.2 for bubbly and slug flow, and C_0=0 for near zero void fraction and 1.0 for high void fraction.

Zuber and Findlay approximated the drift velocity (V_{vj}) for bubbly and slug flow regimes as:

$$V_{vj} = V_{\infty}\left(1- < \alpha >\right)^{n}; 0 < n < 3 \qquad \text{(Eq. 3.27)}$$

where V_{∞} is the bubble rise terminal velocity in the liquid. Others extended the drift velocity analysis to annular flow. However, in annular flow there is little difference between the vapor volumetric flow rate and the total volumetric flow rate, and V_{vj}, is insignificant.

It's important to notice that while the basic equation 3.17 is analytically achieved and valid for every flow pattern and gravity condition, the Zuber and Findlay analysis of distribution parameter and drift velocity was analyzed for earth-gravity conditions. Nevertheless the theoretical model could be applied also in zero gravity. Moreover the analysis of C_0 and V_{vj} for slug flow doesn't have any meaning if approached with the velocity distribution model of equations 3.20 and 3.21. In fact the alternation of slugs and full liquid doesn't allow a constant velocity and concentration shape as the study of Findlay and Zuber [28] requires.

3.5 MARTINELLI ANALYSIS

From the conservation of the linear momentum for a two-phase one-dimensional flow system an expression for the total pressure drop can be written. It states that the overall pressure drop $\left(\frac{dp}{dz}\right)$ is due to friction pressure drop $\left(\frac{dp}{dz}F\right)$, acceleration pressure drop $\left(\frac{dp}{dz}a\right)$ and body force pressure drop $\left(\frac{dp}{dz}z\right)$ as shown in equation 3.28.

$$\left(\frac{dp}{dz}\right)=\left(\frac{dp}{dz}F\right)+\left(\frac{dp}{dz}a\right)+\left(\frac{dp}{dz}z\right) \qquad \text{(Eq. 3.28)}$$

In the current study the microgravity conditions allow us to ignore the body term. Further, the spatial acceleration term is zero because the system is adiabatic. Analyzing the frictional pressure drop it's assumed by Martinelli and Lockhart [30] that it's equal to the pressure drop for one-phase flow multiplied by a correction term Φ_{fo} called the two-phase flow frictional multiplier. The relationship is shown in equation 3.29.

$$-\left(\frac{dp}{dz}F\right)=-\left(\frac{dp}{dz}F\right)_{fo}\bullet\Phi_{fo}^{\ 2} \qquad \text{(Eq. 3.29)}$$

Thus the two-phase multiplier consists of friction pressure drop correction term from one phase flow to two-phase flow.

Assuming that the friction factor may be expressed in terms of the Reynolds number by the Blasius equation it can be shown that equation 3.28 implies that the two-phase flow multiplier Φ_{fo} can be also expressed as in equation 3.30. A broad theoretical approach to these considerations is in Collier [31].

$$\Phi_{fo}{}^{2} = \left[1 + x\left(\frac{\nu_{fg}}{\nu_{f}}\right)\right] \bullet \left[1 + x\left(\frac{\mu_{fg}}{\mu_{g}}\right)\right]^{0.25} \qquad \text{(Eq. 3.30)}$$

Where x is the flow quality, ν is the specific volume and μ is the viscosity.

Verifying this using data, Martinelli and his co-workers [30] argued that the two-phase multiplier could be correlated uniquely as a function of a parameter X called the Martinelli parameter:

$$X^{2} = \frac{\left(\frac{dp}{dz}F\right)_{f}}{\left(\frac{dp}{dz}F\right)_{g}} \qquad \text{(Eq. 3.31)}$$

Where $\left(\frac{dp}{dz}F\right)_{f}$ is the frictional pressure drop of the liquid and $\left(\frac{dp}{dz}F\right)_{g}$ is the frictional pressure drop of the gas phase. In other words X is equal to the

square root of the ratio of the frictional pressure drop in the pipe if the liquid flowed alone to the frictional pressure drop if the gas flowed alone.

The parameter X^2 can be derived also from the properties of the fluid as:

$$X^2 = \left(\frac{1-x}{x}\right)^{1.75} \left(\frac{\mu_f}{\mu_g}\right)^{0.25} \left(\frac{\rho_f}{\rho_g}\right)^{0.25} \qquad \text{(Eq. 3.32)}$$

Where x is the flow quality, ρ is the density and μ is the viscosity.

Martinelli [30] postulated, subject to experimental verification, that the void fraction is dependent on X. Martinelli assumed also that the correlation between α and X is independent of the flow regime. On the contrary, in the current study it's shown that the Martinelli parameter describes something about the flow pattern because it is dependent on the flow regime. This fact could be understood considering that the Martinelli parameter is dependent on the properties of the two phases and the flow quality, like the flow pattern should also be. Anyway at this time it's not yet theoretically clear why X has some relationship with the void fraction and the flow pattern.

Figure 3.16 shows the dependence of the void fraction and of the two-phase multipliers for different flow conditions as a function of the Martinelli parameter [30].

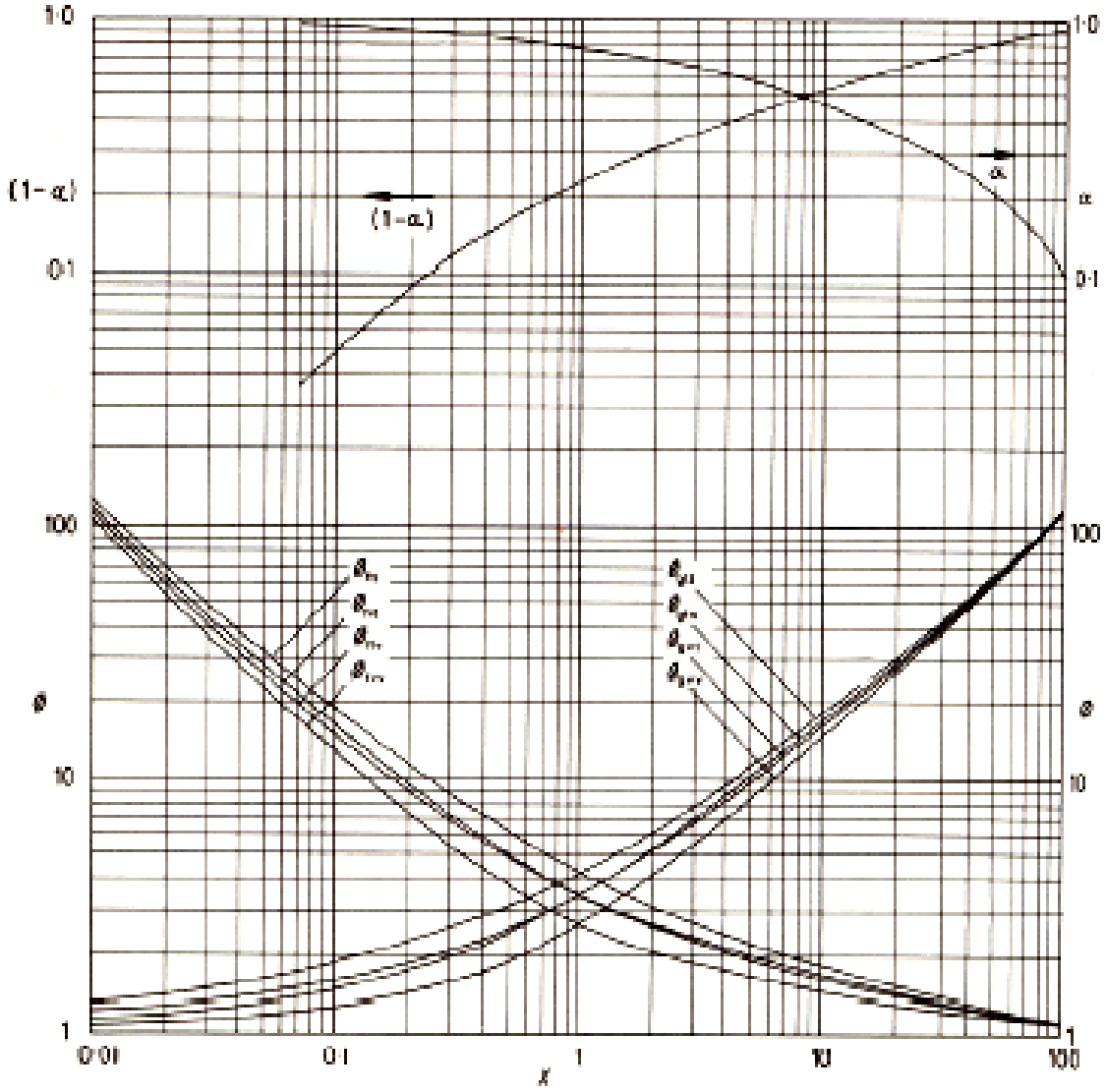

Fig. 3.16. Lockhart-Martinelli correlation

An analytical expression of the relationship between the void fraction and the Martinelli parameter (figure 3.16) is given by Lockhart and Martinelli [30] for isothermal two-phase flow in pipes. They proposed equation

$$\alpha = \left[1 + \left(\frac{1}{X}\right)^{-1.45}\right]^{-0.8} \qquad \text{(Eq. 3.33)}$$

Wang [32] with the same purpose proposed equation 3.33.

$$\alpha = \left[1 + \left(\frac{1}{X}\right)^{-0.8}\right]^{-0.378} \qquad \text{(Eq. 3.34)}$$

Both these correlations agreed with their experimental data.

In the Martinelli study one of the first postulates is that the static pressure drop for the liquid phase must equal the static pressure drop for the gaseous phase regardless of the flow pattern, as long as an appreciable radial static pressure difference does not exists. In the current study X is considered a general independent parameter and so slug flow is correlated with that parameter.

Butterworth [33] considered several correlations which have been proposed for predicting void fraction in co-current gas-liquid flows. He stresses that this approaches neglects the possible effects of the following factors:

- Flow Regime
- Gravity condition of the channel

- Rate of change of quality with length due to evaporation or condensation.

In particular the first two factors are crucial for this study and they will be verified with new data from the current experiment. The third factor is not applicable because the experiment is adiabatic.

3.6 CHAPTER SUMMARY

In the first part of this chapter a presentation of the statistical approach used in this study was given. In particular the analysis of the void fraction data, the PDF, the Cumulative Probability Function and a set of parameters for an analytical description were provided. A code was written and tested in order to evaluate the approach. It was shown that the set of parameters gives useful information from sets of simulated data. The presentation of two different theoretical approaches to two-phase flow modeling was shown: the Lockhart-Martinelli Parameter and the Drift Flux.

CHAPTER IV

RESULTS

4.1 INTRODUCTION

Two-phase flow data for zero-g conditions were obtained in the current research program, and these data support the modeling presented here. In this chapter a description of the codes used for the processing of the raw data and for the zero-g characterization period is presented. In addition an overview of the test matrix development for the January and February 2001 flight for the Foster Miller two-phase flow flight series is provided. In particular the gravity profile, the visual identification with the digital camera, and the validation of the sensors are analyzed.

4.2 DATA ACQUISITION CODE

In this study two codes were developed for the processing of data.

The first consists of the data processing from the instrument voltage raw data to the void fraction data. The Data Acquisition System described in chapter II provides as output a file which recorded all the following values for all the flight period: time, pressure drop, temperatures, flow rates, density, acceleration in the

three dimensions, and void fractions for all the sensors. In every parabola, a flow pattern determined visually is given. The code collects all this data for every flow pattern and converts it from voltage or current to dimensional values.

Figure 4.1 is a graph of the algorithm governing the code.

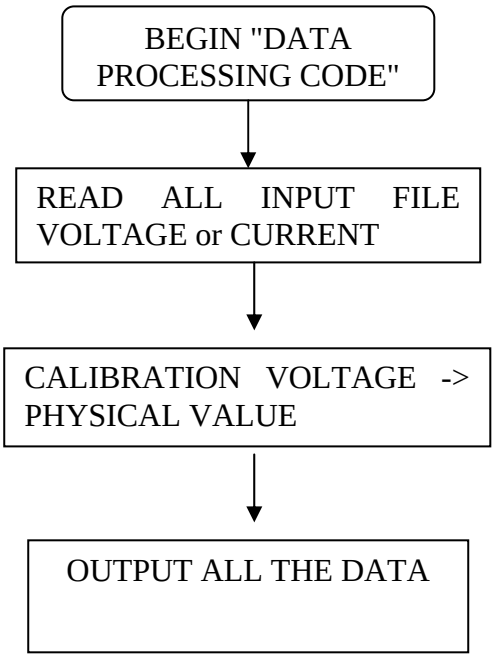

Fig. 4.1. Algorithm of the first code

The second code selects the zero-g period in every parabola. This part of the analysis of the results is very important because an error in this section could results in an incorrect identification of the zero-g period. In particular for the

current study the zero-g period begins when for *n* seconds $\frac{g_z}{9.8}$ is less than a *limit value* plus a *gap*. The time *gap* is necessary to allow the fluid to be completely developed. For the current study the values for the parameters are shown in table 4.1

Table 4.1. Proposed parameters for the zero gravity selector code

Quantity	**Value**
n (seconds)	2
Limit	0.05
Gap (seconds)	5

It can be seen that the zero-g period starts 5 seconds after the moment that for two seconds the vertical acceleration is below 0.05/g. These values are reasonable in order to consider only a zero-g period and with totally developed flow.

Figure 4.2 shows the flow diagram.

Using the two codes in sequence the output all the data expressed as real dimension only for the zero-g period. The analysis of this is in chapter V.

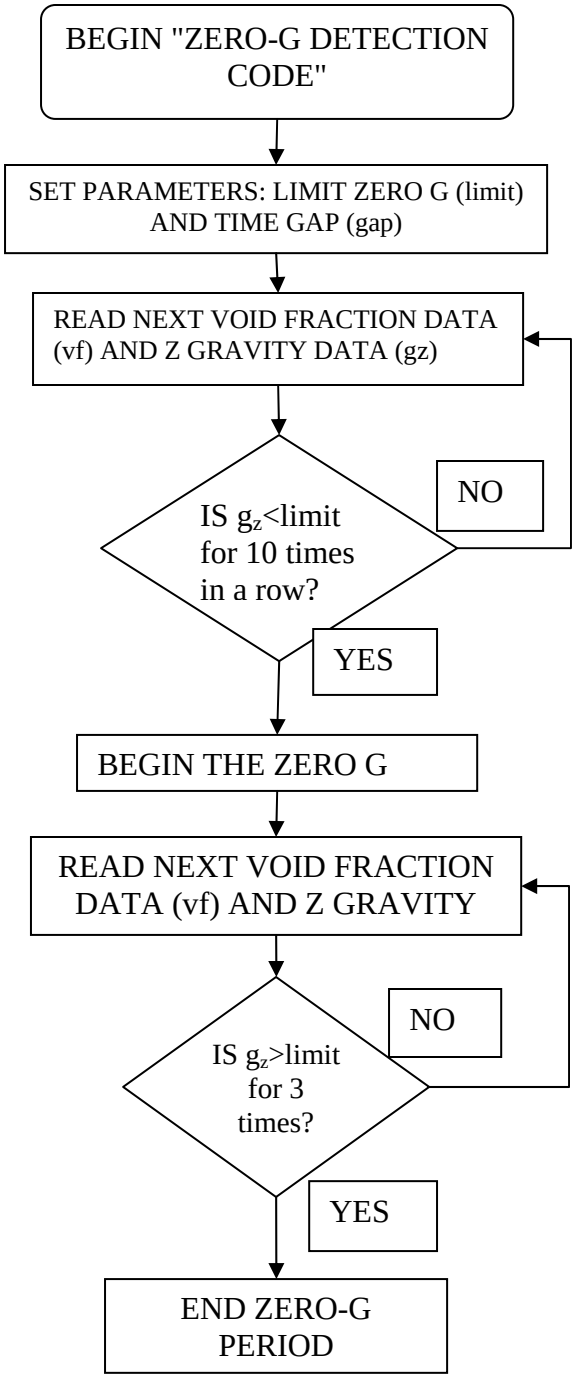

Fig. 4.2. Basic zero-g code performance

4.3 INSTRUMENT TEST

The performance of the Foster Miller two-phase flow test bed was analyzed by Hulbert [19]. The validation of the CREARE Inc. Probe as a valid void fraction device was conducted by Crowley [22] [24] and more recently by Chan [23].

In the current experiment, various parabolas were executed with the channel filled full of freon or gas in order to check the response of the void fraction instrumentation. This was done for two reasons. First, the value of the voltage from the sensors in an empty and a full channel are necessary for the correlation used in the code. Second, because in the current study, the fluctuation of the void fraction is analyzed, and so it's necessary to test the variance of the measurement due to the instrumentation and not to the real flow void fraction fluctuation.

Table 4.2 shows the results for the void fraction measurement variance for the channel full of liquid in comparison with the one found by Vince and Lahey [14] and Jones and Zuber [13].

Table 4.2. Comparison void fraction variance for full liquid channel

	This study	**Vince and Lahey**	**Jones and Zuber**
Variance	0.0014%	0.1600%	2.2000%

It’s noticed that the current study found a better stability of the instrument, so all the fluctuation of the void fraction is due to a real variation of the void fraction and not to any instrument error.

4.4 RESULTS

At it was said in chapter III, in the Forster Miller test bed a Kodak digital video camera is used in order to have a visual classification of the flow pattern (second column table 4.3). The videos are taken between the two capacitance devices through an ultem transparent tube (figure 2.1).

Figures 4.3 through 4.5 are example of the shots taken with the camera for annular flow, transition flow and slug flow with the Data Acquisition System interface.

The acceleration profiles were analyzed for every parabola by the code in order to select the 0-g period. The acceleration collected was in all the three dimensions: vertical, horizontal and lateral. Figure 4.6 shows a classical trend of the accelerations in a parabola (I.D. 23).

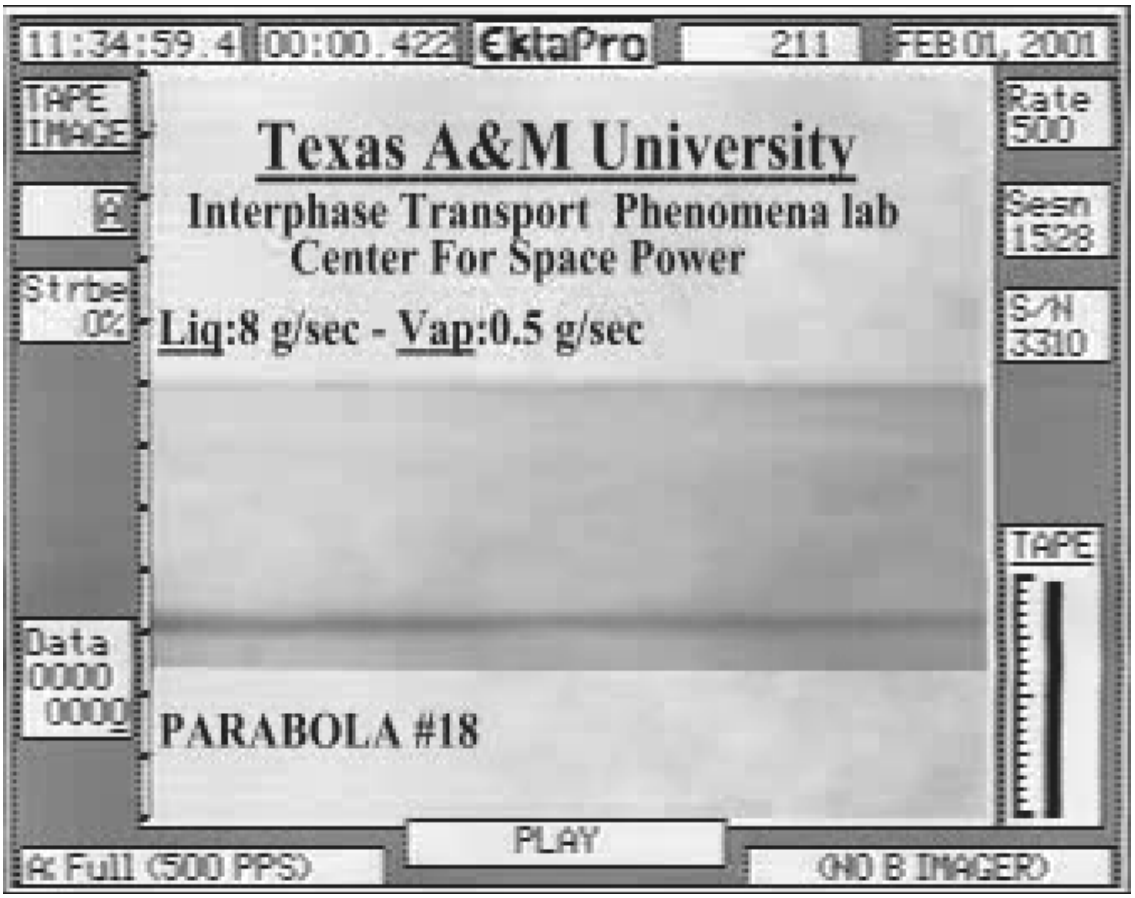

Fig. 4.3. Digital image of annular flow

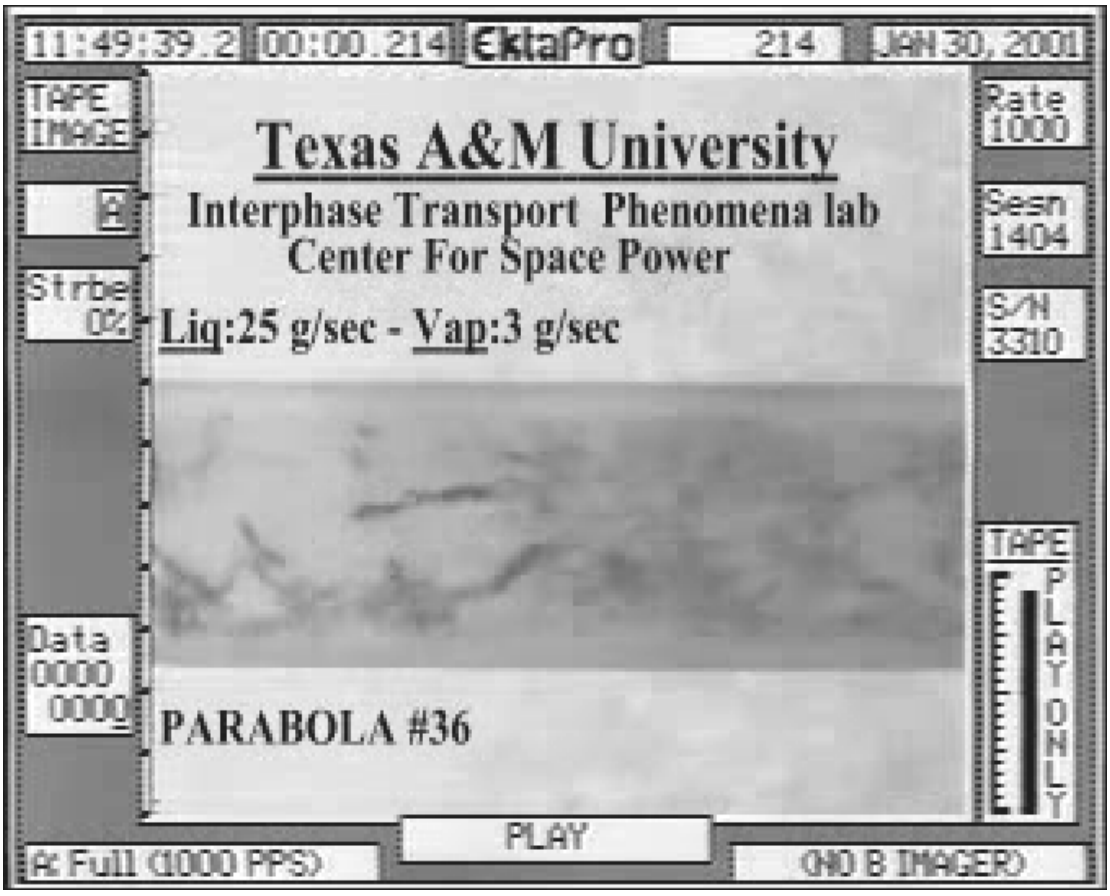

Fig. 4.4. Digital image of transition flow

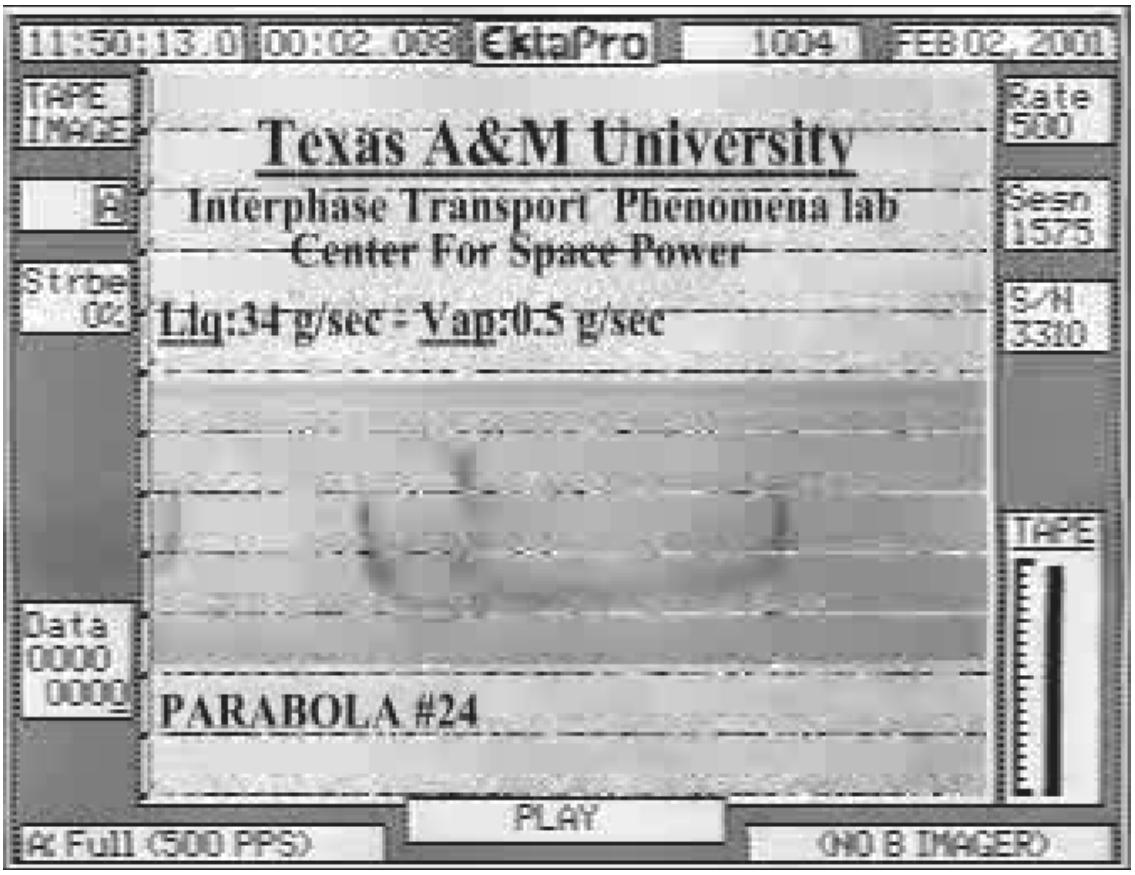

Fig. 4.5. Digital image of slug flow

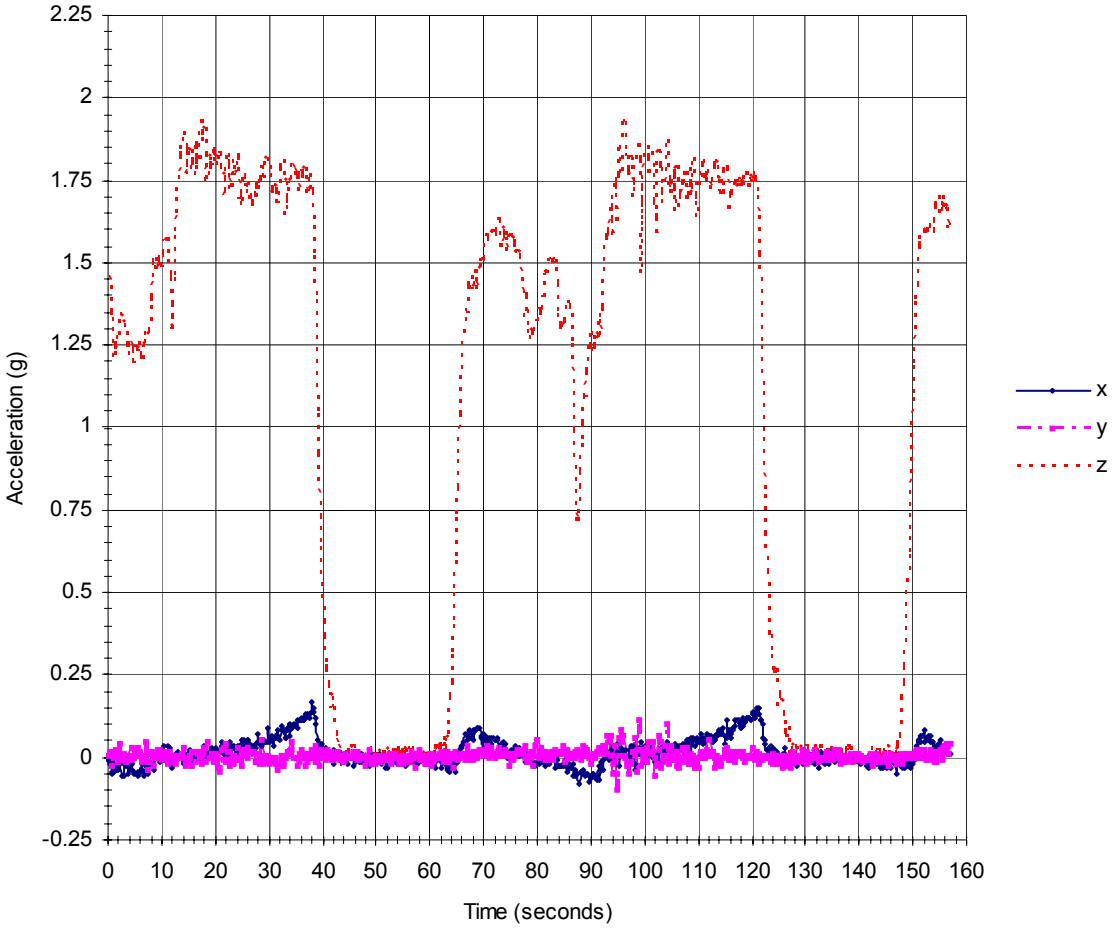

Fig. 4.6. General acceleration profile for parabola I.D. 23

In this section the system condition and the measured void fraction values are given. As said in chapter II, the sensor used is the 3mm ring. In the days of data collection for this study none of the parabolas reached bubbly flow.

Table 4.3 shows all the parabolas, including for each, the net 0-g time calculated by the code, the average of the void fraction from the 3mm ring sensor, the densities of the phases and the mass flow rates. The temperature and pressure drop data are collected by the system but not presented here because they are not relevant for the purpose of the current study.

4.5 CHAPTER SUMMARY

In this chapter the data from the January and February 2001 flights are presented. The codes of data processing and zero gravity period determination are presented. Testing of the instrumentation and results are introduced.

Table 4.3. Results for the 3mm ring sensor

Parabola I.D.	*Flow Pattern*	*0-g period(s)*	*void fraction*	*density liq (Kg/m3)*	*density vap (Kg/m3)*	*mass flow rate liq (Kg/s)*	*mass flow rate vapour (Kg/s)*
42	Annular	10.2	0.957	1366.7	31.6	8.19	8.87
53	Annular	12.0	0.970	1379.8	28.7	7.72	8.43
54	Annular	12.0	0.977	1382.0	28.6	7.43	10.17
55	Annular	12.4	0.990	1383.4	29.1	7.65	14.09
62	Annular	12.8	0.975	1372.5	30.6	4.82	6.46
63	Annular	13.0	0.992	1372.8	30.1	4.50	8.85
64	Annular	14.4	0.996	1373.0	30.2	4.66	10.54
68	Annular	7.0	0.939	1378.6	30.7	1.97	2.02
69	Annular	13.8	0.975	1371.1	30.5	1.88	3.05
2	Transition	15.0	0.463	1364.1	44.8	48.65	2.62
3	Transition	15.4	0.652	1363.8	36.5	50.50	5.65
4	Transition	15.2	0.702	1364.4	39.2	50.05	7.33
10	Transition	14.0	0.499	1368.5	31.8	34.40	2.12
11	Transition	15.6	0.568	1367.9	31.6	34.84	2.91
12	Transition	15.2	0.683	1368.3	31.1	34.14	4.58
13	Transition	15.2	0.747	1368.8	30.9	34.11	6.12
14	Transition	12.2	0.812	1371.8	31.2	34.54	8.75

Table 4.3 continued

Parabola I.D.	Flow Pattern	0-g period(s)	void fraction	density liq (Kg/m3)	density vap (Kg/m3)	mass flow rate liq (Kg/s)	mass flow rate vapour (Kg/s)
15	Transition	15.2	0.845	1372.6	31.1	34.32	10.71
18	Transition	11.0	0.581	1382.0	34.8	25.95	2.46
22	Transition	13.6	0.762	1380.7	31.1	24.79	4.33
16	Transition	15.0	0.877	1377.3	28.8	25.59	9.57
27	Transition	14.2	0.864	1376.5	30.3	34.98	12.36
30	Transition	12.8	0.636	1371.6	31.0	17.10	1.99
31	Transition	8.2	0.736	1375.3	31.6	16.62	3.04
32	Transition	11.2	0.809	1370.5	31.5	16.67	4.40
33	Transition	13.2	0.863	1368.6	31.4	16.58	6.23
34	Transition	11.4	0.897	1370.0	31.5	16.59	8.30
35	Transition	14.6	0.915	1366.9	30.9	16.47	9.97
49	Transition	11.8	0.794	1377.8	29.8	8.34	2.05
51	Transition	11.6	0.911	1379.7	29.0	8.11	4.39
52	Transition	13.6	0.940	1377.8	28.7	8.09	6.30
58	Transition	16.2	0.750	1369.2	31.2	5.10	0.99
59	Transition	12.6	0.866	1371.5	30.9	5.05	2.08
60	Transition	12.4	0.912	1371.3	30.5	5.15	3.08
67	Transition	10.2	0.870	1373.4	30.4	2.00	1.02
1	*Slug*	14.2	0.448	1365.8	31.5	50.86	1.02
8	*Slug*	13.8	0.378	1369.3	30.6	34.43	0.54
9	*Slug*	15.0	0.494	1367.3	31.4	33.51	1.00
16	*Slug*	11.8	0.449	1353.2	30.8	26.94	0.53
17	*Slug*	10.4	0.553	1371.5	30.9	27.33	1.04
36	*Slug*	12.0	0.643	1370.8	30.0	12.18	0.53
37	*Slug*	13.0	0.668	1369.8	30.1	12.07	1.07
47	*Slug*	13.6	0.653	1374.9	31.1	8.73	0.52
48	*Slug*	12.0	0.710	1374.6	30.7	8.66	1.01
57	*Slug*	12.2	0.783	1372.6	31.5	5.43	0.49
66	*Slug*	15.0	0.809	1369.9	31.7	2.13	0.54

CHAPTER V

DATA ANALYSIS

5.1 INTRODUCTION

This chapter describes three different analyses of the January and February 2001 flight Foster Miller experiment data. The first consists of the statistical analysis and includes the analysis of the transient data, the PDF (using several parameters), the Cumulative Density Function (using descriptor factors) and an analysis of the dependence of those values on the superficial velocities. The second analysis consists of the Lockhart-Martinelli examination. Finally the results are investigated using the Drift Flux approach. All these methods are developed in chapter III. The goal is to develop some parameters or factors that can be considered valid flow pattern identifiers and to apply the theoretical model to the collected data.

In the current study the flow regimes are visually identified by digital camera recording. In general, the literature refers to a superficial vapor velocity and superficial liquid velocity graphical representation. It is not an attempt of the current thesis to analyze the flow regime transitions but report them in order to have an immediate comparison with different studies. It's clear that the found data shown in figure 5.1 follows the general literature [34].

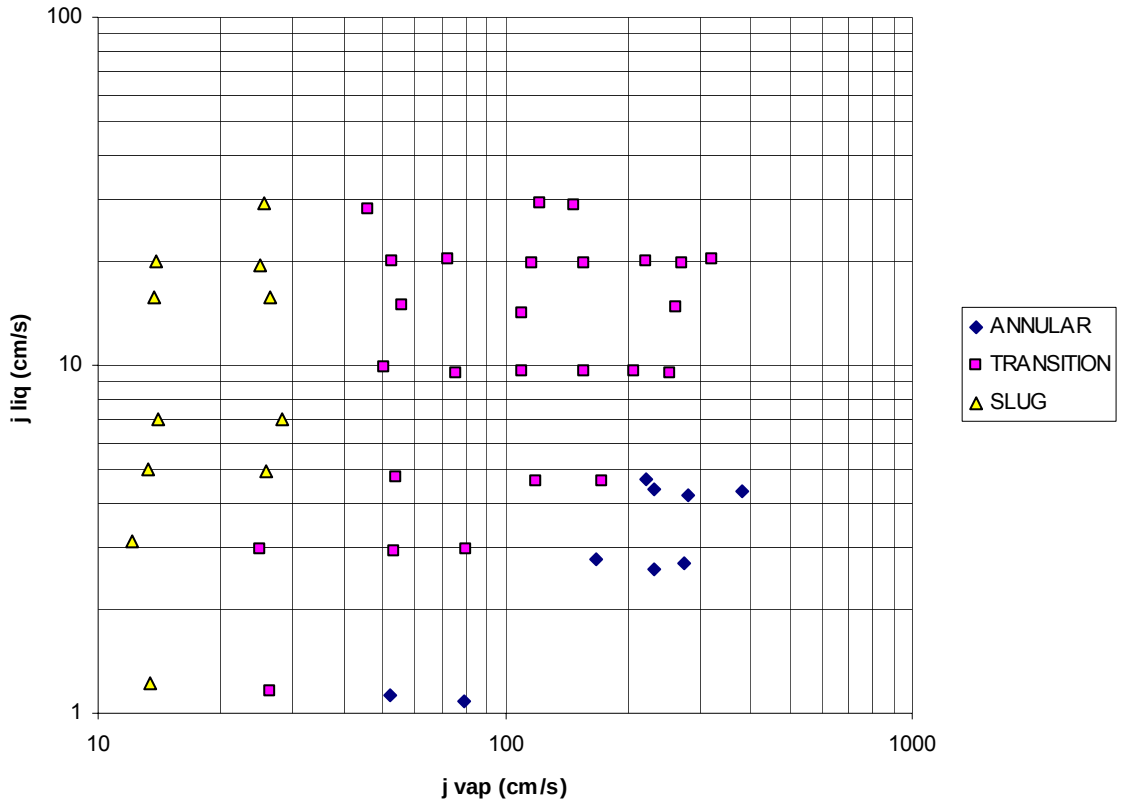

Fig. 5.1. Superficial liquid velocity vs. superficial gas velocity

5.2 STATISTICAL ANALYSIS

Figures 5.2 through 5.10 show a set of graphs from the void fraction sensor for three flow pattern test points (slug point 9, transition point 4, and annular point 42). The first graph is the measured void fraction vs. time at 100Hz, the

second is the Probability Density Function (PDF) and the third the Cumulative Probability Function (F) of the signal.

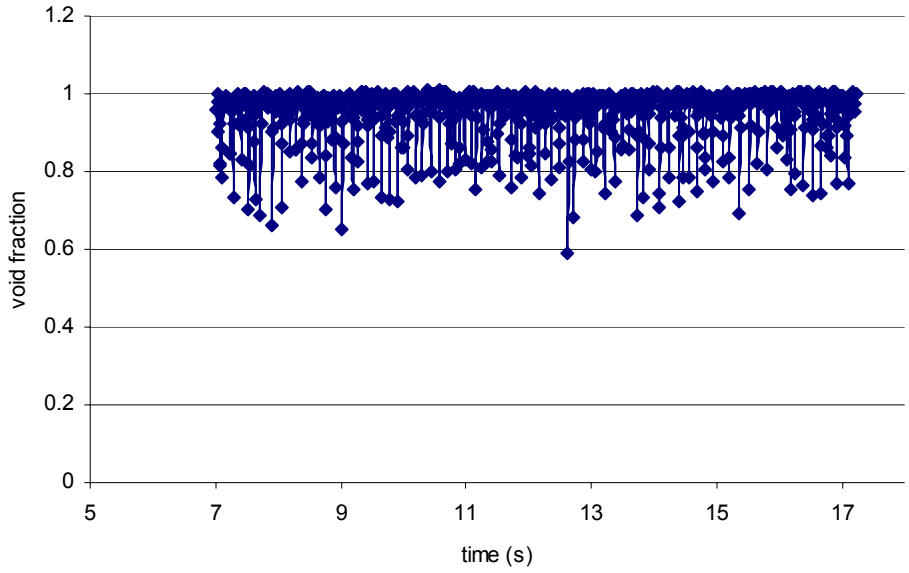

Fig. 5.2. Sample data for annular flow at 100Hz, test point 42

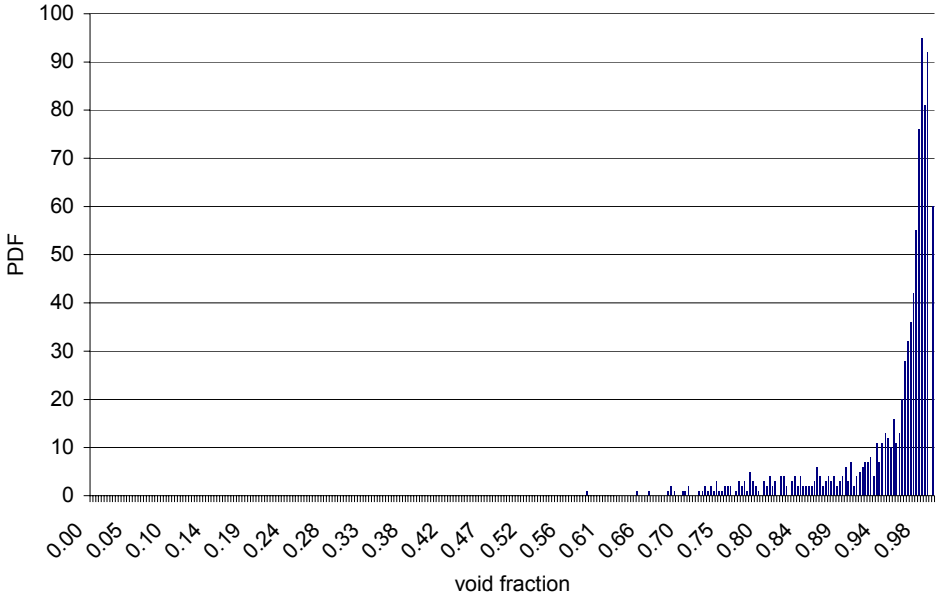

Fig. 5.3. PDF for annular flow, test point 42

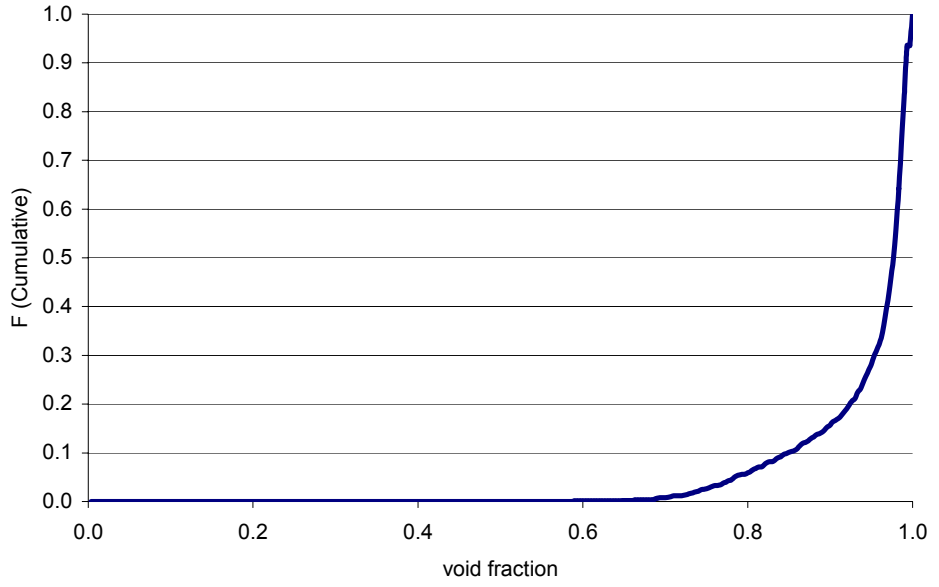

Fig. 5.4. Cumulative probability function for annular flow, test point 42

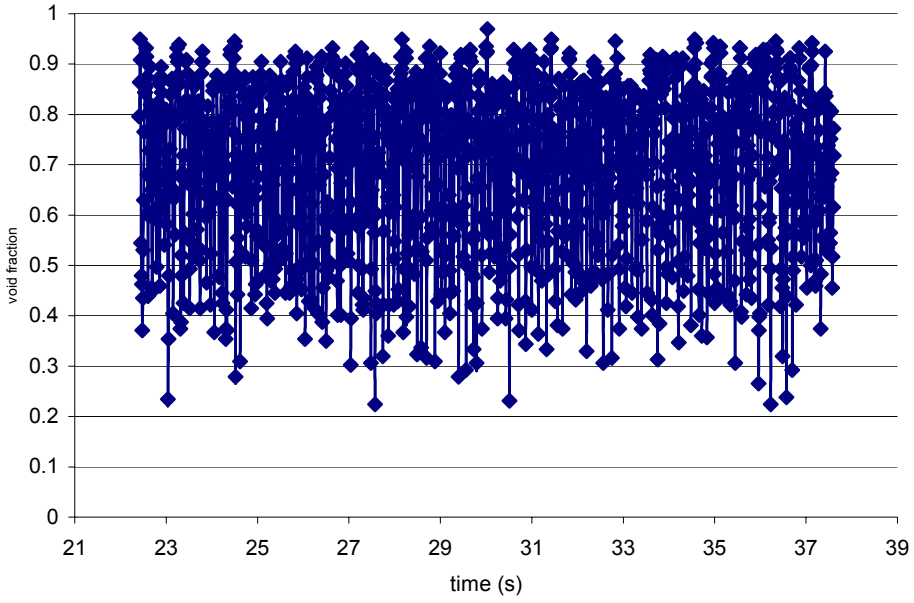

Fig. 5.5. Transient behavior for transition flow for 100Hz, test point 4

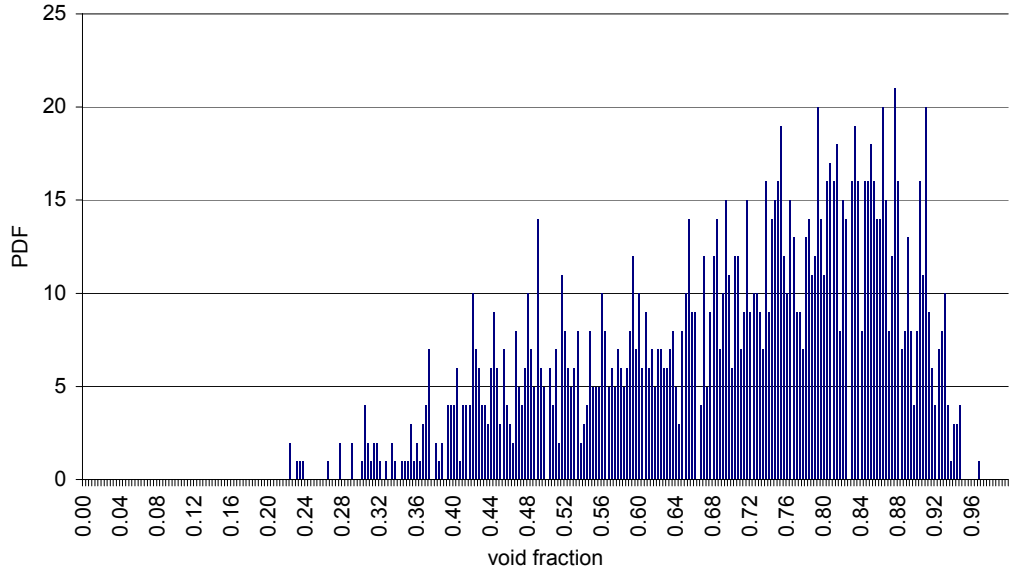

Fig. 5.6. PDF for transition flow, test point 4

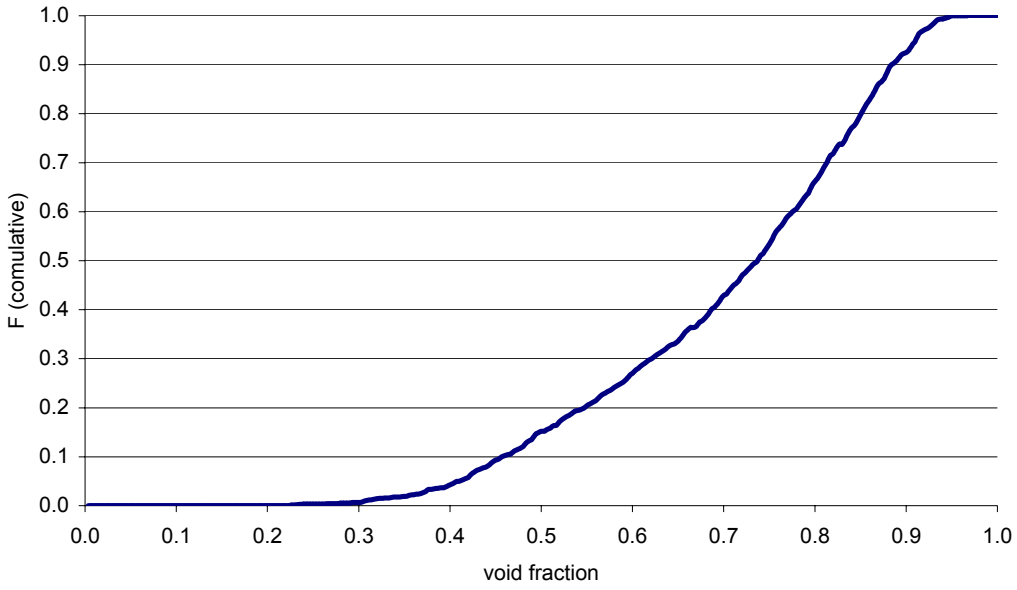

Fig. 5.7. Cumulative probability function for transition flow, test point 4

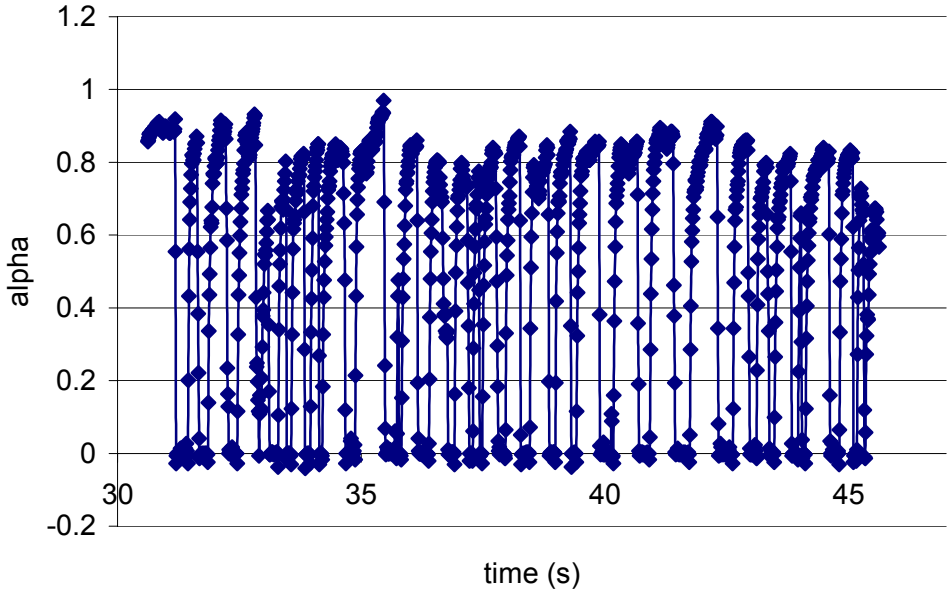

Fig. 5.8. Raw data for slug flow at 100Hz, test point 9

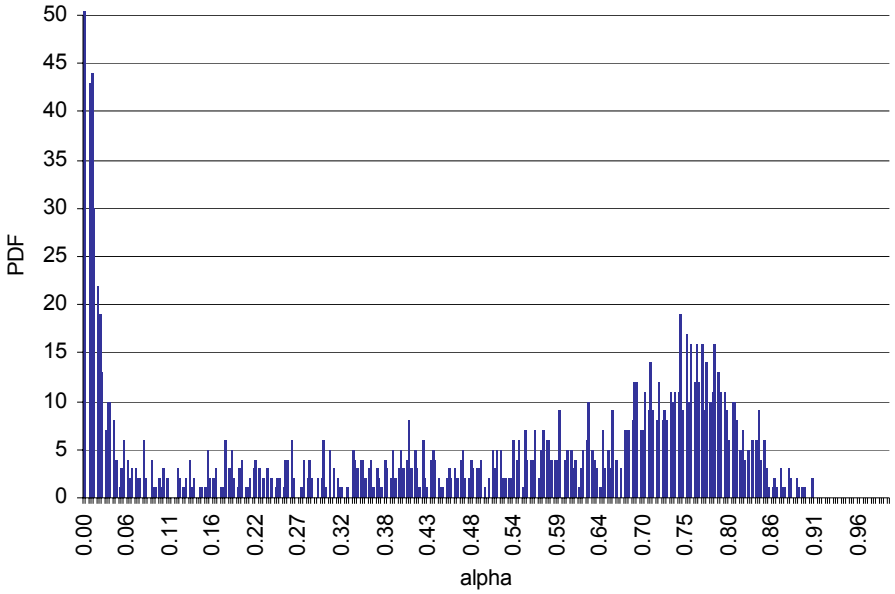

Fig. 5.9. PDF for slug flow, test point 9

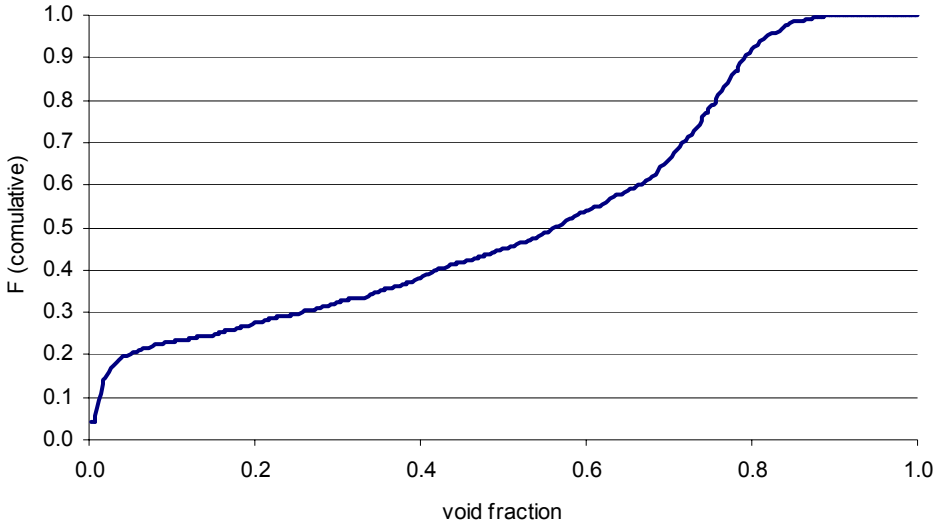

Fig. 5.10. Cumulative probability function for slug flow, test point 9

From the characteristics of the void fraction we can notice a strong difference between different flow patterns. In fact for annular flow the graph shows high void fraction values and a small fluctuation, while for slug flow the graph illustrates the intermittent high and low values of the void fraction due to the presence of Taylor bubbles. The transition void fraction data show a very wide distribution.

All these considerations are better represented by the PDF for the different flow patterns: it's right peaked for annular flow, two peaked for slug flow and wide for transition flow.

Consequently the Cumulative Probability Function shows an increased slope from annular to transition. It's interesting to notice the trend of the slug Cumulative Function: it's very sloping for low void fractions, and then it increases slowly until the second peak in the PDF that create another increasing in the slope of the Cumulative function.

It's important at this point to apply the analysis introduced in chapter III in order to have an objective and unique set of descriptors. The parameters analyzed at all the test points are: mean, variance, SNR, coefficient of skewness, coefficient of kurtosis, HHV, LAD.

Table 5.1 shows all of these for every test point arranged by flow pattern.

Table 5.1. Statistical parameters for all the test points.

test point	flow pattern	void fraction (mean)	variance	SNR	skewness	Kurtosis	LAD	HHV
42	A	0.957	0.00425	0.00444	-0.1536	5.2918	-134.514	0.9767
53	A	0.970	0.00364	0.00376	-0.1416	4.9385	-134.425	0.9767
54	A	0.977	0.00263	0.00269	-0.1201	4.9048	-135.653	0.9767
55	A	0.990	0.00114	0.00115	-0.0798	5.2427	-138.924	0.9800
62	A	0.975	0.00272	0.00279	-0.1538	8.7813	-137.940	0.9833
63	A	0.992	0.00082	0.00083	-0.0932	-17.9335	-141.651	0.9867
64	A	0.996	0.00060	0.00060	-0.0739	-30.9744	-141.877	0.9867
68	A	0.939	0.00749	0.00798	-0.2996	13.4467	-130.392	0.9600
69	A	0.975	0.00261	0.00268	-0.1787	-27.4339	-140.705	0.9867
2	T	0.463	0.03498	0.07550	-0.0485	-10.6987	11.278	0.4767
3	T	0.652	0.03001	0.04604	-0.0925	-15.6577	-45.203	0.6833
4	T	0.702	0.02574	0.03667	-0.0998	-13.7305	-60.284	0.7367
10	T	0.499	0.04447	0.08919	-0.0772	-6.7357	0.282	0.5300
11	T	0.568	0.04210	0.07408	-0.0920	-19.2146	-20.194	0.6033
12	T	0.683	0.03255	0.04763	-0.1328	-14.5336	-54.693	0.7233
13	T	0.747	0.02624	0.03514	-0.1401	-15.2528	-73.715	0.7900
14	T	0.812	0.01776	0.02186	-0.1433	0.2693	-93.264	0.8567
15	T	0.845	0.01429	0.01692	-0.1346	-17.8715	-102.947	0.8833
18	T	0.581	0.04323	0.07439	-0.1305	-0.6237	-24.076	0.6300
22	T	0.762	0.03035	0.03982	-0.1861	-7.6748	-78.317	0.8100
26	T	0.877	0.01196	0.01364	-0.1489	-17.3119	-112.400	0.9133
27	T	0.864	0.01061	0.01228	-0.1238	-10.0503	-108.651	0.8967
30	T	0.636	0.04775	0.07506	-0.1464	-0.5628	-40.498	0.6967
31	T	0.736	0.03012	0.04095	-0.2045	0.6849	-70.033	0.7867
32	T	0.809	0.02299	0.02842	-0.2011	1.1399	-92.212	0.8567
33	T	0.863	0.01714	0.01986	-0.2059	-8.3893	-108.337	0.9133
34	T	0.897	0.01022	0.01139	-0.1605	1.7607	-118.367	0.9333
35	T	0.915	0.00793	0.00867	-0.1555	-17.5637	-123.570	0.9467
49	T	0.794	0.02321	0.02923	-0.2008	1.1621	-87.818	0.8467
51	T	0.911	0.01268	0.01391	-0.2364	4.0775	-121.836	0.9500
52	T	0.940	0.00786	0.00836	-0.1916	-12.8281	-128.847	0.9667
58	T	0.750	0.03257	0.04341	-0.2520	-291.9088	-74.728	0.8000
59	T	0.866	0.01857	0.02144	-0.2639	3.1911	-109.311	0.9200
60	T	0.912	0.01233	0.01351	-0.2408	4.7792	-122.996	0.9567
67	T	0.870	0.01676	0.01926	-0.3538	7.9796	-110.465	0.9233
1	S	0.448	0.09612	0.21476	-0.1011	-5.9609	9.929	0.5600
8	S	0.378	0.11727	0.31036	-0.0071	-4.9616	-26.048	0.6767
9	S	0.494	0.13276	0.26861	-0.1551	-8.0329	-41.551	0.7633
16	S	0.449	0.14856	0.33123	-0.0772	-1.7846	-59.684	0.7800

Table 5.1 continued

test point	flow pattern	void fraction (mean)	variance	SNR	skewness	Kurtosis	LAD	HHV
17	S	0.553	0.12934	0.23372	-0.2673	-1.2602	-63.479	0.8067
36	S	0.643	0.16286	0.25346	-0.3673	-1.0539	-105.117	0.9133
37	S	0.668	0.07051	0.10552	-0.3554	-6.9894	-64.818	0.7600
47	S	0.653	0.16345	0.25017	-0.3739	-5.8158	-110.019	0.9367
48	S	0.710	0.06312	0.08892	-0.3860	1.5729	-73.543	0.8000
57	S	0.783	0.11814	0.15080	-0.5986	1.2242	-123.635	0.9600
66	S	0.809	0.09546	0.11805	-0.6683	-23.7718	-122.940	0.9400

All the parameters will now be discussed. In particular, their physical meaning and their usefulness as a flow pattern identifier will be investigated. Moreover a comparison with the previous literature is proposed showing differences and analogies.

5.2.1 Variance

Figure 5.11 shows the dependence of the variance on the measured void fraction for all the test points.

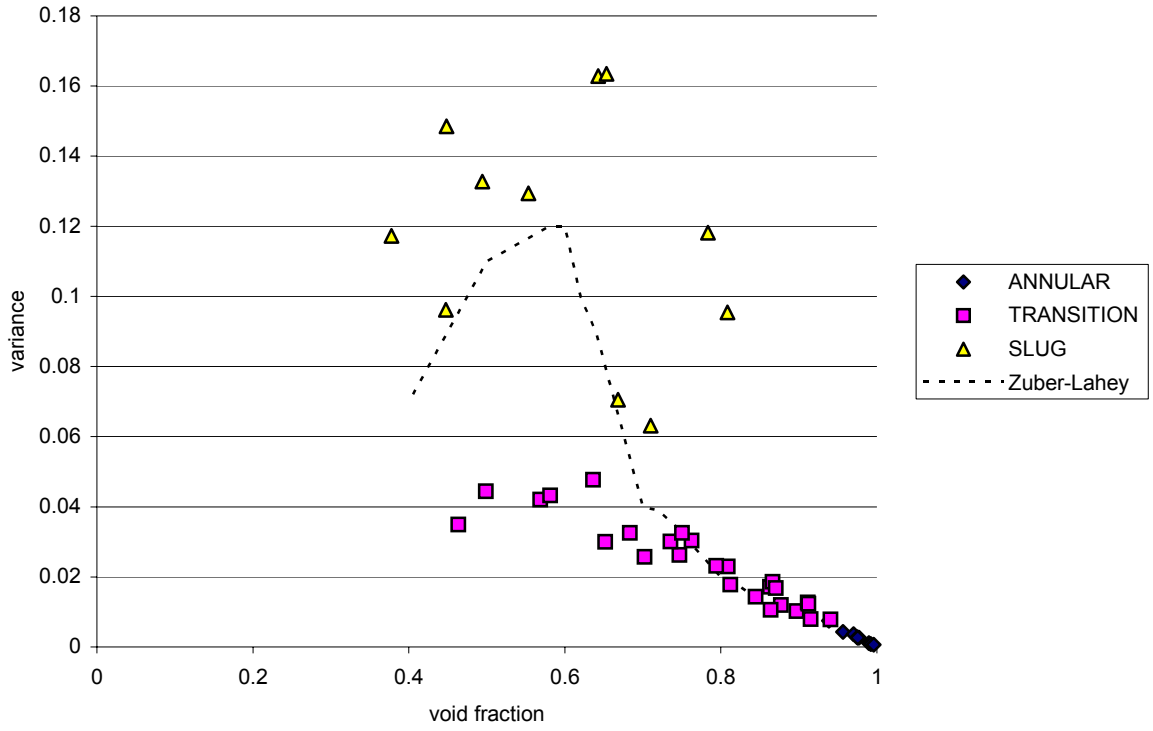

Fig. 5.11. Void fraction variance vs. void fraction

The graph could be divided in three variance regions: for variance from 0 to 0.005 where only annular flow exists, from 0.005 to 0.05 where only transition and more than 0.05 where only slug flow exists. As previously explained reasonably the variance increases from annular to slug.

Despite this fact the variance of the void fraction for slug flow considering only the Taylor bubble region is smaller than for annular. This occurs because the velocity difference between the phases is small in slug flow, and then the shear force in the interface is small and this brings to a smoother surface, while

for annular the shear is bigger due to a larger difference in the velocities and so it brings a more turbulent interface. Moreover, there is an almost linear correlation between the void fraction and its variance for annular and transition flow.

Note the spread distribution for variance for slug flow. The wide range of the values is due to the fact that all the slug parabolas have different Taylor bubble configurations.

The result for void fraction from 0.6 to 1 is in accordance with Vince and Lahey [14] experiments. Different values have been found for smaller void fraction (from 0.4 to 0.6, in the slug region) due to the fact, as said before, that they have a strong relation with the slug configuration. So we can conclude that reasonably the two studies agree on the basic configurations.

Moreover it's expected that the variance for annular flow in zero gravity is smaller in microgravity than in earth-gravity conditions. This happens because the absence of buoyancy, the annular regime can be reached for smaller velocities in microgravity, and so the shear is reduced and the interface smoother.

In conclusion, the variance is seen as a good parameter for flow pattern identification for this experiment using the classification shown in table 5.2.

Table 5.2: Variance regions for the classification of the flow pattern.

Flow pattern	**Variance**
Annular	0<Var<0.005
Transition	0.005<Var<0.05
Slug	Var>0.05

5.2.2 Signal Noise Ratio (SNR)

As shown in chapter III, SNR should be more relevant than the variance alone because it shows the ratio of the variance over the mean (void fraction)(it's not in an absolute scale but in a mean-weight scale). Consequently this parameter doesn't depend directly on the value of the void fraction but only on the fluctuations.

Figure 5.12 shows the dependence of the SNR with the measured void fraction.

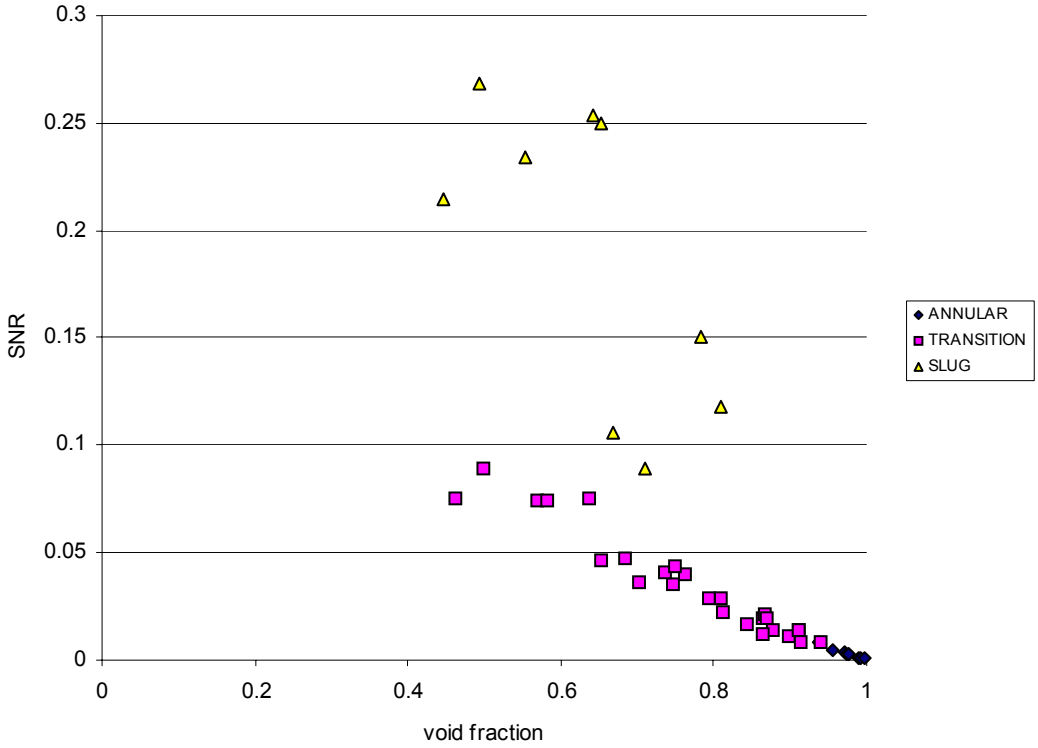

Fig. 5.12. SNR vs. void fraction for all the test points

The graph shows three SNR regions (table 5.3). Thus this parameter could be a good flow pattern identifier for this experiment.

Table 5.3. SNR regions for the classification of the flow pattern.

Flow pattern	**SNR**
Annular	0<SNR<0.008
Transition	0.008<SNR<0.09
Slug	SNR>0.09

5.2.3 Skewness

The coefficient of skewness is computed in accordance with equation 3.6. Its meaning is explained in chapter III. Figure 5.13 is a plot of the coefficient of skewness vs. the void fraction.

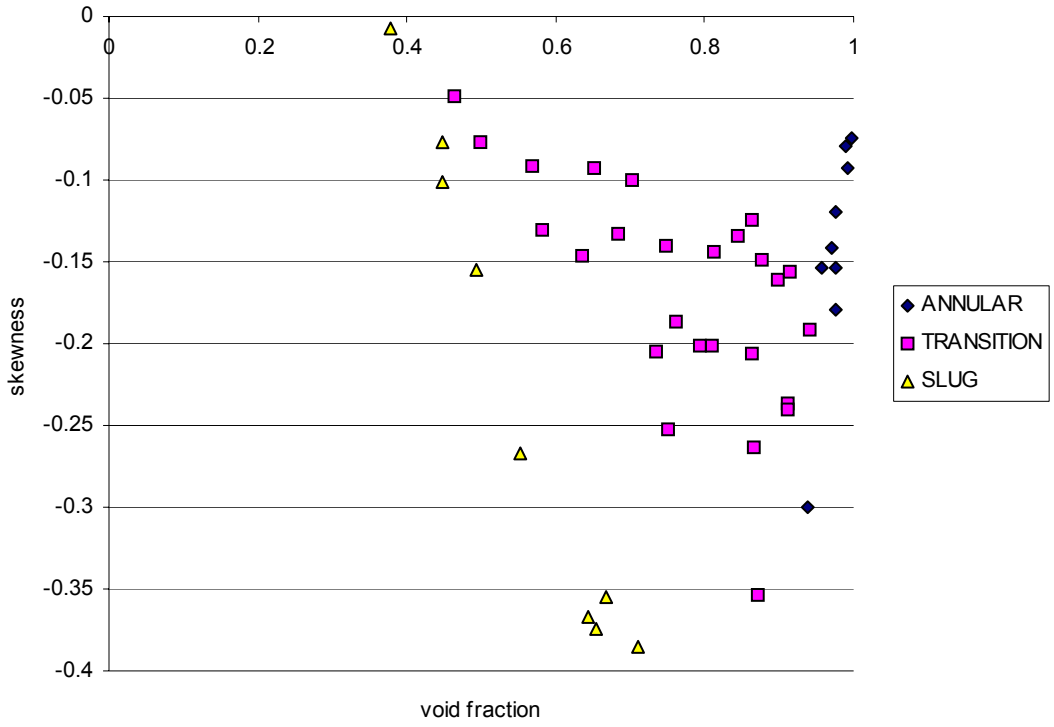

Fig. 5.13. Skewness coefficient vs. void fraction for all test points.

A large skewness coefficient means a right-tailed distribution and a small means a left-tailed distribution. An interesting remark is that in general slug flow

has a smaller skewness than transition flow for same void fraction. It's reasonable because the two-peak slug distribution consist of a more left-tailed PDF shape. Additionally annular flow assumes small values because the distribution has a small left tail.

The trend of the current experiment for annular and transition is close to the one that Vince-Lahey [14] found as shown in figure 5.14.

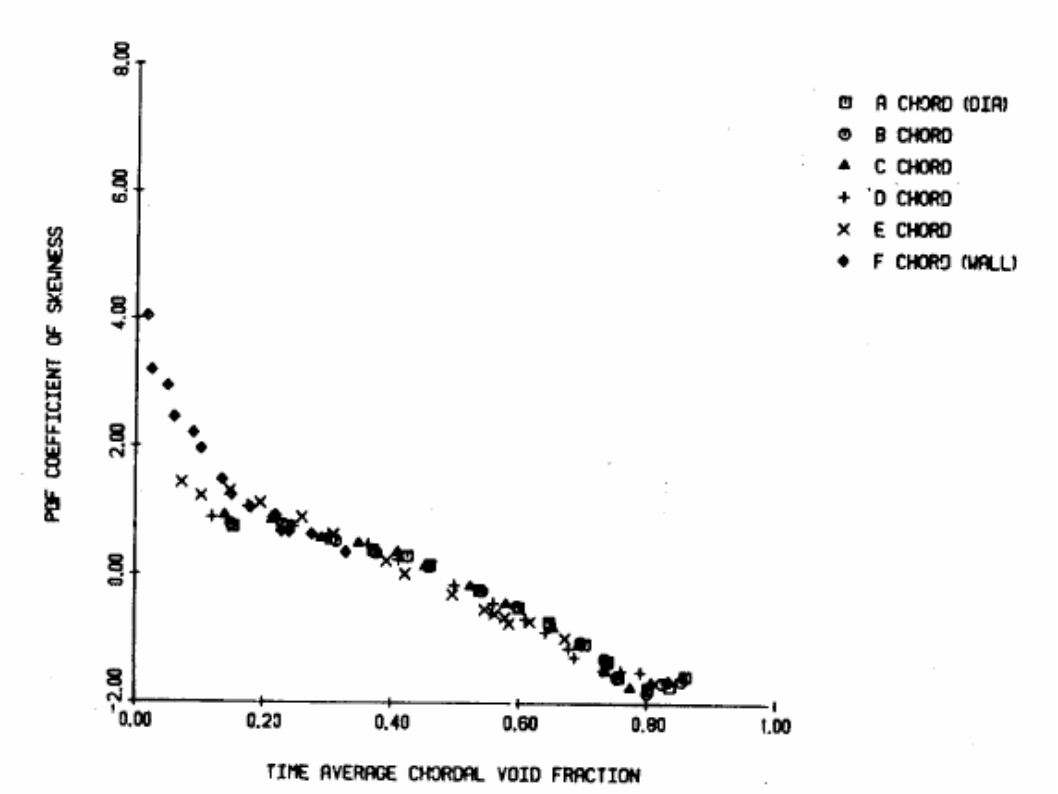

Fig. 5.14. Vince-Lahey skewness vs. void fraction

The values of the coefficient of skewness are different probably due to a different definition of the statistical moment but the trend (not the scale) is similar. The present work and Lahey both have a skewness minimum for a void fraction equal to 0.8-0.9 and they are equal to zero around a void close to 0.4. The skewness for slug flow in the present work is clearly different from the other flow patterns and from Vince-Lahey [14].

Figure 5.13 does not present any straight threshold classification but a regional classification in the skewness-void fraction space.

Anyway the unique categorization due to the complexity and the inaccuracy of this parameter results in a more complicated identification than variance and SNR.

5.2.4 Kurtosis

Figure 5.15 shows the dependence of the coefficient of kurtosis on void fraction.

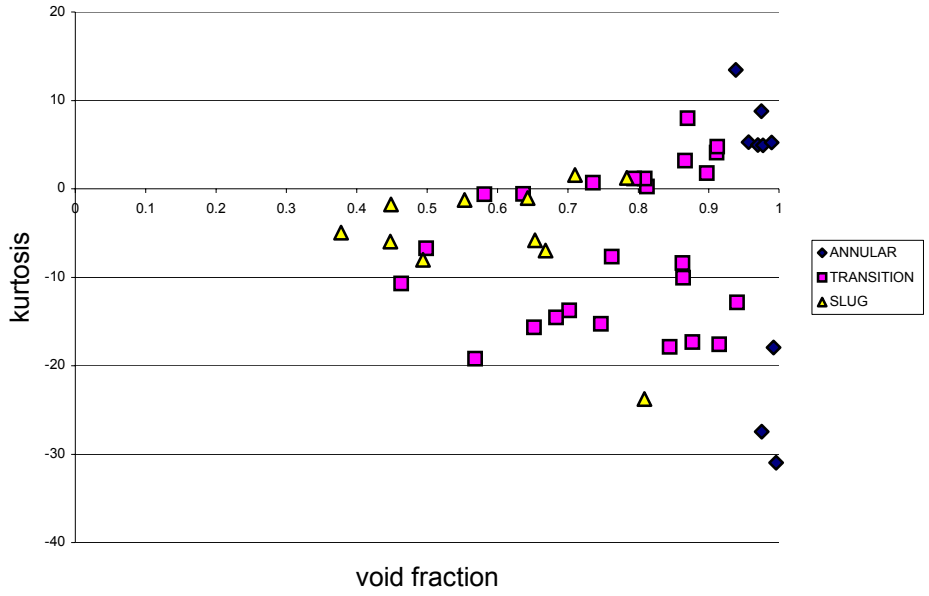

Fig. 5.15. Coefficient of kurtosis vs. void fraction for all test points

This parameter fails the requirements to be a valid flow pattern identificator. Vince and Lahey [14] found a different distribution. The discrepancy between the data could be explained in different ways. The most probable is that a small variation due inaccuracy in the measurements results in a large disparity in the void fraction values and even more large difference in the calculation of the fourth statistical moment.

5.2.5 Half High Value (HHV)

The Half High Value (HHV) is computed as described by equation 3.10 and its meaning is explained in chapter III. Figure 5.16 is a plot of the HHV vs. the void fraction.

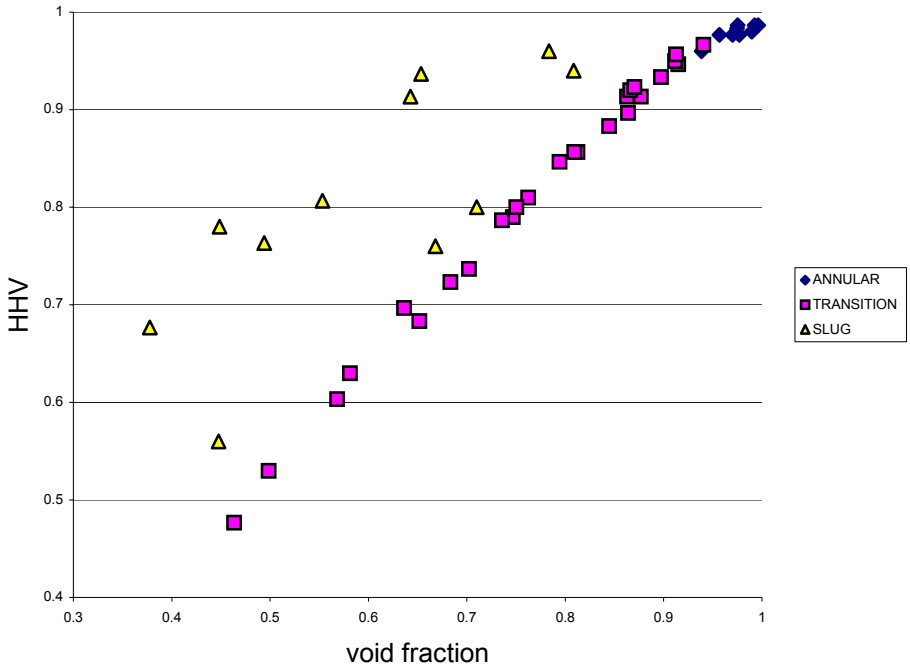

Fig. 5.16. HHV vs. void fraction for all test points

Figure 5.16 is in perfect accordance with the expectations. It presents high values for annular flow (from HHV=0.97 to HHV=0.99) because the Cumulative function increases strongly for large void fraction values.

HHV for slug flow is out of the transition-annular trend line and assume larger values. In addition, for equal values of the void fraction HHV is greater for slug than for transition flow. This is due to the presence of the left peak in the slug distribution that moves the Cumulative function left.

The plot in figure 5.16 could be a good flow pattern identifier. Annular and transition flow are in an almost linear correlation while slug has an out side behavior. As mentioned before it's due to the variability of the slugs, in particular

with the length of the Taylor bubbles. Table 5.4 summarizes the identification criterion for HHV analysis.

Table 5.4. HHV regions for the classification of the flow pattern

Flow pattern	**HHV**
Annular	HHV>0.97
Transition	HHV<0.97 and HHV≈alpha
Slug	HHV<0.97and HHV>alpha

5.2.6 Linear Area Difference (LAD)

Figure 5.17 shows the dependence of the LAD on void fraction.

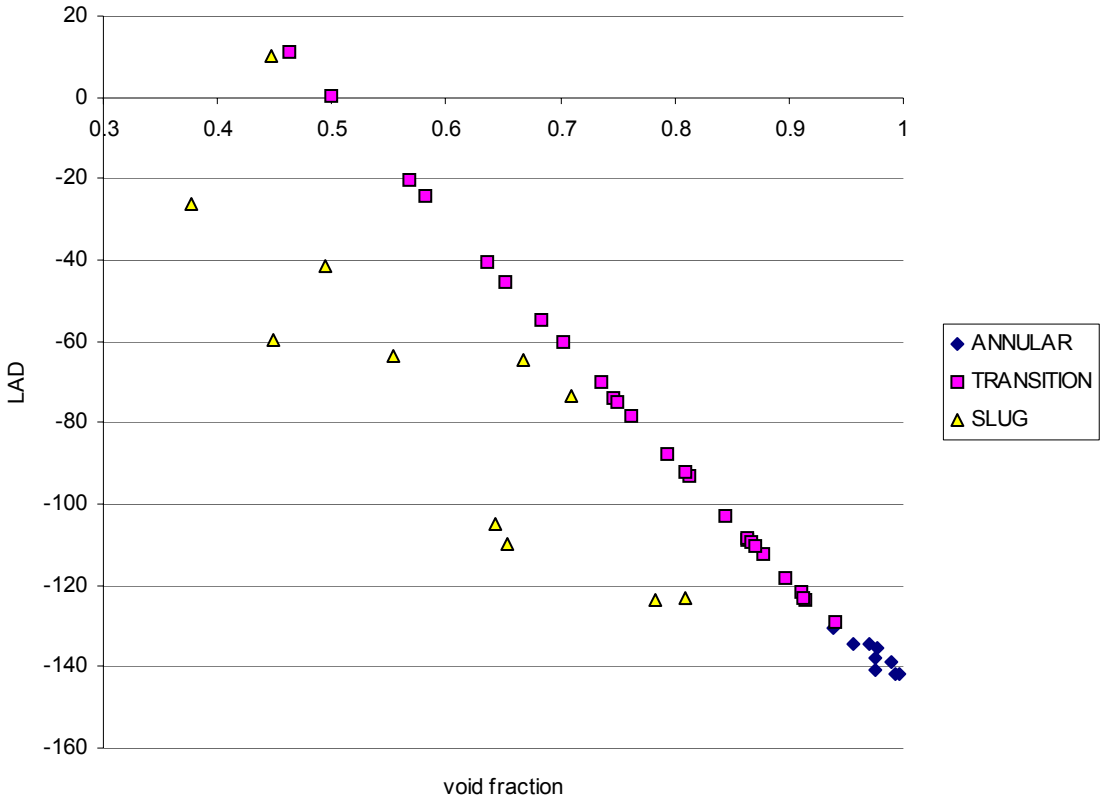

Fig. 5.17. LAD vs. void fraction

This graph is helpful for flow pattern identification. Annular flow has a very negative LAD as expected because annular flow assumes only high values for void fraction. Transition values sit on an almost linear trend line (R^2=0.9998). Furthermore, slug flow is out of the trend-line. In fact, the slug LAD is smaller than the transition LAD for equal void fraction values because the Cumulative function is flat for middle-values. This happens because in slug flow few points

with a void fraction between the one of annular and full water were detected. Table 5.5 summarizes the proposed identification criterion for LAD.

Table 5.5. LAD regions for the classification of the flow pattern

Flow pattern	**LAD**
Annular	LAD<-130
Transition	LAD>-130 and LAD≈-300alpha+148
Slug	LAD>-130 and LAD<-300alpha+148

For both HHV and LAD the transition are set in a linear correlation with the void fraction. For HHV R^2=0.9945 and for LAD R^2=0.998. The reason why could be explained by the fact that the transition PDF distributions have almost the same shape for different void fractions. In fact, the values are spread for all the void fractions. In other words, they have the same shape for different void fraction means and so the area and the half high value are strictly dependent on the void fraction mean.

This result is particularly significantly. In fact for this system, knowing the LAD or HHV, with a linear correlation it's possible to estimate the void fraction values.

The HHV and LAD have shown an excellent capability to indicate the different flow pattern and in particular to distinguish and describe the two-peak distribution of slug flow from the others. This approach is much more efficient than Annunziato and Girardi [15], where the attempt of the description of the PDF shape was purely analytical but difficult functionally with experimental data.

A particular aspect that has to be investigated is how much the superficial velocities affect the parameters just described. This is important because an eventual independency from the velocities enlarges the applicability of these considerations. Figures 5.18 to 5.23 show the statistical parameter dependence with the liquid velocity.

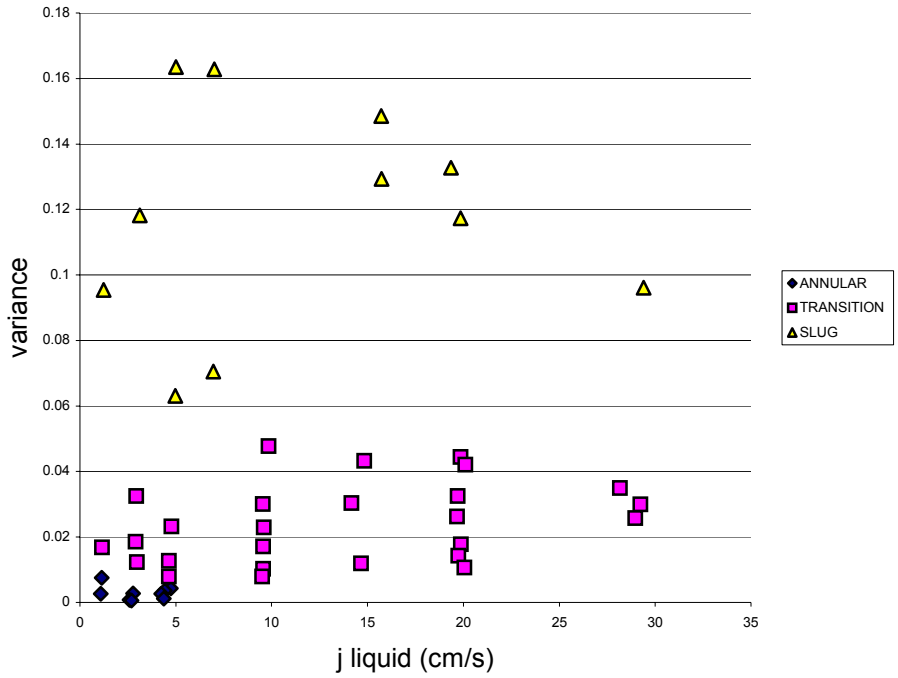

Fig. 5.18. Variance dependence on the superficial liquid velocity

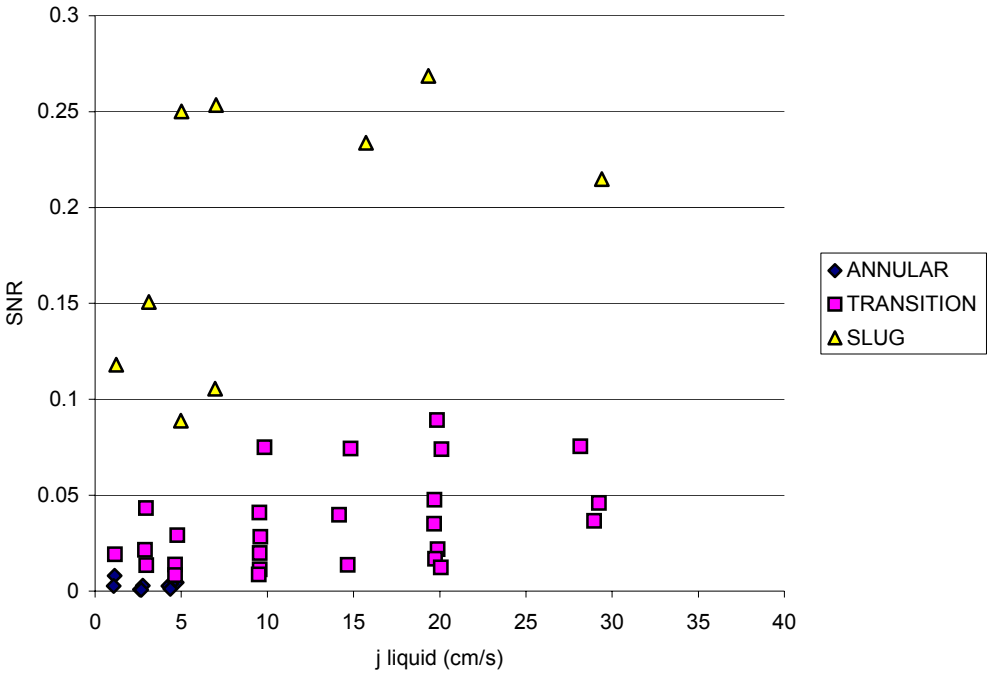

Fig. 5.19. SNR dependence on the superficial liquid velocity

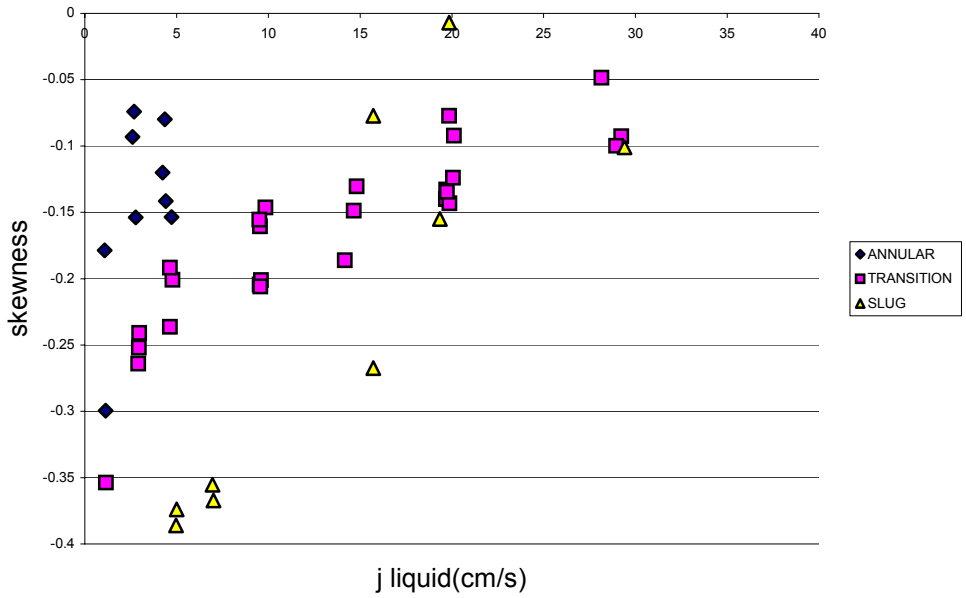

Fig. 5.20. Coefficient of skewness dependence on the superficial liquid velocity

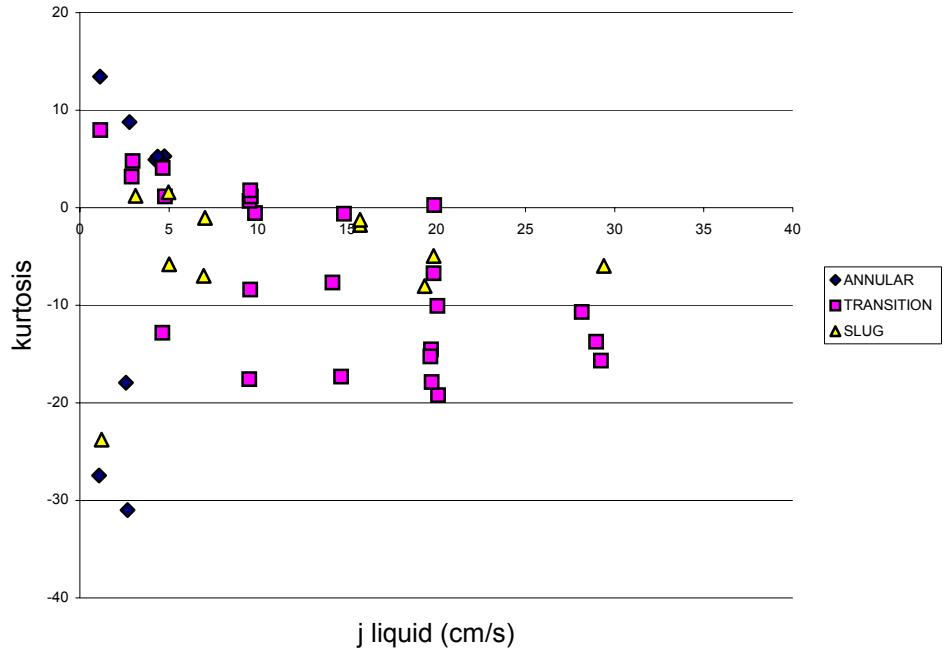

Fig. 5.21. Coefficient of kurtosis dependence on the superficial liquid velocity

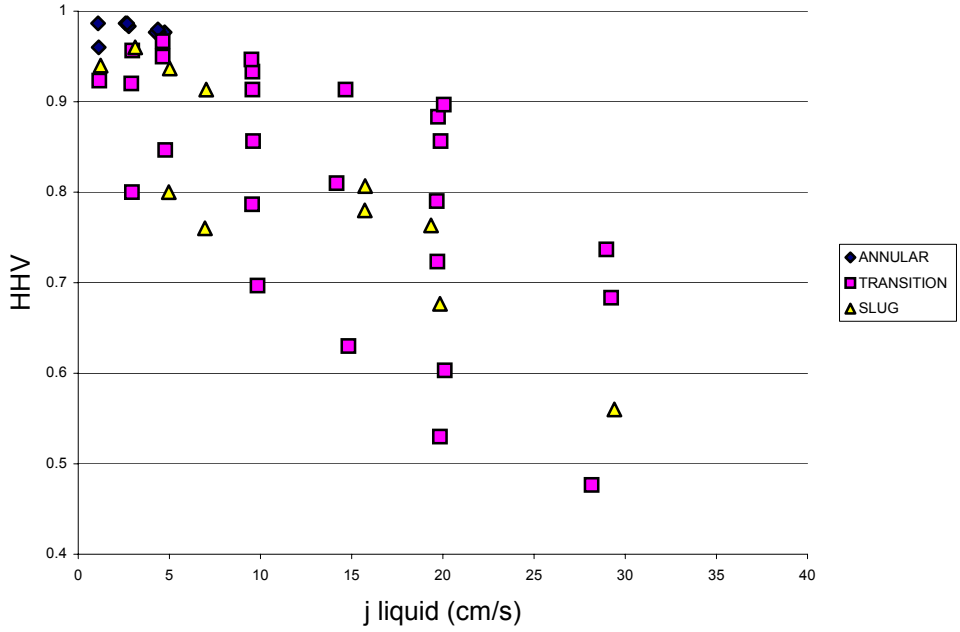

Fig. 5.22. HHV dependence on the superficial liquid velocity

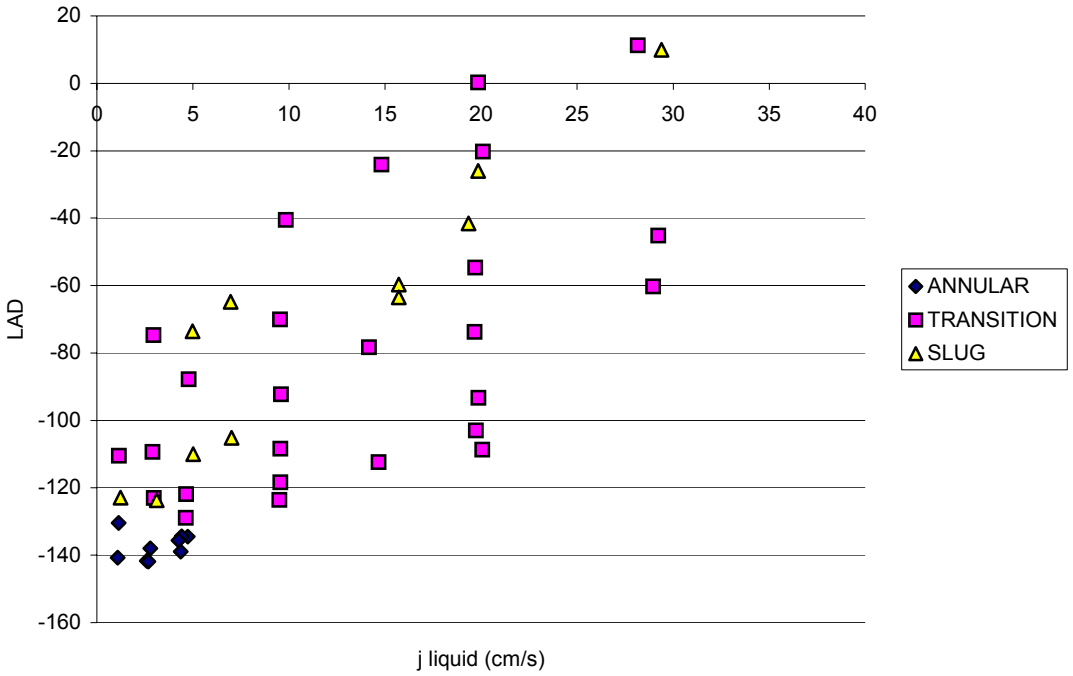

Fig. 5.23. LAD dependence on the superficial liquid velocity

Vince and Lahey [14] claimed that momentum is strongly sensitive to the liquid phase velocity. Instead from the graphs just presented the statistical momentum in the current experiment is not related with the superficial vapor velocity. In fact from figure 5.18 to 5.23 no correlations are shown in any graphs and the statistical parameters vary independently from the liquid phase velocity.

Now investigate the dependence of variance on vapor superficial velocity in figures 5.24 through 5.27.

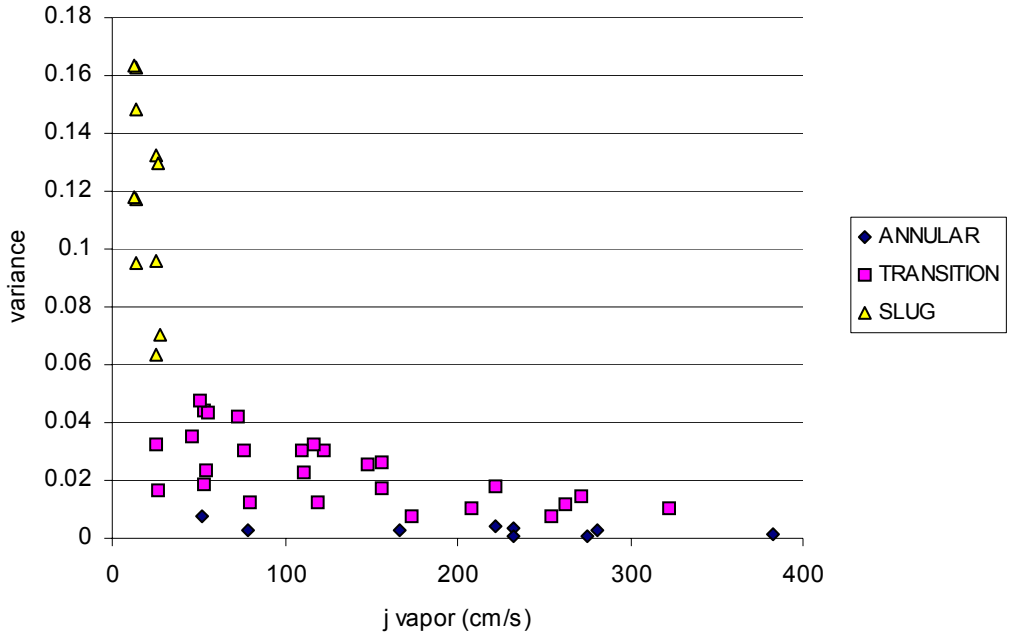

Fig. 5.24. Variance dependence on the superficial vapor velocity

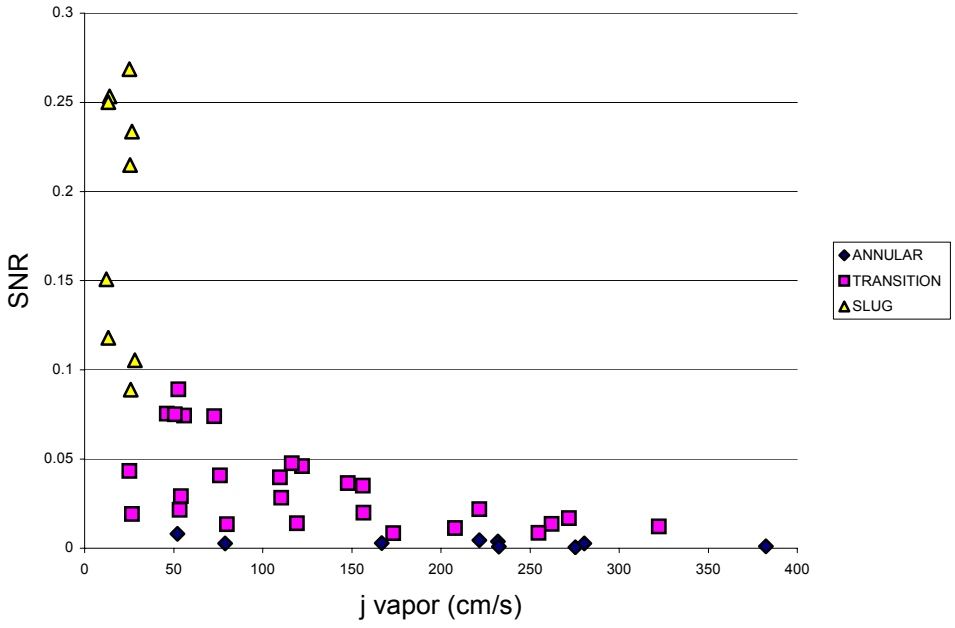

Fig. 5.25. SNR dependence on the superficial vapor velocity

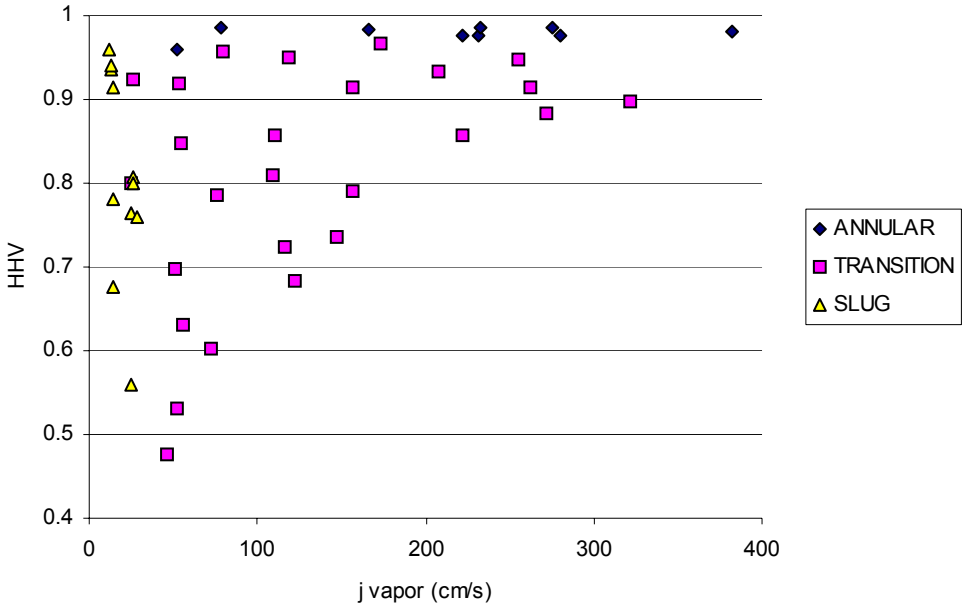

FIg. 5.26. HHV dependence on the superficial vapor velocity

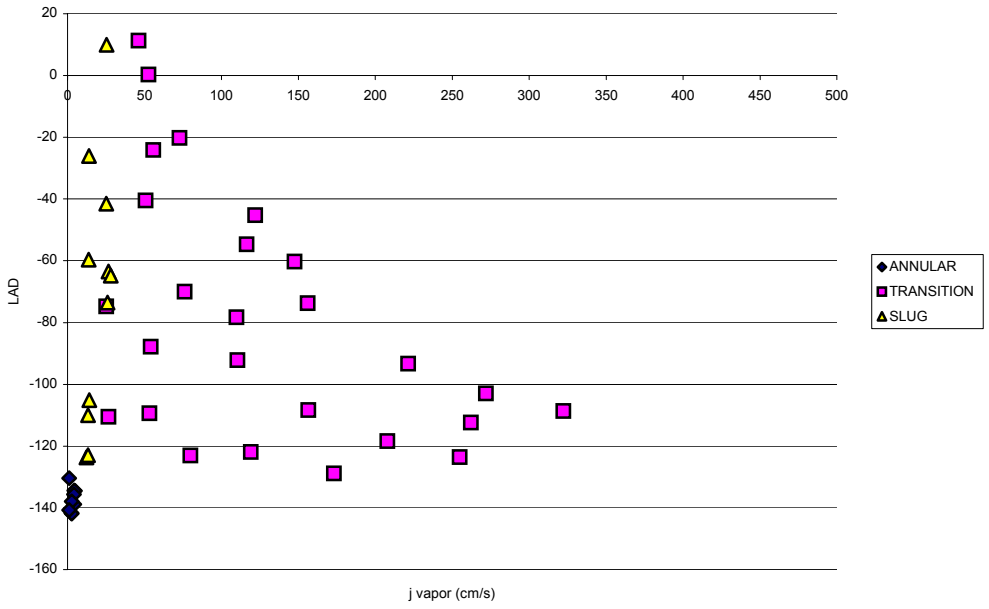

Fig

5.27. LAD dependence on the superficial vapor velocity

Notice that the variance and the SNR for slug flow depend somewhat on the vapor velocity but without any specific and relevant relationship. In fact the only relationship is the one that underline that the different flows, and so different statistical parameters, stand under specific values of superficial velocities, as will be analyzed later. So the relationship is more explainable as relationship between the flow pattern and the velocities rather than the statistical parameter and the velocities. In addition it's noticed that while for slug flow somewhat there is dependence, for annular flow the vapor velocity doesn't affect the parameters. This could be explained by the fact that for slug flow the physical configuration of the flow pattern is more strongly determined by the vapor phase velocity than for annular flow. In fact for example vapor velocities determine the length of the Taylor bubble or the frequency for slug flow while it establishes nothing in particular for annular flow (in fact the shape is anyway the same for the considered superficial velocities).

The coefficients of skewness and of kurtosis don't show any relevant dependence with the vapor superficial velocity.

5.3 LOCKHART-MARTINELLI ANALYSIS

Figure 5.28 shows the measured void fraction as function of the Martinelli parameter evaluated for each point from equation 3.32.

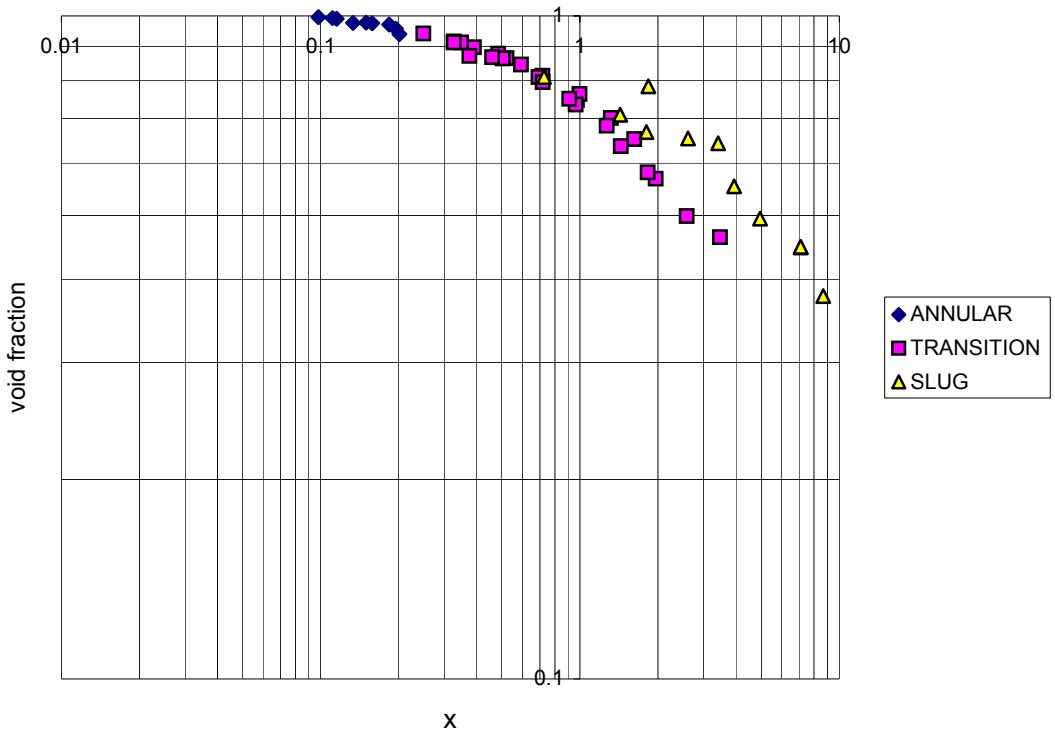

Fig 5.28. Martinelli parameter vs. void fraction for different flow patterns for all test points

Another plot of the void fraction as function of the inverse Martinelli parameter is provided in figure 5.29 because all the literature [30] [32] represent their data in that form.

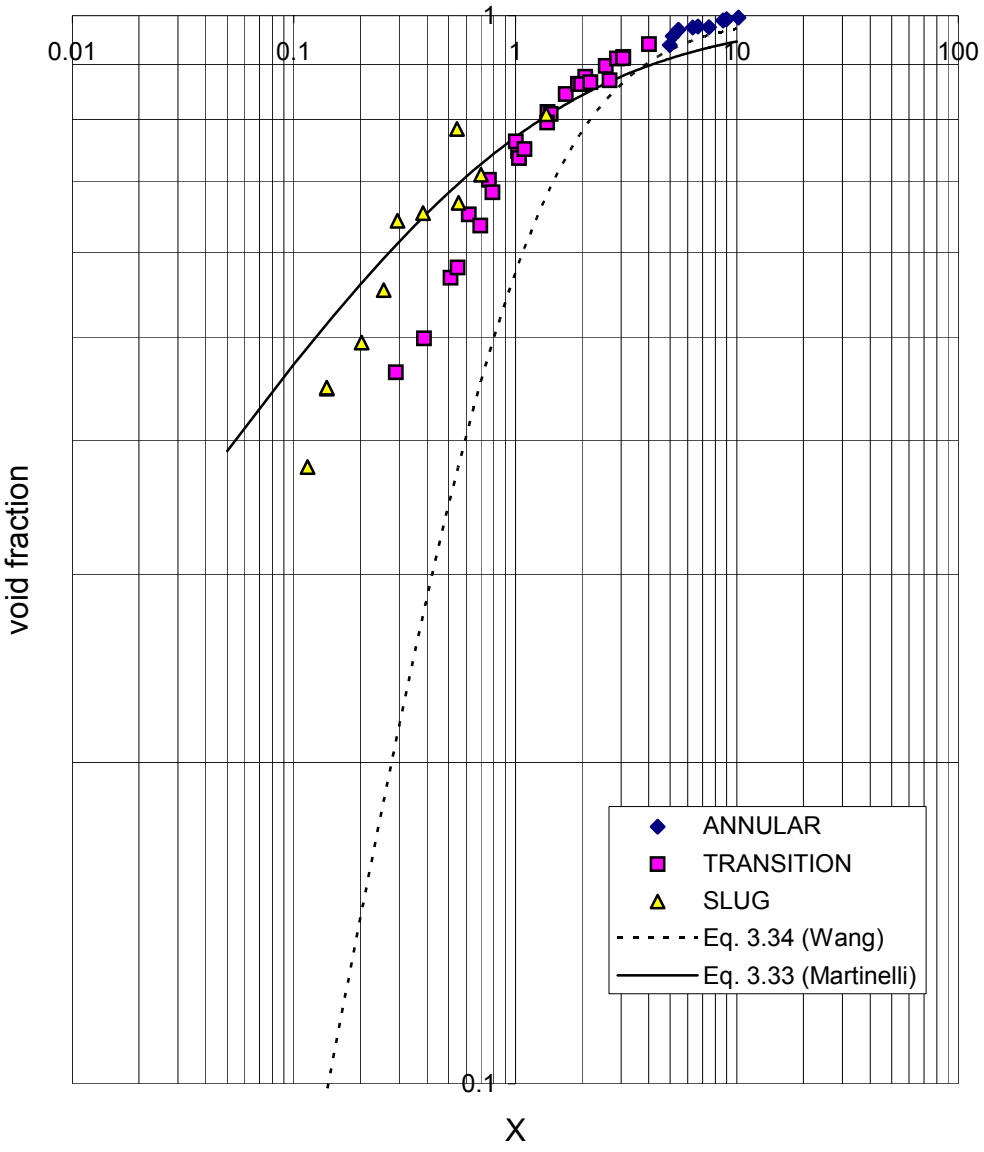

Fig 5.29. Inverse Martinelli parameter vs. void fraction for different parameters

A difference between the slug and the transition-annular data is obvious. This fact underlines in particular the difference that occurs between the slug and the other flow regimes. In fact the Martinelli parameter has high values for annular

flow and then quite mixed for transition and slug. In the transition-slug region for the same values of void fraction slug flow has a greater value of the Martinelli parameter than the transition phase.

In figure 5.29 Equations 3.33 and 3.34 are shown. A relevant discrepancy between the Wang (Eq. 3.34) correlation and the experimental data is noticed, while the Martinelli correlation (Eq. 3.33) seems to be closer to the data. As noted it seems that slug flow follows a slightly different correlation. It could be that for earth gravity conditions slug flow follows the trend of the transition-annular phase like all the 1-g literature suggested [30] [32], while in microgravity conditions it presents some discrepancy from the other flow patterns. This could happen because for slug flow some aspects became crucial in earth-condition and are absent in zero gravity such as buoyancy. The discrepancy is revealed only for slug flow because the buoyancy strongly governs slug flow more than any other pattern.

As said in chapter III at the time it's not clear yet what the Martinelli parameter has to do with the flow pattern, and so figure 5.28 and 5.29 show one more time the correlation but no theoretical explanation is provided.

The next figures illustrate the relationship of the Martinelli parameter with the previously developed statistical parameters.

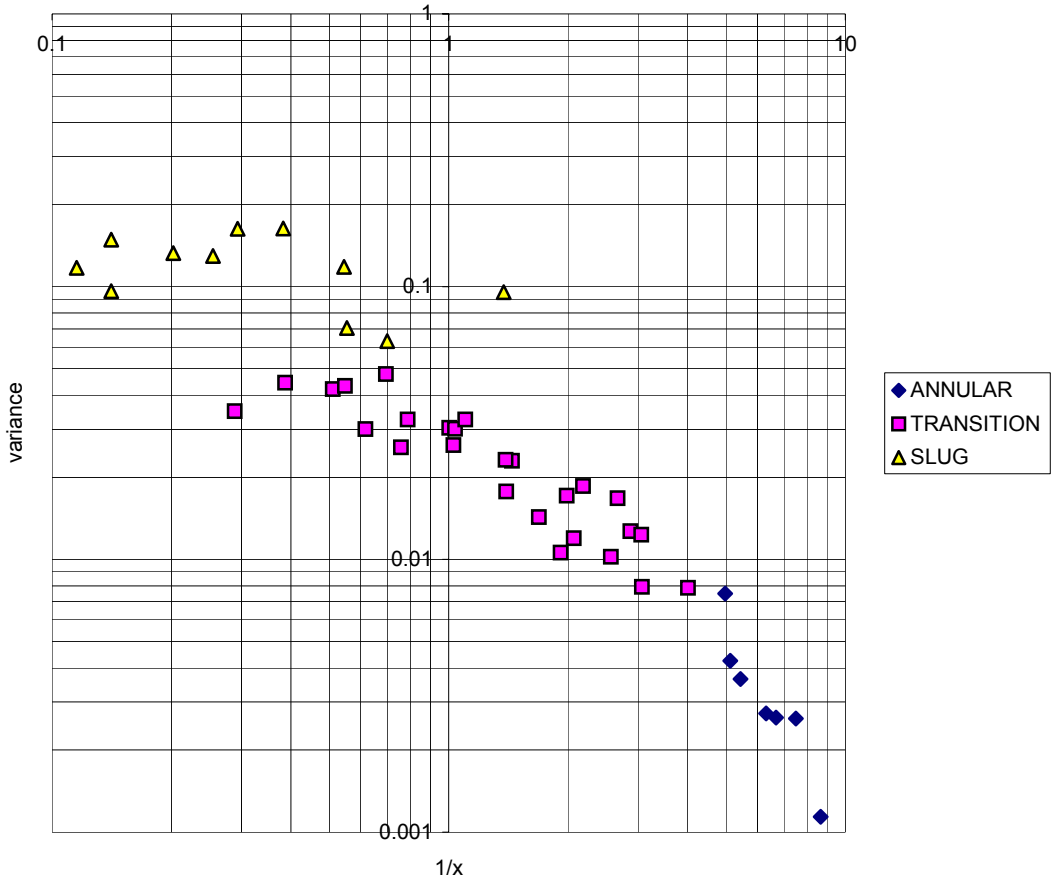

Fig 5.30. Inverse Martinelli parameter vs. variance for different flow patterns

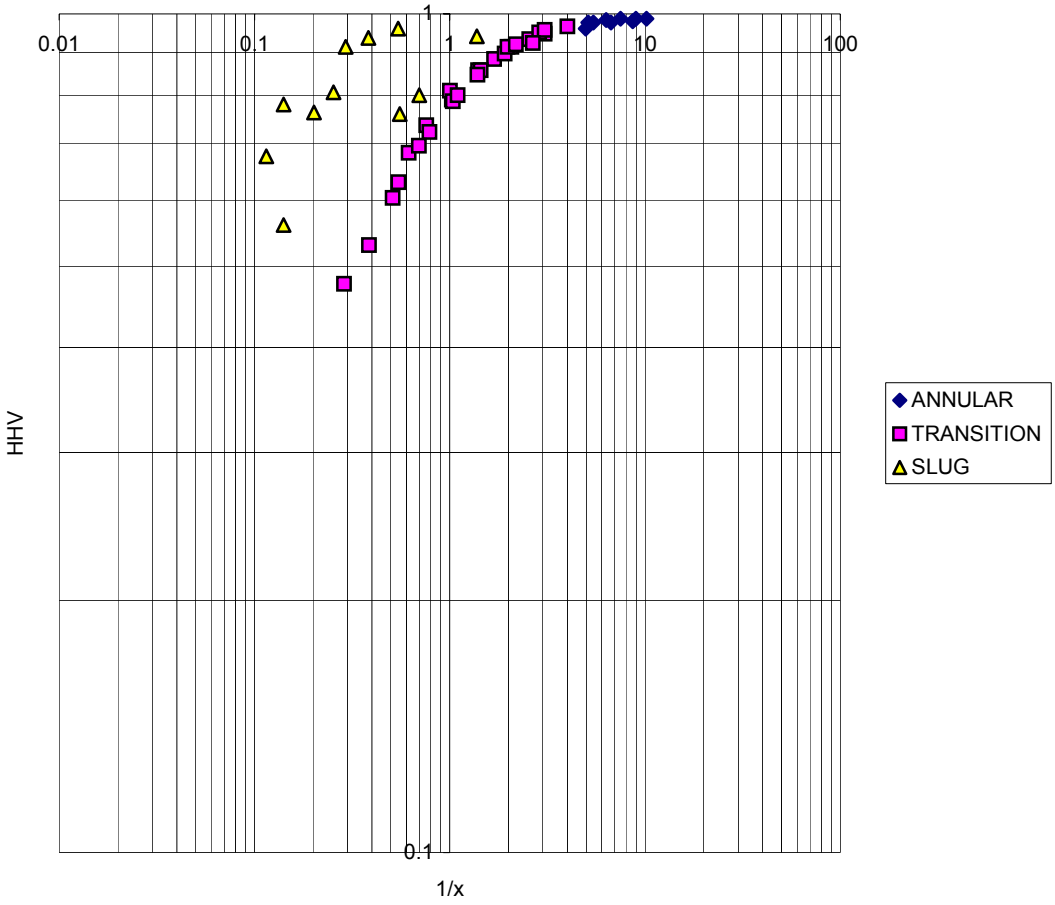

Fig 5.31. Inverse Martinelli parameter vs. HHV for different flow pattern

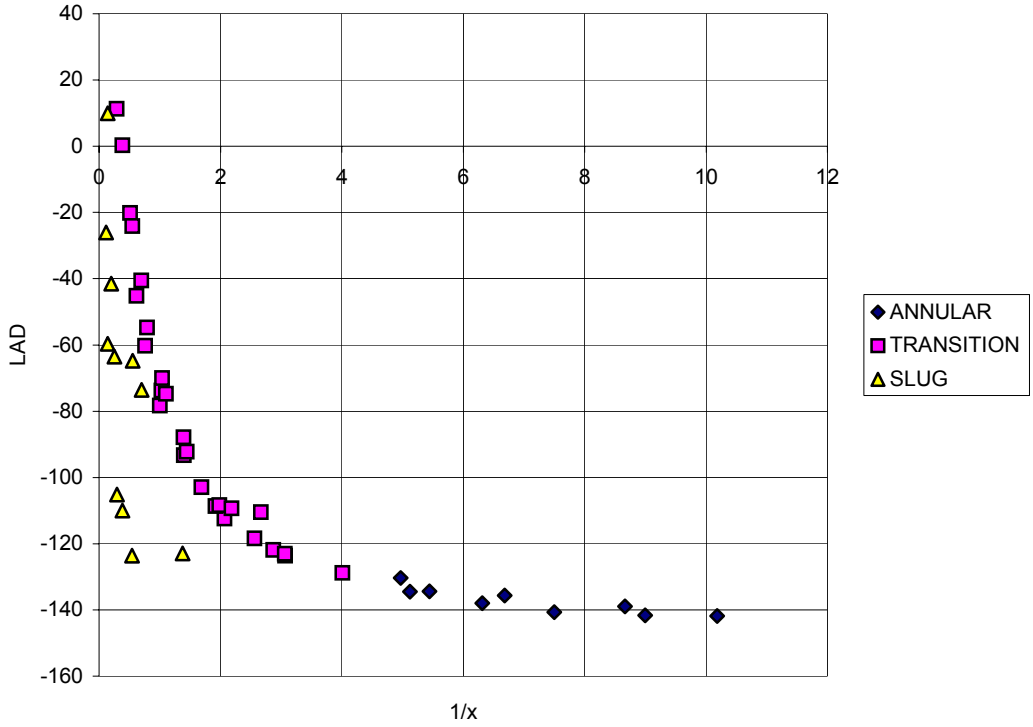

Fig 5.32. Inverse Martinelli parameter vs. LAD for different flow pattern

Figures 5.30 through 5.32 show good correlations with the Martinelli parameter. This result was expected because that's another consequence of the fact that both the statistical parameter and the Martinelli parameter are linked with the flow pattern (Figure 5.28 and 5.29). The fact that the parameters plotted in the graph are from separated and different analysis (statistical and flow property) underlines the importance of the current results.

It's important to note one more time, the outlier slug flow behavior in all the graphs. This fact leads to a new explanation of slug flow statistics. In fact, it's clear that slug flow should not be considered a periodic time combination of

bubbly and annular flows, as Jones and Zuber [13] proposed, but it should be considered a totally different flow regime governed by its own basic equation and with its characteristic performance. The same conclusion could have been achieved from the physical analysis of the slug flow. In fact it's clear that it's a capillary dominated flow regime that occurs for low superficial velocities, different from the conditions of the annular and bubbly flow.

Other statistical dependences were shown, such as analyzing the ratio of the superficial velocities as a function of the measured void fraction and of the statistical parameters. The results are plotted in figure 5.33 through 5.36. In figure 5.34 the other results from the 0-g literature are shown.

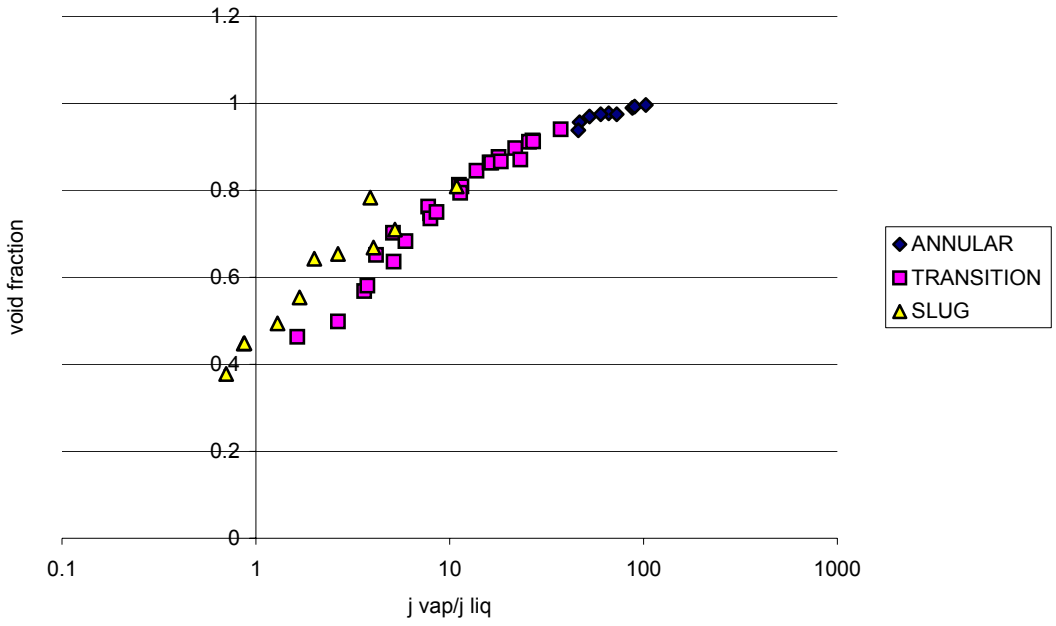

Fig 5.33. Void fraction data for the current study (0-g)

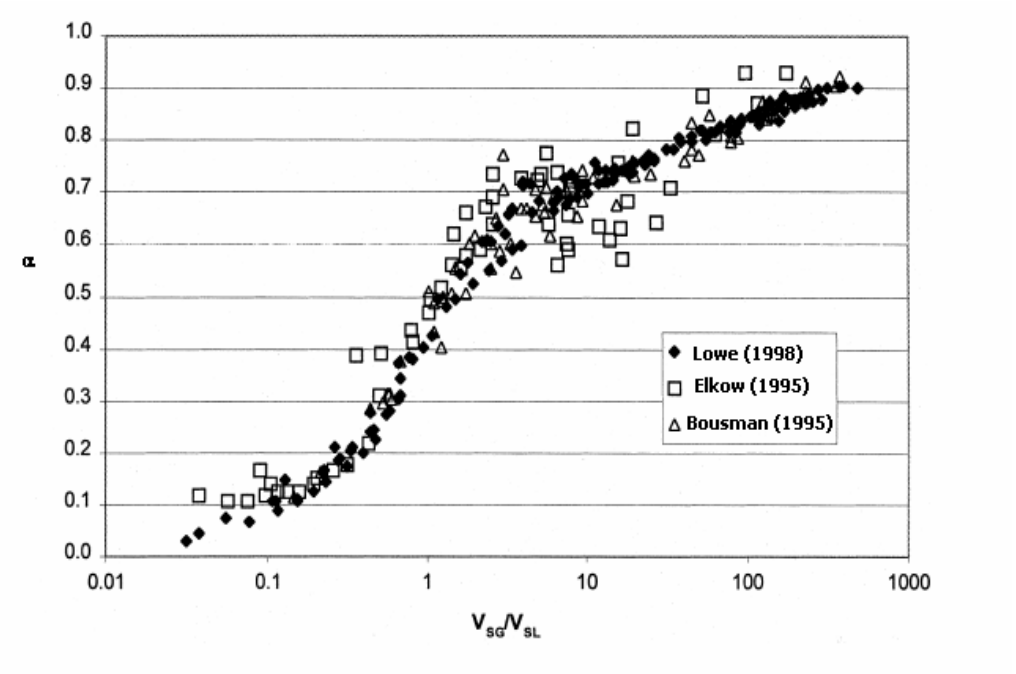

Fig 5.34. Void fraction data from the literature (0-g)

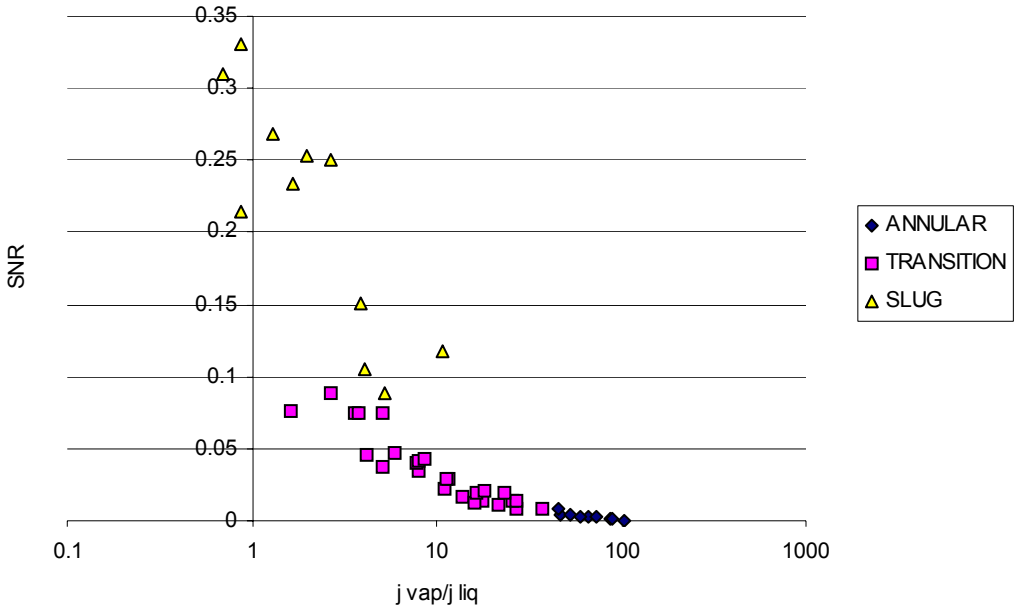

Fig 5.35. SNR dependence on the phases ratio superficial velocities

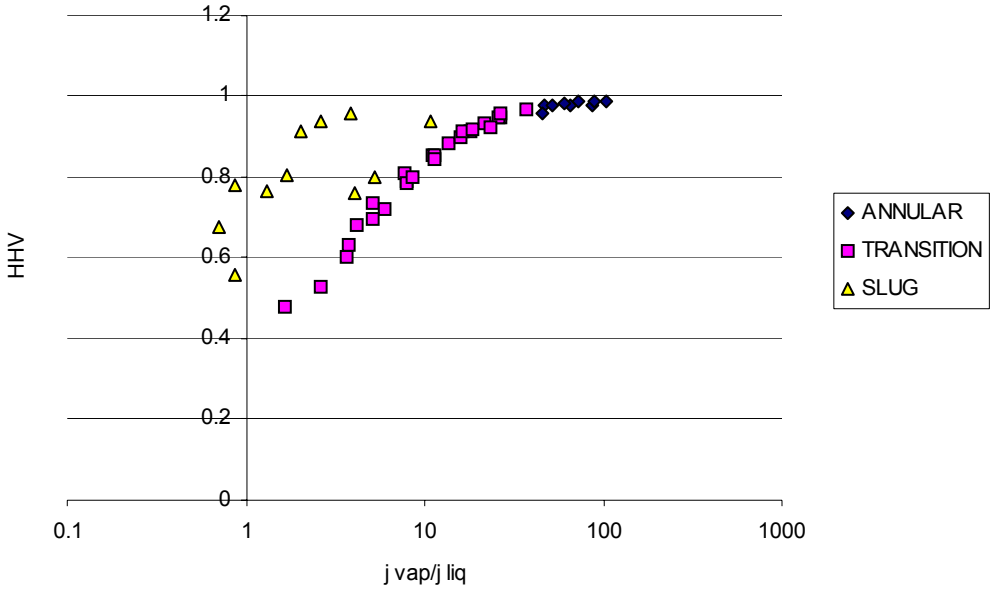

Fig 5.36. HHV dependence on the phases ratio superficial velocities

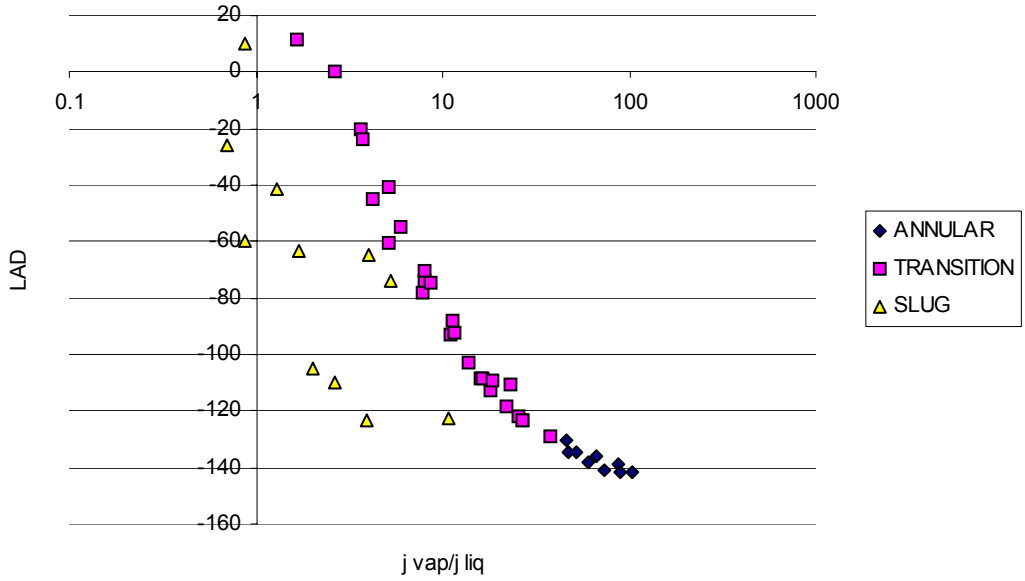

Fig 5.37. LAD dependence from the phases ratio superficial velocities

A good accordance of results is verified. It's shown one more time the good correlation between the statistical parameters and the velocity ratio because of their relation with the flow pattern.

In addition from figures 5.34 to 5.37 two main conclusions could be reached:

First, we notice two main regions of flow patterns in figure 5.33: for the ratio greater than 50 only annular flow is present, while below 50, transition and slug flow occur. Physically this means that the difference of the phase velocities for annular flow is large and the vapor moves faster than the liquid phase. This allows us to consider this ratio a good flow pattern identificator.

Secondly for same void fraction slug flow exists at a smaller value of the superficial velocities ratio and it's approaching 1. This means that the relative velocity between the vapor and the liquid is smaller for slug flow than for transition flow. This fact is physically reasonable, in fact the Taylor bubble is entrapped with liquid and so the velocities should be closer than annular and transition, where the vapor is free to flow at any velocities in the centerline.

Furthermore this fact confirms the results from the Martinelli analysis, where it was shown that the behavior of the slug flow and the inadequacy of considering the slug as a periodic time combination of bubbly and annular flows.

It's important to notice one more time that the values found of the ratio of the velocities is smaller in microgravity condition than in earth condition due to the absence of buoyancy that implies that annular flow is reached at smaller velocities.

5.4 DRIFT FLUX ANALYSIS

Using the Drift Flux Analysis we can analyze the data from the present experiment. In particular we could be able to notice the eventual linear correlation of equation 3.17 between the ratio of the superficial vapor velocity and the void fraction and the mixture superficial velocity. This graph is shown in figure 5.38.

In Figure 5.38 also the trend line and the homogeneous model prediction are shown. As previously seen, the two parameters to be analyzed are the distribution parameter C_0 and the drift velocity u_{gj}. Zuber and Findlay [28] suggested that C_0 and u_{gj} are strongly functions of the flow regime.

Table 5.6 shows the results for the current experiment.

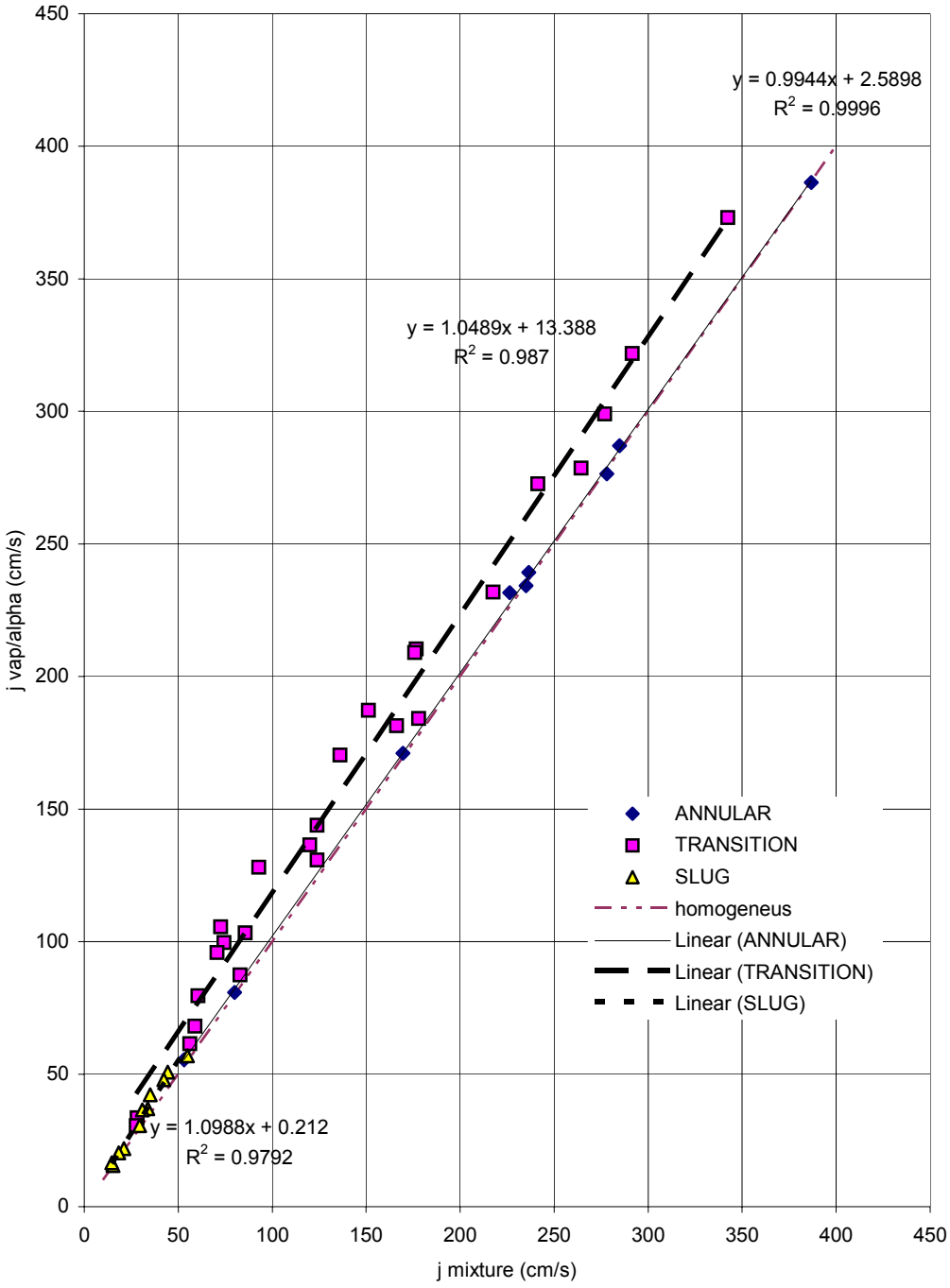

Fig 5.38. Ratio of the superficial vapor velocity and the void fraction vs. mixture superficial velocity

Table 5.6. C_0 and u_{gj} for different flow patterns

	SLUG	TRANSITION	ANNULAR
C_0	1.0988	1.0489	0.994
u_{gj} (cm/s)	0.212	13.388	2.5898

Collier [31] suggested that the value of u_{gj} for annular and transition is not very representative of any property because the analysis of the drift velocity could have meaning only for $u_{gj}<0.05j$ when the drift velocity is significant compared with the total volumetric flux, and in the current experiments several data are out of that range.

Anyway we analyze it as a pure correlation result and so we consider it accurate and valid even though there are particular physical reasons that explain the data.

The value for u_{gj} for slug flow close to zero is empirically supported because, as Janicot and Dukler [35] concluded, studies of movie films taken during slug flow showed that gas bubbles in the liquid slug and the Taylor bubble move at the same velocity. So we can assume that the liquid phase is moving with almost the same velocity of the bubbles entrapped in the liquid phase. This

means that the drift velocity (the velocity of the vapor that pass through a section moving at j velocity) should be small.

The value for u_{gj} for transition flow is larger than for annular. This could be due to the fact that j is typically higher for annular than for transition, and so the velocity of the vapor that passes through the moving imaginary surface with velocity j is larger in transition than in annular. In other word the liquid phase is slower in transition than in annular.

Also in this case it's important to analyze the differences between zero and earth gravity conditions. In particular for annular flow the value of Vvj is expected to be smaller than in earth-condition because of the lower velocities of the phases.

In addition, more results for the C_0 value are noticed. In order to have a better understanding of C_0,it is better to go back to the physical definition given in chapter 3. C_0 can have two physical interpretations: it could be seen as an empirical correcting factor of the one-dimension homogeneous theory or it could be seen from the analysis of the concentration profile of the phases in the duct section. A further consideration should be done in case of slug flow. In fact from the second interpretation, it follows that C_0 for slug flow has no meaning (there are two different velocities profile in time transient, full water and slug) while the first C_0 is still a parameter with a physical sense.

Besides that for annular and transition, the closer the value of C_0 is to 1, the closer the fluid is to homogeneous model behavior where all the phases have

the same velocity and the velocity is constant over the duct section. The values found in this microgravity condition experiment are almost 1 for all the flow patterns (table 5.6), so in zero gravity condition it seems that we are approaching a fluid with more “homogeneous” properties and velocity constant over the section. In other words it seems that in microgravity we are approaching a fluid with a constant velocity profile through the duct section. Instead of the earth-gravity conditions Zuber and Finlay [28] suggested C_0=1.2 for bubbly and slug flow, and C_0=0 for near zero void fraction and 1.0 for high void fraction.

The results of this study are reasonable. In fact, Colin et al. [34] analyzed the influence of gravity on void distribution in two-phase gas-liquid flow in adiabatic pipe 4cm I.D. using air and potassium chloride added to water. They found that the local void fraction dependence on the radius in the duct follows figure 5.39.

So the concentration profile is almost constant for zero-gravity conditions, and that’s means from the previous analysis (in particular figure 3.15) that C_0 should be close to 1, as the present data shows. Moreover, the large profile difference from zero-gravity and earth conditions is noteworthy.

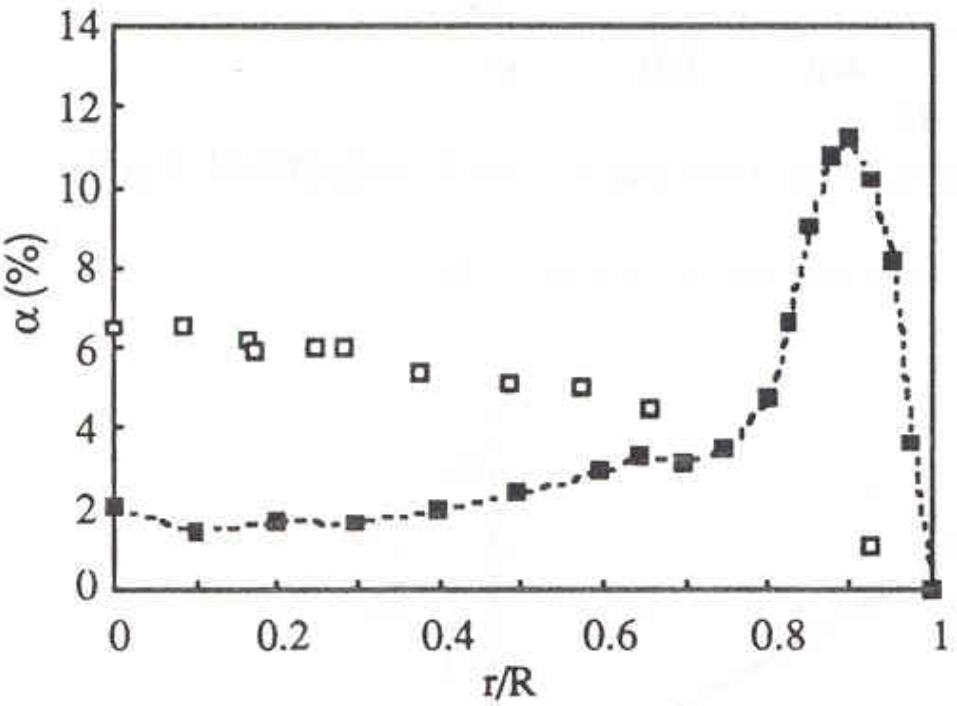

Fig. 5.39. Concentration profile from Colin et al. [34] in dependence of the relative radial position for earth gravity conditions (black square) and microgravity conditions (white square)

5.5 CHAPTER SUMMARY

This chapter described three different analyses of the CREARE Inc. Void Fraction data and other data from the experiment.

The first one consists of statistical analysis and includes the analysis of the transient data, the PDF and the Cumulative Density Function. It was found that the variance, SNR, skewness, HHV and LAD could be considered good flow

pattern identifies. Moreover no dependence of the parameters with the liquid superficial velocity was found.

The second analysis consists in the Lockhart-Martinelli examination. It was found that the void fraction data approximates the original Martinelli correlation and the abnormal trend of the slug flow pattern was noticed and explained.

Finally the Drift Flux approach was analyzed and explanation of the C_0 values collected.

The desire to identify some parameters or factors that can be considered valid flow pattern identificators is accomplished, although more experimental data are needed to validate the thesis.

CHAPTER VI

CONCLUSION

Knowledge of the two-phase flow state is fundamental for two-phase flow system design and operation. Flow configuration is important for engineering correlations of heat and mass transfer, pressure drop, and wall shear. However, it is somewhat subjective since it is mostly defined by experimental observation, resulting in an approximate and equivocal definition. Thus, there is need for a better, objective flow regime identification. The void fraction is a key parameter in monitoring the operating state of a two-phase system and several tools have been developed in order to measure it. Thus, purpose of this study is to use the void fraction and other parameters of the system to achieve a model for flow pattern identification.

An experimental program using Foster-Miller two-phase flow test bed and Creare Inc. capacitance void fraction sensors was conducted in the microgravity environment of the NASA KC-135 aircraft. Several data types were taken for each phase, such as flow rate, superficial velocity, density and transient void fraction at 100Hz. A clear sight tube and a digital camera was added for visual observation and recording of the flow.

Two different codes were built in order to collect all the results and to match the data with the zero-gravity period and to provide a preliminary analysis.

Several analytical approaches were pursued, including a statistical approach, Martinelli analysis, and Drift Flux analysis.

The statistical approach consisted in the analysis of the fluctuation of the void fraction using the probability density function examined by statistical moments (variance, skewness, and kurtosis) and the cumulative density function analyzed by the Linear Difference Area and Half High Value.

The Martinelli approach consists in the investigation of the Martinelli parameter in dependence with the other quantities and the flow pattern.

The Drift flux approach is an extension of the model for a microgravity environment.

Important and consistent results for flow pattern identification were achieved.

From the statistical point of view it was found that the variance and SNR are good flow patterns indicators (bigger for slug and smaller for annular). The coefficient of skewness was found in accordance with the literature but not useful for the identifications of the flow pattern. The coefficient of kurtosis did not present any relevant characteristic properties. The Half High Value (HHV) and the Linear Area Difference (LAD) are useful for the identification of an annular region, for a clear linear trend for transition and annular and for the out-lier behavior for slug. It’s also shown that there is no influence of the velocities in these results.

From the Martinelli analysis could be concluded that the slug flow has a different trend in comparison with annular and transition and in general the

Martinelli parameter is a good flow pattern identifier. It's also shown that the ratio of the superficial velocities provide a good indicator for all the three regions.

Analyzing the Drift Flux model it was found that in microgravity the value of C_0 is close to 1 for all the flow patterns. That brings us to a constant velocity profile in the duct section.

This work is a preliminary void fraction statistical analysis, Martinelli analysis and Drift Flux analysis. The current study shows that several parameters and approaches could be used to identify the flow regime. However, further tests also including other flow regimes and transitional regions, e.g., bubbly and mist flow would enhance the methods outlined in this thesis.

REFERENCES

[1]. J. Fabre, Two-phase Flow and Applications at Microgravity, Aerospace Institute Aeronautics and Astronautics Short Course, Reno, Nevada, January 10-12, 1992

[2]. G. W. Govier and M. M. Omer, The Horizontal Pipeline Flow of Air-Water Mixtures, The Canadian Journal of Chemical Engineering, 40, (1962), 93.

[3]. N. Miller and R. E. Mitchie, The Development of a Universal Probe for Measurement of Local Void Fraction in Liquid/Gas Two-Phase Flow Systems, 11th National ASME/AIChE Heat Transfert Conference, Section Two-Phase Flow Instrumentation, American Society of Mechanical Engineering, New York (1969).

[4]. V. E. Schrock, Radiation Attenuation Techniques in Two-Phase Flow Measurements, 11th National ASME/AIChE Heat Transfer Conference, Section Two-Phase Flow Instrumentation, American Society of Mechanical Engineering, New York (1969).

[5]. D.C. Lowe, K.S. Rezkallah, Flow Regime Identification in Microgravity Two-Phase Flow Using Void Fraction Signal, International Journal of Multiphase Flow, 25 (1999), 433-457

[6]. J. M. Delhaye, Hot-Film Anemometry in Two-Phase Flow, 11th National ASME/AIChE Heat Transfer Conference, Section Two-Phase Flow Instrumentation, American Society of Mechanical Engineering, New York (1969).

[7]. N. Reinecke, G.Petritsch, M. Boddem and D. Mewes, Tomographic Imaging of the Phase Distribution in Two-Phase Slug Flow, International Journal of Multiphase Flow, 24 (1998), 617-634

[8]. E. Fransolet, M. Crine, D. Toye and P. Marchot, Electrical Resistence Tomography Sensor Simulations: Comparison with Experiments, Measurament Science and Technology, 13 (2003), 1239-1247

[9]. J.F. Lafferty and F.G. Hammitt, A Conductivity Probe for Measuring Local Void Fractions in Two-Phase Flow, Nuclear Application, 3 (1967), 317-322

[10]. D.C. Barber and B.H. Brown, Applied Potential Tomography, (Review Article). Journal Physics E Science Instrumentation, 17 (1984), 723 - 733.

[11]. K.A. Dines and R.J. Lytle, Analysis of Electrical Conductivity Imaging, Geophysics 46 (1981), 1025 – 1036

[12]. J. J. M. Geraets and J. C. Borst, A Capacitance Sensor for Two-Phase Void Fraction Measurement and Flow Pattern Identification, International Journal of Multiphase Flow, 14 (1988), 305-320

[13]. O. C. Jones, Jr. and N. Zuber, The Interrelation Between Void Fraction Fluctuations and Flow Patterns in Two-Phase Flow, International Journal of Multiphase Flow, 2 (1975), 273-306.

[14]. M. A. Vince and R. T. Lahey, Jr., On the Development of an Objective Flow Regime Indicator, International Journal of Multiphase Flow, 8 (1982), 93-124.

[15]. M. Annunziato, G. Girardi, Statistical Method to Identify Two-Phase Regimes: Experimental Results for Vertical Large Diameter Tubes, 2nd International Conference, London, England: 19-21 June 1985. Paper G5.

[16]. C.H. Song, H.C. No and M.K. Chung, Investigation of Bubble Flow Developments and its Transition Based on the Instability of Void Fraction Waves, International Journal of Multiphase Flow, 21 (1995), 381-404

[17]. D.C. Lowe, K.S. Rezkallah, Flow Regime Identification in Microgravity Two-Phase Flow Using Void Fraction Signal, International Journal of Multiphase Flow, 25 (1999), 433-457

[18]. K.J. Elbow and K.S. Rezkallhah, Statistical Analysis of Void Fluctuation in Gas-Liquid Flows Under 1-g and μ-g Conditions Using a Capacitance Sensor, International Journal of Multiphase Flow, 23 (1997), 833-844

[19]. Hurlbert, K.M., Flow Dynamics for Two-Phase Flows in Partial Gravities, Ph.D. dissertation, Department Mechanical Engineering, University of Houston, Dec 2000.

[20]. S. Benner, G. Durback, K. Kolos, and R. Bayt, A Breadboard Flight Experiment for Two-Phase Flow Visualization in Microgravity, Proc. 33rd Aerospace Sciences Meeting & Exhibit, Reno, Nevada, January 9-12, 1995, AIAA-95-0696.

[21]. M. Wheeler, An experimental and Analytical Study of Reduced Acceleration Two-Phase Flow Frictional Pressure Drop, Master's Thesis, Nuclear Engineering Department, Texas A&M University, December 1992

[22]. C. J. Crowley, P. J. Magari, C. M. Martin, and M. E. Hill, A Void Fraction Instrument for Two-Phase Flow In Dielectric Liquids, Proc. 34th Aerospace Sciences Meeting & Exhibit, Reno, Nevada, January 15-18, 1996, AIAA-96-0925.

[23]. Jae Chang, Statistical Comparison of Void Fraction Instrumentation in Microgravity Environment, Master Thesis, Texas A&M University, Department Nuclear Engineering, 1999

[24]. C.J. Crowley, W.B. Chen, Scaling of Multiphase Flow Regimes and Interfacial Behavior at Microgravity, Final Report, CREARE Inc., TM-2086, December 2001

[25]. K. Marsden and F. Best, Vertical Acceleration Environment in the NASA KC-135, Environmental Systems Conf. Colorado Springs, Colorado, SAE, July 12-14 (1993).

[26]. P. A. W. Lewis and E. J. Orav, Simulation Methodology for Statisticians, Operations Analysts, and Engineers, Wadsworth & Brooks/Cole Advanced Books & Software, Pacific Grove, California (1989).

[27]. E. Parzen , On Estimation of a Probability Density Function and Mode, The Annals of Mathematical Statistics, 33 (1962), 1065-1076.

[28]. N. Zuber, J.A. Findlay, Average Volumetric Concentration in Two-Phase Flow Systems, Journal of Heat Transfer, Transaction of the ASME, 87 (1965), 453-468

[29]. G.B. Wallis, One-dimension Two-phase Flow, McGraw-Hill Book Company, New York, 1969

[30]. R.W. Lockhart, R.C. Martinelli, Proposed Correlation of Data for Isothermal Two-Phase Two-component Flow in Pipes, Chemical Engineering Progress, 45 (1949), 39-48.

[31]. John G. Collier, Convective Boiling and Condensation, McGraw Hill, New York, 1972.

[32]. L.P. Wang, V.P. Carey, R. Greif and D. Abdollahian, Experimental Simulation and Analytical Modeling of Two-Phase Flow Under Zero-gravity Condition, International Journal of Multiphase Flow, 16 (1990), 407-419

[33]. D. Butterworth, A Comparison of some Void Fraction Relationship for Co-current Gas-liquid Flow, International Journal Multiphase Flow, 1 (1974), 845-850

[34]. C.Colin, A.Kamp, J.Fabre, Influence of Gravity on Void Distribution in Two-Phase Gas-liquid Flow in Pipe, Advanced Space Research, 13, (1993), 141-145

[35]. A.Janicot, A.E. Dukler, A Model for Gas-liquid Flow at Reduced Gravity Conditions", AIChE Journal, 39 (1993), 1101-1106.

VITA

Luca Valota was born on April 15, 1980 to Giacomo Valota and Adelisa Manfredi in Calcinate (BG), Italy. He graduated from Liceo Scientifico Edoardo Amaldi in Trescore (BG), Italy. He received his Bachelor of Science degree in Nuclear Engineering from Politecnico di Milano in May 2002. His permanent address is Via Virgilio 1, Gorlago (BG), 24060, Italy.